TEMPORAL, GEOCHEMICAL, ISOTOPIC, AND METALLOGENIC STUDIES OF MID-CRETACEOUS MAGMATISM IN THE TINTINA GOLD PROVINCE, SOUTHEASTERN YUKON AND SOUTHWESTERN NORTHWEST TERRITORIES, CANADA

by

R. SCOTT HEFFERNAN

B.Sc. Specialization in Geology, University of Alberta – Edmonton, Alberta, 1998

A THESIS SUBMITTED IN PARTIAL FULFILLMENT OF
THE REQUIREMENTS FOR THE DEGREE OF

MASTER OF SCIENCE

IN

THE FACULTY OF GRADUATE STUDIES

(Department of Earth and Ocean Sciences)

We accept this thesis as conforming
to the required standard

THE UNIVERSITY OF BRITISH COLUMBIA

June 2004

Library Authorization

In presenting this thesis in partial fulfillment of the requirements for an advanced degree at the University of British Columbia, I agree that the Library shall make it freely available for reference and study. I further agree that permission for extensive copying of this thesis for scholarly purposes may be granted by the head of my department or by his or her representatives. It is understood that copying or publication of this thesis for financial gain shall not be allowed without my written permission.

R. SCOTT HEFFERNAN
Name of Author *(please print)*

JUNE 21/2004
Date (dd/mm/yyyy)

Title of Thesis: TEMPORAL, GEOCHEMICAL, ISOTOPIC, and METALLOGENIC STUDIES of MID-CRETACEOUS MAGMATISM IN THE TINTINA GOLD PROVINCE, SOUTHEASTERN YUKON and SOUTHWESTERN NORTHWEST TERRITORIES, CANADA

Degree: M. Sc. Year: 2004

Department of EARTH & OCEAN SCIENCES
The University of British Columbia
Vancouver, BC Canada

Abstract

The Tintina Gold Province (TGP) of east-central Alaska, Yukon Territory, and the southwestern Northwest Territories comprises a very large number of gold (± base metal) deposits and occurrences that are spatially and temporally related to mid-Cretaceous intrusions. Intrusions in the eastern Selwyn Basin, south of MacMillan Pass and east of Frances Lakes, include some of the largest bodies within the TGP and are the focus of this study. Magmatic rocks of the TGP have been divided into individual plutonic suites on the basis of crystallization age, lithology, mineralogy, geochemistry, and spatial distribution, as well as metallogenic association. From ~111 Ma to ~99 Ma, magmatism is thought to reflect the formation of a southwest-facing continental magmatic arc, represented by the Whitehorse – Coffee Creek suite, and that the coeval Anvil and Cassiar suites formed in a back-arc environment. The younger Tay River, Tungsten and Tombstone plutonic suites successively stepped inboard between 99 Ma to 89 Ma. However, the processes leading to such volumetrically significant magmatism remains poorly understood.

Intrusions within the study area range in composition from granite to granodiorite with subordinate diorite and are characteristically calc-alkaline, peraluminous to weakly metaluminous, relatively reduced, and typically contain only biotite as the dominant mafic phase. Sixteen new U-Pb ages, ranging from ~107 Ma to ~91 Ma, constrain a temporal framework for plutonism across the region that is consistent with the progressively "inboard younging" pattern of magmatism observed in the northern and western portions of the TGP. Geochemical (major, trace and rare earth elements) characteristics, together with geochronology indicate that the Anvil, Tay River, Tungsten, and Tombstone plutonic suites as originally defined farther to the northwest do continue southeastward and into the southwestern Northwest Territories. Initial Sr ratios and epsilon Nd values (n=20; age corrected for T = 100 Ma) range from 0.70853 to 0.72243 and –6.0 to –17.5, respectively. Lead isotopic compositions (n=20) show relatively narrow ranges for $^{206}Pb/^{204}Pb$, $^{207}Pb/^{204}Pb$, and $^{208}Pb/^{204}Pb$ ratios of 19.397 to 19.772, 15.697 to 15.829, and 39.461 to 39.883, respectively. All radiogenic isotope systematics indicate that these magmas have interacted extensively with or were derived entirely from continental crust. Several spatial and temporal trends are apparent in the data including an increase in overall REE abundance and εNd values, and a decrease in Sr_{inital}, values with decreasing age (broadly moving from west to east). These trends may reflect differences in the nature of the underlying basement, potential magma source(s), and/or the melt producing processes that were involved.

Lead isotope compositions of feldspars from various intrusions and sulphides from associated precious- and base metal deposits and occurrences define narrow and overlapping ranges indicating that the metals in many of the mineral deposits (and prospects) in the region are mostly derived from the mid-Cretaceous TGP intrusions.

Table of Contents

Abstract ii

Table of Contents iv

List of Tables vii

List of Figures viii

Acknowledgements ix

Chapter 1

Introduction

Introduction 1

Methodology 3

Field Work and Sampling 3

U-Pb Geochronology 3

Lithogeochemistry 3

Radiogenic Isotopic Studies 4

Presentation 4

References 5

Chapter 2

Temporal, geochemical and isotopic studies of mid-Cretaceous magmatism in the Tintina Gold Province in southeastern Yukon and southwestern Northwest Territories: Constraints on the tectonomagmatic evolution of the northern Cordillera

Introduction 6

Geologic Overview 7

Pre-Mesozoic Tectonic History 7

Mesozoic and Cenozoic Deformation 8

Mid-Cretaceous Intrusions 9

U – Pb Geochronology........10

Samples and Methodology........10

Results........11

Discussion........18

Lithogeochemistry........19

Analytical Techniques........19

Results........20

Discussion........21

Isotope Geochemistry........22

Analytical Techniques........22

Sr and Nd Isotope Results........23

Pb Isotope Results........24

Discussion........24

Nature of Magma Sources........24

Tectonic Setting of Mid-Cretaceous Magmatism........27

Where does the Tintina Gold Province go?........29

Conclusions........30

References........31

Chapter 3

Lead isotope signatures of Tintina Gold Province intrusions and associated mineral deposits from southeastern Yukon and southwestern Northwest Territories: Implications for exploration in the southeastern Tintina Gold Province

Introduction........66

Regional Metallogeny........67

Geologic Background........67

Lead Isotope Study..68

Samples and Analytical Techniques..68

Results...69

Discussion..70

Conclusions..71

References..71

Chapter 4

Summary and Directions for Future Research

Summary...78

Directions for Future Research..80

References..81

Appendix 1

Analytical Precision

Analytical Precision...82

List of Tables

Table 2.1 U-Pb sample locations and descriptions 38

Table 2.2 U-Pb analytical data for southeastern Tintina Gold Province intrusions 39

Table 2.3 Geochemistry sample locations and descriptions 42

Table 2.4 Major, trace, and REE analytical data 43

Table 2.5 Pb isotope data 47

Table 2.6 Sr and Nd isotope data 48

Table 3.1 Location and descriptions of intrusion-related deposits and occurrences 73

Table 3.2 Pb isotope data from feldspar and sulphide mineral separates 74

Table A.1 Replicate Standard Analyses 83

List of Figures

Figure 1	Location of the study area within the Tintina Gold Province	2
Figure 2.1	Map of Cretaceous volcanic and plutonic rocks in Yukon and Alaska	49
Figure 2.2	Morphogeological belts of the Canadian Cordillera	50
Figure 2.3	Location of U-Pb samples	51
Figure 2.4	U-Pb concordia plots for intrusions in the southeastern Tintina Gold province (1 through 16)	52
Figure 2.5	Map of plutonic suites in the southeastern Tintina Gold Province	56
Figure 2.6	Location of lithogeochemistry and radiogenic isotope samples	57
Figure 2.7	Total alkalis versus silica plot	58
Figure 2.8	Geochemical classification plots (cordilleran vs. ferroan, modified alkali lime index, Shand's Index)	59
Figure 2.9	Primitive mantle normalized REE diagrams (A-D)	60
Figure 2.10	Tectonic discriminant plots	61
Figure 2.11	Thorogenic, uranogenic, and $^{208}Pb/^{206}Pb$ vs. $^{207}Pb/^{206}Pb$ plots for intrusions in the southeastern Tintina Gold Province	62
Figure 2.12	Initial $^{87}Sr/^{86}Sr$ and εNd data for intrusions in the southeastern Tintina Gold Province	63
Figure 2.13	Compiled Pb isotope data from the northern Cordillera	64
Figure 2.14	Map of Tintina Gold Province with Tintina Fault displacement restored	65
Figure 3.1	Location of the study area within the Tintina Gold Province	75
Figure 3.2	Map of Cretaceous volcanic and plutonic rocks in Yukon and Alaska	76
Figure 3.3	$^{207}Pb/^{206}Pb$ versus $^{208}Pb/^{206}Pb$ plot of lead isotope ratios from Tintina Gold Province intrusions	77

Acknowledgements

Special thanks go to, my supervisor Dr. Jim K. Mortensen for his caffeine-fuelled harangues, Drs. Janet Gabites and Rich Friedman for their expert tutelage, patience, and guidance through the dark world that is geochronology and isotope geochemistry, and Drs. Dick Tosdal and Steve Rowins for their roles on my supervisory committee.

Many thanks go to all those that in one way or another shared in this experience, in particular Mr. Jefferson and the gang.

Most importantly, to John and Marty Heffernan and the rest of my family I say thank you for your endless support.

Chapter 1

Introduction

The Tintina Gold Province (TGP) is an arcuate belt of Early to Late Cretaceous intrusive rocks and associated gold-rich mineral deposits and occurrences which extends from east-central Alaska into southwestern Northwest Territories (Fig.1; Smith, 2000). In central and western Yukon, discrete plutonic suites have been recognized on the basis of their age, lithological, and geochemical characteristics, as well as their metallogenic associations (e.g., Mortensen et al., 2000). The connection between individual plutonic suites and their metallogenic associations has proven to be valuable as an exploration tool, enabling exploration companies to target specific groups of intrusions. Intrusions in the southeastern Yukon include some of the largest bodies within the TGP; however little is known regarding their ages or geochemical affinities, highlighting the need for a temporal and geochemical framework to guide future exploration in this large region.

A field and laboratory based geochronological, geochemical, and isotopic study was undertaken in order to investigate the southeastern extension of well-established plutonic suites currently recognized in central and western Yukon. New data reported in this thesis help constrain the tectonomagmatic evolution of the region in mid-Cretaceous time, and have implications for genetic and exploration models recently developed for gold and base metal mineralization associated with intrusions in this area (e.g., Lang et al., 2000). Funding for this project was provided by several organizations. Analytical costs (including U-Pb geochronology, Sr, Nd, Pb isotopic analyses, and whole rock geochemistry) were covered by a NSERC Discovery Grant (to J.K. Mortensen) and a NSERC Collaborative Research and Development Grant (to J.K. Mortensen and the Mineral Deposit Research Unit at the University of British

Columbia). The Yukon Geological Survey also contributed funding for lithogeochemical analyses and provided logistical support in the field. Additional logistical support and funding for fieldwork was provided by Hudson Bay Exploration and Development Co. Ltd. and a Hugh E. McKinstry Grant to the author.

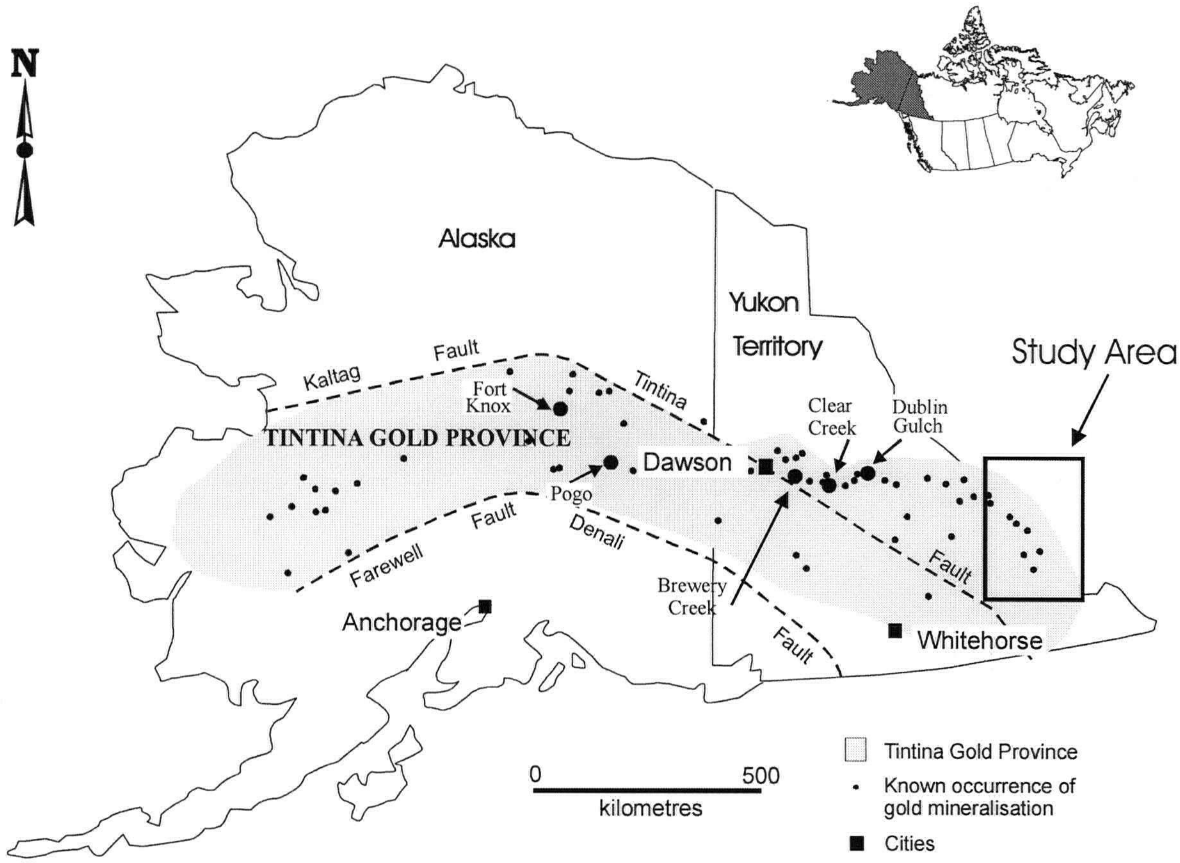

Figure 1. Map of Alaska and Yukon Territory showing the extent of the Tintina Gold Province and the locations of gold deposits and occurrences within (after Mortensen et al., 2000). The main study area is outlined by the box.

Methodology

Field Work and Sampling

Field work was carried out by the author during the 1999 and 2000 field seasons while employed by Hudson Bay Exploration and Development Company Ltd., and working in conjunction with geologists from the Yukon Geological Survey. Limited mapping traverses were completed in and adjacent to several of the intrusions and numerous mineral occurrences and deposits were examined and sampled. Samples of fresh plutonic rocks and mineralized wallrocks and intrusives were collected for petrographical, geochronological, geochemical, and isotopic studies. Additional samples were provided by V. Sterenberg (DIAND Yellowknife), which allowed sample coverage to be expanded to include the southeasternmost extension of the TGP.

U-Pb Geochronology

Previous geochronologic studies, which mainly utilized K-Ar and Rb-Sr dating methods, indicate broadly mid-Cretaceous ages for intrusions in the study area (e.g., Gordey and Anderson, 1993). However these data are too imprecise and sparse to permit direct comparison with recently developed plutonic suite designations elsewhere in the TGP (e.g., Mortensen et al., 2000). Crystallization ages determined by U-Pb dating of zircon, monazite, and titanite was employed in this study to provide a temporal framework for magmatism in the study area and to assess possible extensions of known plutonic suites into the area. All U-Pb sample preparation and analyses were carried out by the author and staff of the Pacific Centre for Isotopic and Geochemical Research (PCIGR) at the University of British Columbia.

Lithogeochemistry

Lithogeochemical analyses including major, trace and rare earth element (REE) concentrations were utilized to characterize the composition of plutonic rocks and to aid interpretation of the paleotectonic setting in which mid-Cretaceous magmatism in the study area occurred. All samples were prepared by the author and analyses were done by ALS Chemex Laboratories in North Vancouver, British Columbia, utilizing a combination of X-ray fluorescence (XRF) and inductively coupled plasma mass spectrometry (ICP-MS) techniques.

Radiogenic Isotopic Studies

Isotopic studies can provide important information concerning the source of magmas, to evaluate contributions from mantle versus crustal sources, and to identify potential metal sources in mineral occurrences. A representative suite of samples of intrusive rocks providing the broadest temporal and geographical coverage was selected for Rb-Sr, Sm-Nd, and Pb-Pb isotopic analysis. Sulphides from skarn occurrences associated with the plutonic rocks were also sampled for common Pb isotopic study to evaluate possible genetic relationships between skarn mineralization and the mid-Cretaceous magmatism. All sample preparation was done by the author. Common Pb analyses were carried out by the author and staff of the PCIGR at the University of British Columbia. Rb-Sr and Sm-Nd isotopic analyses of rock powders previously prepared for whole rock geochemistry were conducted by Dr. R. Creaser in the Radiogenic Isotope Facility at the University of Alberta.

Presentation

The results of this research project are presented as two research papers (Chapters 2 and 3) that will be submitted to international refereed journals. Chapter 2 focuses on the nature of intrusive rocks within the study area, and incorporates field observations as well as geochronological, petrographic, geochemical, and isotopic data obtained during the course of this study. These data are used to differentiate between individual plutonic suites throughout the study area. Discussion focuses on the mid-Cretaceous tectonomagmatic evolution of the area, and specifically the nature of source(s) of magmatic components, and interpretation of the paleotectonic setting through comparison with data from the western and northern portions of the TGP, the southern Canadian Cordillera and global analogues.

Chapter 3 combines conclusions regarding the nature of magmatism drawn from Chapter 2 with results of common Pb isotopic investigations of intrusions and associated mineral occurrences in order to constrain genetic and exploration models for intrusion-related mineralization in the study area.

Chapter 4 provides a synopsis of conclusions from chapters 2 and 3, outlines outstanding questions raised from this study and suggests directions for potential future research.

References

Gordey, S.P., and Anderson, R.J., 1993. Evolution of the northern Cordilleran miogeocline, Nahanni map area (105I), Yukon and Northwest Territories: Geological Survey of Canada Memoir 428, 214 p.

Lang, R.L., Baker, T., Hart, C.J.R., and Mortensen, J.K. 2000. An exploration model for intrusion-related gold systems. Society of Economic Geologists Newsletter, no. 40-1, pp. 6-15.

Mortensen, J.K., Hart, C.J.R., Murphy, D.C., and Heffernan, S. 2000. Temporal evolution of Early and Mid-Cretaceous magmatism in the Tintina Gold Belt. *In:* The Tintina Gold Belt: Concepts, exploration, and discoveries, British Columbia and Yukon Chamber of Mines Cordilleran Roundup Special Volume 2, Vancouver, British Columbia, pp. 49-57.

Smith, M. 2000. The Tintina Gold Belt: An emerging gold district in Alaska and Yukon. *In:* The Tintina Gold Belt: Concepts, exploration, and discoveries, British Columbia and Yukon Chamber of Mines Cordilleran Roundup Special Volume 2, Vancouver, British Columbia, pp. 1-3.

Chapter 2

Temporal, geochemical and isotopic studies of mid-Cretaceous magmatism in the Tintina Gold Province in southeastern Yukon and southwestern Northwest Territories: Constraints on the tectonomagmatic evolution of the northern Cordillera

Introduction

The Tintina Gold Province (TGP) of east-central Alaska, Yukon Territory, and the southwestern Northwest Territories comprises a very large number of gold (± base metal) deposits and occurrences that are spatially and temporally related to mid-Cretaceous intrusions (Fig. 2.1, inset). Magmatism within the TGP occurred in a variety of tectonic settings and was superimposed on diverse terranes of the northern Cordillera. Recent investigations (e.g., Mortensen et al., 2000) have lead to the subdivision of plutonic rocks in the region into individual plutonic suites on the basis of crystallization age, lithology, mineralogy, geochemistry, and spatial distribution, as well as their metallogenic signature (Fig. 2.1). From ~111 Ma to ~99 Ma, magmatism is thought to reflect the emplacement of a continental magmatic arc, represented by the Whitehorse – Coffee Creek suite (WCCS), with the coeval Anvil (APS) and Cassiar (CPS) suites forming in a back-arc environment. The younger Tay River (TRPS), Tungsten (WPS) and Tombstone plutonic suites (TPS), successively stepped inboard between 99 Ma to 89 Ma, but it remains unclear how much, if any, of a subduction-related component is present in these plutonic suites.

This study focuses on intrusions that compose the southeastern extent of the TGP, which have received little attention thus far. The individual plutonic suites defined farther to the northwest appear to project into this area; however prior to this study there was insufficient data available to determine whether the suites extend into the study area. An additional question concerns the reason why magmatism appears to terminate abruptly to the southeast. This paper presents new age, geochemical and isotopic data for intrusions in this region. The data also help to constrain potential source materials and provide insight into the tectonic setting in which these magmas were generated.

Geologic Overview

Pre-Mesozoic Tectonic History

Ancestral North America (Laurentia) was mostly assembled by circa 1.9 Ga. In the region of what is now the northern Canadian Cordillera, the westernmost margin is believed to consist of the enigmatic Nahanni domain and the Fort Simpson arc (see Welford et al., 2001; their Fig.12). These crustal elements formed during the waning stages of the accretionary Wopmay Orogen and are recognized largely on the basis of distinct aeromagnetic signatures and isotopic correlations between basement drill core from the northern Cordillera and basement gneisses of the southern Cordillera (Villenueve et al, 1991; Ross, 1991). Since the amalgamation of Laurentia, the western margin has been subject to episodic rifting and the deposition of passive margin miogeoclinal successions (Monger and Price, 1979; Gabrielse and Yorath, 1991, Ch.18). In the northern Cordillera, sedimentation took place in four main periods: 1.84-1.71 Ga Wernecke Supergroup, 1.815-1.5 Ga Muskwa assemblage, 1.2-0.78 Mackenzie Mountain Supergroup, and 0.8-0.54 Ga Windermere Supergroup; each representing a variety of depositional environments (Ross et al., 2001; Aitken and McMechan, 1991, Ch.5). The Meso- and Neoproterozoic assemblages are overlain by dominantly Paleozoic clastic and carbonate rocks of the Selwyn Basin and Mackenzie Platform. Recent seismic studies have shown these thick sedimentary successions, plus crystalline basement layers, form a tapering wedge that composes most of the crust (25-30 km) underlying the Foreland and Omineca belts whereas

Windermere and younger strata compose only the uppermost ~5km of this section (Cook et al., 1999; Welford et al., 2001, Fig. 12; Snyder et al., 2002, Fig. 1B).

Although the controls on the distribution of Proterozoic sedimentation remain somewhat uncertain (Gabrielse and Yorath, 1991), Cecile et al. (1997) have argued that the geometry of the latest Precambrian rifting of the western margin of Laurentia that underlies was fundamental in influencing Paleozoic sedimentation and subsequent Mesozoic deformation (discussed in next section). The northeast trending Liard Line (Fig. 2.2) is a zone defined by Paleozoic facies patterns and is interpreted to represent an ancient transfer fault separating an upper plate margin (Macdonald High) on the south from a lower plate margin (Meilleur River Embayment) on the north (Cecile et al., 1997).

Mesozoic and Cenozoic Deformation

Historically, intrusions throughout the region have been collectively referred to as the Selwyn Plutonic Suite (Anderson, 1983, 1987, 1988; Pigage and Anderson, 1985; Gordey and Anderson, 1993). Intrusions of the southeastern TGP were emplaced into Late Precambrian to Mesozoic strata of the Selwyn Basin and define the eastern limit of the Omineca Belt in the northern Cordillera (Fig. 2.2). Selwyn Basin strata consist mostly of turbiditic sandstones, deep water limestones, shale and chert which were deposited contemporaneously with shallow water carbonate rocks and sandstones of the Mackenzie platform to the north and west (Gordey and Anderson, 1993). Jurassic through Paleoene collisional deformation, resulting from the accretion of allochthonous terranes to the west (Monger and Price, 1979; Gabrielse and Yorath, 1991), produced the northeast-verging Selwyn and Mackenzie fold belts. The former is characterized by small- to large-scale, open to tight folds with associated axial planar cleavage whereas the latter formed large scale, broad open folds. The different styles of deformation reflect varying competency of the strata involved; weak, thin-bedded siliciclastic strata of the Selwyn Basin versus the competent thick carbonate sections of the Mackenzie platform (Gordey and Anderson, 1993), respectively. Palinspastic reconstructions suggest crustal shortening of approximately 30% or about 50 to 70 km in this area, which is significantly less than the 200 km of contemporaneous shortening observed in the southern Canadian Cordillera (Gabrielse and Yorath, 1991; Gordey and Anderson, 1993; Cecile et al., 1997). The emplacement of mid-Cretaceous intrusions post-dates regional compressional deformation (folding and thrusting) but is pre- to syn-kinematic with respect to other major faults within the region (Gordey and Anderson, 1993; Murphy, 1997). The only known extrusive equivalents to these plutonic rocks in the region are caldera-filling, welded dacitic tuffs of the South Fork Volcanics (Gordey, 1988), which are considered to be comagmatic with the Tay River suite intrusions (Mortensen et al., 2000).

Mid-Cretaceous Intrusions

Mid-Cretaceous intrusions in southeastern Yukon and southwestern Northwest Territories form simple to complex, single to multi-phase stocks, plutons and batholiths. Contacts with adjacent wallrocks are typically steep (>65°) and are characterized by prominent oxidized, rusty weathering metamorphic aureoles that are less than a few hundred meters in width. The presence of andalusite-bearing hornfels within contact aureoles and known stratigraphic thicknesses indicate a possible range of 3.3 to 11.6 km for depth of emplacement (Gordey and Anderson, 1993). A limited amount of aluminum-in-hornblende thermobarometric data for some of the intrusions in the region (Heffernan, unpub. data) also suggest shallow emplacement levels, and possibly further constrain emplacement depths to less than ~6 km.

Major intrusive phases consist mainly of medium-grained, massive to megacrystic granodiorite, quartz monzonite, and granite. Porphyritic (plagioclase ± hornblende ± biotite) phases and aplite dykes are locally abundant, particularly near the margins. Biotite and magnetite ± ilmenite are the dominant ferromagnesian phases. Hornblende is noticeably absent except within the Coal River Batholith. Common accessory minerals include apatite, zircon, allanite, and monazite or titanite. See Table 2.3 for a complete list of sample lithologies. Weak to moderate alteration of hornblende (if present) and biotite to chlorite and epidote, and sericitization of plagioclase are ubiquitous, but generally weak.

U – Pb Geochronology

Samples and Methodology

U-Pb geochronology was used to constrain crystallization ages of intrusions within the study area. Samples were collected from surface exposures of individual intrusions or from different phases of composite intrusions to provide the broadest geographical coverage throughout the region. Table 2.1 provides a summary of samples, including the name of the intrusive body sampled, UTM coordinates and a brief lithologic description of samples for which crystallization ages are being reported.

Zircon, monazite and/or titanite was separated from 3-15 kilogram samples using conventional crushing, grinding, and Wilfley table techniques, followed by heavy liquid and magnetic separation steps. Mineral fractions for analysis were selected based on grain size, quality, morphology, and magnetic susceptibility. Most zircon fractions were abraded prior to dissolution using the technique of Krogh (1982) in order to minimize the effects of post-crystallization lead loss. A small number of zircon fractions (see table 2.2) were not abraded; nor were all monazite and titanite fractions. All geochemical separations and mass spectrometry were done in the Pacific Centre for Isotopic and Geochemical Research (PCIGR) at the University of British Columbia. Samples were dissolved in concentrated HF and HNO_3 in the presence of a mixed $^{233\text{-}235}U$-^{205}Pb tracer. Separation and purification of Pb and U employed ion exchange column techniques modified slightly from those of Parrish et al. (1987). Pb and U were eluted separately and loaded together on a single Re filament using a phosphoric acid silica-gel emitter. Isotopic ratios were measured using a modified single collector VG-54R thermal ionization mass spectrometer equipped with a Daly photomultiplier. Most measurements were done in peak switching mode on the Daly detector. U and Pb analytical blanks were in the range of 1-2 pg and 1-9 pg, respectively, during the course of this study. U fractionation was determined directly on individual runs using a mixed $^{233\text{-}235}U$ tracer, and Pb isotopic ratios were corrected for a fractionation of 0.43%/amu, based on replicate analyses of the NBS-981 Pb standard and the values recommended by Thirwall (2000). All analytical errors were propagated through the age calculations using the numerical technique of Roddick (1987). All errors are reported at the 2σ level and are included with analytical results in Table 2.2.

Results

Sixteen of the thirty-one samples processed for U-Pb dating returned well-constrained ages. Nine samples did not yield minerals amenable for analyses and an additional six samples require further work to clearly resolve an age. Numbered sample locations (Fig. 2.3) and concordia plots (Fig. 2.4) correspond to samples as discussed below.

1. Mt. Billings Batholith (99-SH-022): This sample is a medium-grained biotite granodiorite that was collected from the southern portion of the Mt. Billings Batholith (Fig. 2.3). A moderate amount of fair to good quality zircon was recovered. Two fractions (A and B) of clear, colorless elongate prisms with minor inclusions and one fraction (C) of clear, colorless stubby equant prisms were moderately abraded and analyzed. All three fractions were discordant (Fig. 2.4). A regression line through all three points (MSWD=0) has a lower intercept age of 106.4 ± 0.4 Ma and is interpreted as the igneous crystallization age. The calculated upper intercept age of 1.87

Ga indicates a mainly Mesoproterozoic average age for an inherited zircon component contained within the sample.

2. *Mt. Billings Batholith (00-SH-001):* This sample is a weakly foliated, fine- to medium-grained biotite granodiorite. The sample was collected from surface, close to the margin of the northern end of Mt. Billings Batholith (Fig. 2.3). Very little zircon was recovered from the sample. Most zircon grains were either clear to pale brown, with 'cloudy' inherited cores or were brown to dark brown and contained a very high abundance of inclusions. The sample also yielded a quantity of euhedral clear yellow monazite grains containing very minor bubble-shaped inclusions. Two fractions of monazite, composed of 2 to 3 tabular grains with wedge-shaped terminations, were analyzed. Fractions M4 and M6 overlap each other and plot above concordia (Fig. 2.4), due to excess ^{206}Pb from the decay of ^{230}Th (Parrish, 1990). Assuming no post-crystallization Pb loss, a conservative crystallization age of 103.5 +/- 1.1 Ma is assigned based on the range of $^{207}Pb/^{235}U$ ages of the two monazite fractions.

3. *Mt. Billings Batholith (SH-073):* This sample is a massive, fine-grained, biotite granite collected from surface in the vicinity of the Tia skarn occurrence (Minfile # 105H 073) at the northern end of the Mt. Billings Batholith (Fig. 2.3). The sample contained a small amount of very fine (≤100 μm) monazite and a very small amount of zircon. Monazite grains were clear pale yellow, had no visible zoning, were virtually inclusion free, and had a subhedral flat/tabular morphology. Two fractions (M4 and M6) were analyzed and yielded similar results (Fig. 2.4). A crystallization age of 100.8 +/- 2.3 Ma is assigned based on the range of $^{207}Pb/^{235}U$ ages.

4. *Mt. Billings Batholith (SH-070):* This sample of fine- to medium-grained granite was collected from the Cali skarn occurrence (Minfile # 105H 070) located at the northern end of the

Mt. Billings Batholith (Fig. 2.3). The sample yielded a small amount of moderate to good quality monazite and a very small amount of poor quality zircon. Three fractions of monazite were analyzed. Monazite fractions M5 and M6 each consisted of several grains of clear, pale yellow, broken, stubby prismatic grains. These fractions yield nearly concordant analyses with $^{207}Pb/^{235}U$ ages of 104.6 ± 0.5 Ma and 104.4 ± 0.8 Ma respectively. Fraction M4 was a single grain of the same morphology of fractions M5 and M6 except that it was of poorer clarity due to a higher content of micro-inclusions. Fraction M4 yielded a slightly older $^{207}Pb/^{235}U$ age of 106.3 ±1.6 Ma. A conservative crystallization age of 105.8 ± 2.2 Ma is assigned based on the $^{207}Pb/^{235}U$ age range of all three fractions.

5. Coal River Batholith (99-SH-008): This sample is a medium-grained hornblende biotite granodiorite collected from the central portion of Coal River Batholith (Fig. 2.3). Abundant clear, colorless, prismatic zircon grains of varying morphology were recovered. Most of the zircon were quite fine (<104 μm) and of excellent quality. Three moderate- to strongly-abraded fractions of the coarsest grains were analyzed. Fractions B and C (tabular morphology) yielded different but concordant results and fraction D (elongate morphology) was slightly discordant (Fig. 2.4). With no evidence of inheritance having affected the sample and assuming that fractions C and D have been affected by post-crystallization Pb loss (2-3 times higher U concentration than fraction B), a crystallization age of 95.6 ± 0.4 Ma is assigned based on the $^{206}Pb/^{238}U$ age of concordant fraction B.

6. Coal River Batholith (99-SH-006): This sample is a medium-grained hornblende biotite granodiorite collected from the central portion of the batholith, southwest of sample 99-SH-008 (Fig. 2.3). A large quantity of moderate to excellent quality, colorless to pale yellow zircon with variable morphologies was recovered. Three strongly abraded fractions of zircon, each of a different morphology, were analyzed (Fig. 2.4). Most zircon grains in all fractions contained very minor colorless to pale brown rod- and bubble-shaped inclusions. Fractions A and B are concordant with $^{206}Pb/^{238}U$ ages of 97.1 ± 0.2 Ma and 96.9 ± 0.3 Ma, respectively. Based on these two fractions, a crystallization age of 96.9 ± 0.4 Ma is assigned. Fraction C was also concordant, but with a slightly younger $^{206}Pb/^{238}U$ age (95.4 ± 0.2 Ma). This fraction is interpreted to have suffered minor post-crystallization Pb loss.

7. Caesar Lakes pluton (99-SH-013): This sample of fine-grained biotite granite was collected from near the southern end of the pluton (Fig. 2.3). A moderate amount of variable quality zircon and a small amount of monazite was recovered. Three fractions of unabraded zircon and one fraction of monazite were analyzed. Zircon fractions F and H, which consisted of square prisms with abundant colorless to dark bubble-shaped inclusions and rod-shaped inclusions parallel to the c-axis of the zircons, yielded discordant results (Fig. 2.4). Fraction I also contained abundant inclusions but zircons grains were very elongate with length to width ratios of 5 to 15 and was only slightly discordant. The one fraction of monazite (M4) consisted of three yellow, inclusion free, euhedral grains and plots above concordia with a $^{207}Pb/^{235}U$ age of 97.1 ± 0.5 Ma. The three zircon fractions plot slightly below concordia and yield non-overlapping Pb/Pb ages, indicating the presence of small amounts of inherited zircon in each fraction. The monazite age (97.1 ± 0.5 Ma) is taken as the best estimate for a crystallization age of this sample.

8. Tuna stock (99-SH-016): This sample of fine- to medium-grained biotite monzogranite was collected in the vicinity of the porphyry style Tuna mineral occurrence (Minfile # 105H 082)(Fig. 2.3). Abundant monazite of good quality was recovered. Four fractions of the coarsest, clearest euhedral grains were analyzed. All fractions (M3 – M6) plot together on or slightly above concordia (Fig. 2.4). A crystallization age of 97.1 ± 2.0 Ma is assigned based on the total range of $^{207}Pb/^{235}U$ ages from all results.

9. *Mulholland pluton (98-HAS-06)*: This sample is a hornblende biotite granodiorite containing K-feldspar megacrysts up to 3cm. The sample was collected on surface from the Mulholland pluton located in the northeast portion of the study area (Fig. 2.3). Abundant clear, colorless to pale brown, stubby to elongate prismatic zircon was recovered. Three fractions were analyzed (Fig. 2.4). Fraction A consisted of strongly abraded, coarse (> 134 μm) elongate prisms that contained abundant fractures and rod-shaped inclusions parallel to the c-axis of the zircons. A crystallization age of 97.7 ± 0.2 Ma is assigned based on the concordant analyses for this fraction. Fraction C was also composed of elongate prisms but was not abraded. This fraction was discordant and likely reflects post-crystallization Pb loss. Fraction B was discordant and is interpreted to contain an inherited, older component as 'cryptic' cores that could not be distinguished visually.

10. *Rudi pluton (98-Z-C-028):* This sample is a medium-grained biotite monzogranite collected on surface from the northernmost intrusion sampled in this study (Fig. 2.3). A small amount of good quality monazite was recovered. Three fractions of the coarsest grains, with the fewest bubble-shaped inclusions, and analyzed. Fractions M2, M3, and M4 yielded very similar, concordant results (Fig. 2.4). A crystallization age of 98.0 ± 1.2 Ma is given based on the $^{207}Pb/^{235}U$ ages of all three fractions.

11. *Patterson stock (98-HAS-12):* This sample is a fine-grained biotite granodiorite from the south-easternmost intrusion in the study area (Fig. 2.3). The sample was collected from one of many small, scattered exposures of this body. A small amount of zircon of poor to moderate quality was recovered. Four fractions of different morphologies were moderately abraded and analyzed. Fraction B (elongate prisms) and fraction D (multi-faceted equant prisms) were discordant, and although no cores were observed, the fractions are interpreted to have contained an older, inherited components (Fig. 2.4). Fraction A consisted of several colorless, clear, inclusion-free flat tabular grains and plots just off concordia. Fraction C was composed of coarse fragments of elongate prisms and contained abundant fractures and bubble- and rod-shaped inclusions that occurred proximal to or parallel to the c-axis of the zircons. Fraction C is concordant and a crystallization age of 97.5 ± 0.3 Ma is assigned for the sample based on the $^{206}Pb/^{238}U$ age of this fraction.

12. *Felsic dyke, near Patterson stock (98-HAS-12a):* This sample is a biotite-plagioclase porphyritic dyke collected close to the previous sample (Fig. 2.3). A moderate amount of good quality monazite was recovered and two fractions were analyzed. Both fractions consisted of several yellow, clear, euhedral (tabular) monazite grains that were virtually inclusion free. The total range of $^{207}Pb/^{235}U$ ages for the fractions is 98.3 ± 1.6 Ma (Fig. 2.4), which is interpreted as the crystallization age of the dyke.

13. *Shannon Creek pluton (99-SH-001):* This sample is a weakly foliated, medium-grained biotite granodiorite (Fig. 2.3). Abundant zircon of variable quality and morphology was recovered, and five strongly abraded fractions were analyzed. Fraction B was concordant with a $^{206}Pb/^{238}U$ age of 97.0 ± 0.2 Ma which is interpreted as the crystallization age. The remaining fractions DA, DB, C, and AA returned discordant results reflecting variable amounts of Pb loss and inheritance.

14. Mt. Appler pluton (98-HAS-02): This sample is a medium-grained biotite monzogranite and was collected at the northern end of the field area (Fig. 2.3). Moderately abundant colorless to pale brown, stubby to elongate prismatic zircon was recovered. Two moderately abraded fractions (D and F) and one unabraded fraction (E) were analyzed and all returned discordant results (Fig. 2.4).

Abundant good quality monazite was also recovered. Five fractions of the best quality grains were analyzed. Fractions M2 and M10 overlap concordia and the remaining fractions (M1, M7, and M8) plot slightly above concordia indicating the presence of excess ^{206}Pb (Fig. 2.4). The $^{207}Pb/^{235}U$ ages of all fractions are within error of each other. A crystallization age of 94.5 ± 0.9 Ma is reported based on the weighted average of all $^{207}Pb/^{235}U$ ages.

15. McLeod pluton (98-HAS-14): This sample is a medium-grained biotite monzogranite with K-feldspar phenocrysts up to 15 mm. It was collected from one of the most easterly intrusions in the study area (Fig. 2.3). A large quantity of colorless to pale brown, stubby to elongate prismatic zircon of variable quality was recovered. Three fractions of zircon were strongly abraded and analyzed. Two fractions (A and B) consisted of elongate grains with inclusions and fractures parallel to the c-axis. The finer fraction (B) was concordant and fraction A was slightly discordant (Fig. 2.4). Fraction C was composed of several clear, colorless tabular grains and also returned slightly discordant results. A crystallization age of 93.9 ± 0.2 Ma is assigned based on the $^{206}Pb/^{238}U$ age of the concordant zircon fraction B. Minor angular fragments of clear, pale to medium honey brown titanite were recovered from a more magnetic separate. One unabraded titanite fraction (T1) yields a concordant (albeit imprecise) analysis with a $^{206}Pb/^{238}U$ age of 92.8 $\pm$ 0.2 Ma. The slightly younger age for the titanite likely reflects minor post-crystallization Pb loss.

16. Big Charlie pluton (99-SH-011): This sample is a fine- to medium-grained biotite monzogranite with K-feldspar megacrysts up to 2.5 cm. The sample was collected from the southeastern region of the study area (Fig. 2.3). Abundant zircon of variable quality was recovered and four fractions were strongly abraded and analyzed. Fraction AA was composed of colorless, elongate, square prisms and yielded a concordant analysis (Fig. 2.4) with a crystallization age of 91.0 ± 0.3 Ma. This is interpreted to give the crystallization age of the sample. The remaining fractions AB, B, and CA were discordant, reflecting an inherited component in each fraction.

Discussion

U-Pb results presented here provide a temporal framework for mid-Cretaceous magmatism throughout the study area. The same 'inboard younging' pattern of magmatism recognized in the northern and western portion of the TGP (Mortensen et al., 2000) is evident in the study area. Four samples from the easternmost Mt. Billings Batholith returned the oldest ages, ranging from ~107 to ~100 Ma, and are correlated with the Anvil plutonic suite (Fig. 2.5).

Samples from intrusions to the north and east of the Mt. Billings Batholith, including the Coal River Batholith, the Tuna Stock, and the Mulholland and Rudi plutons, all return ages <100 Ma. The majority of ages are between ~99 and ~95 Ma, the range of ages that characterizes the coeval Tay River and Tungsten plutonic suites as recognized further north. None of the samples dated in this study are strongly peraluminous or contain both biotite and muscovite, which are characteristics that typify Tungsten suite intrusions. These intrusions are therefore considered part of the Tay River suite (Fig. 2.5). No Tungsten suite intrusions have been identified south of the Cantung mine area thus far.

Among the easternmost intrusions, samples from the Mt. Appler, McLeod, and Big Charlie plutons yielded ages 94.5 ± 0.9 Ma, 93.9 ± 0.2 Ma, and 91.0 ± 0.3 Ma respectively (Fig.

2.5). The relatively young ages correlate with the Tombstone plutonic suite to the northwest (~94 to ~89 Ma) and indicate that the Tombstone plutonic suite, or at least Tombstone age equivalent magmatism, extends into this portion of the Selwyn Basin.

Lithogeochemistry

Major, trace and rare earth element (REE) geochemistry was employed to characterize the composition of mid-Cretaceous plutonic rocks in the study area and to aid in the interpretation of the paleotectonic setting in which the magmatism occurred.

Analytical Techniques

A total of thirty-seven samples were analyzed for their major, trace, and rare earth element (REE) concentrations. Samples were collected from surface exposures at locations shown in Figure 2.6. UTM coordinates, the name of the intrusive body sampled, plutonic suite associations, and brief lithologic descriptions are provided in Table 2.3.

To avoid the effects of surficial processes, weathered surfaces were removed using a rock saw. Samples were then crushed and powdered using a standard jaw crusher and a tungsten carbide ring mill at ALS Chemex Labs Ltd. in North Vancouver, British Columbia. All major, trace and REE analyses were done at ALS Chemex Labs Ltd. in North Vancouver, British Columbia. X-ray fluorescence (XRF) was used for determining major element concentrations and inductively coupled plasma emission mass spectrometry (ICP-MS) methods were used to determine trace and REE concentrations. Replicate analyses of two in-house whole rock standards were used to evaluate analytical precision and accuracy (see Appendix 1). The results, as well as pertinent major and trace element ratios are presented in Table 2.4.

Results

Intrusive rock units in the study area show a limited lithological and mineralogical range, and have been subdivided into specific plutonic suites based largely on the results of geochronology. The results of major element analyses indicate that the intrusions are dominantly granitic and granodioritic in composition with subordinate diorite (Fig. 2.7). Diorite occurs as porphyritic satellite dykes and areally restricted marginal phases and does not form volumetrically significant intrusive phases. The high-K calc-alkaline intrusions have mixed I- and S-type characteristics (Irvine and Baragar, 1971; Le Maitre et al., 1989). Using the classification scheme proposed by Frost et al. (2001; Figure 2.8), with the exception of a few samples with the highest SiO_2 concentrations (Fig. 2.8 A), samples from all three plutonic suites in the study area plot as 'magnesian' or Cordilleran (versus 'ferroan' or A-type) and range from calc-alkalic to alkali-calcic (Fig. 2.8 B). The Anvil Plutonic suite (APS) and Tay River Plutonic suite (TRPS) intrusions are weakly to strongly peraluminous whereas the younger Tombstone Plutonic suite (TPS) intrusions cluster on or very near the metaluminous-peraluminous boundary (Fig. 2.8 C). Major element mobility is considered negligible with the exception of several weakly altered and mineralized samples (e.g. SH-005, SH-008, SH-024, and SH-028a) that account for nearly all scatter observed within the data.

Primitive mantle normalized REE plots (Fig. 2.9 A-C) are virtually identical for all three plutonic suites, displaying steep profiles with negative Nb, Eu, and Ti anomalies (Table 2.4). APS intrusions have La_N/Yb_N values from 4.25 to 18.70 and Eu/Eu* values from 0.05 to 0.84, TRPS intrusions have La_N/Yb_N values from 5.47 to 29.17 and Eu/Eu* values from 0.29 to 0.96, and TPS intrusions have La_N/Yb_N values from 13.00 to 44.18 and Eu/Eu* values from 0.48 to 0.75. Although there is significant overlap between these ranges, the TPS intrusions show more pronounced LREE-enrichment and less prominent Eu anomalies (Fig. 2.9-D). The observed increase in overall REE abundance with decreasing age (APS > TRPS > TPS) also correlates with a general increase from ~700° to ~800°C in calculated zircon saturation temperatures (Table 2.4; Watson and Harrison, 1983).

Discussion

The LREE-enrichment (high La_N/Yb_N values) and negative Nb, Ti and Eu anomalies (Table 2.4 and Fig. 2.9) are characteristics typically ascribed to I-type volcanic arc or subduction-related granitoids (Whalen et al., 1994; Jenner, 1996; Christiansen and Keith, 1996; Morris et al., 2000). More recently however, this same "subduction signature" has been attributed to the partial melting of material previously formed in subduction settings, such as immature sedimentary rocks derived from a continental magmatic arc (e.g., Keskin et al.,1998; Selby et al., 1999; Morris et al., 2000). In such cases, it has been argued that the "subduction signature" is actually inherited from the source rocks that were partially melted.

Immobile trace and REE concentrations have been commonly used to discriminate between tectonic settings for granitic rocks. The results from this study are plotted on Rb versus Yb+Ta, Ta versus Yb, Nb versus Y, and Rb versus Y+Nb discriminant plots of Pearce et al. (1984), as well as the Hf – Rb/10 – Ta*3 and Hf – Rb/30 – Ta*3 discriminant plots of Harris et al. (1986) (Figs. 2.10 A through F). The intrusions display a shared affinity between the 'volcanic arc', 'syn-collisional', and 'within-plate' fields on the discriminant plots of Pearce et al. (1984), plotting on or very near the boundaries between these fields (Fig. 2.10 A to D). On the tectonic discriminant plots of Harris et al. (1986), the intrusions plot entirely within the 'within-plate' and 'late/post-collisional' fields (Fig. 2.10 E and F). Despite these ambiguities, the results appear to indicate that these intrusions did not form in a volcanic arc setting and that they are most likely related to a collisional within-plate tectonic setting. This 'non-diagnostic' feature is common to all plutonic suites present in the field area, and has been observed previously by Lang (2000) for TPS intrusions elsewhere within the TGP, as well as by Logan

(2001) for mid-Cretaceous granitoids in the southern Canadian Cordillera that were also emplaced into the Foreland and Omineca belts.

Isotope Geochemistry

Strontium, neodymium, and lead isotopic studies of the intrusive suites were undertaken to further characterize their composition and possible origin. These data provide insight on the nature, age, and composition of source materials and therefore help constrain the tectonic setting(s) in which this magmatism occurred.

Analytical Techniques

A subset of 20 samples was selected for Sr, Nd, and Pb isotopic study. The location of these samples are denoted with stars in Figure 2.6 and described in Table 2.3. Samples were chosen in order to provide the broadest geographical and temporal coverage of the study area.

Rb-Sr and Sm-Nd isotopic analyses were done at the Radiogenic Isotope Facility at the University of Alberta following the procedures of Creaser et al. (1997) and Holmden et al. (1997). Whole rock powders (prepared by ALS Chemex) were analysed for Rb, Sr, Sm, Nd isotopic compositions and concentrations using isotopic dilution mass spectrometry. Analytical results and errors at the 2σ level are reported in Table 2.5.

Pb isotope geochemistry, including sample preparation, geochemical separations and isotopic measurements were done at the PCIGR at the University of British Columbia. Clean feldspar mineral separates were handpicked, ground and sieved to obtain a 100 – 200 mesh size fraction. The clean plagioclase separates were first leached in dilute HCl, then in a mixture of dilute Hf and HBr, and subsequently dissolved in concentrated Hf. Separation and purification of Pb employed ion exchange column techniques. Samples were converted to bromide, the solution was passed through ion exchange columns in HBr and the lead was eluted in 6N HCl.

The total procedural blank on the trace lead chemistry was 100-110 pg. Approximately 10-25 ng of the lead in chloride form was loaded onto a rhenium filament using a phosphoric acid-silica gel emitter, and isotopic compositions were determined on a Faraday collector in peak-switching mode using a modified VG54R thermal ionization mass spectrometer. The measured ratios were corrected for instrumental mass fractionation of 0.12% per mass unit based on repeated measurements of the N.B.S. SRM 981 Standard Isotopic Reference Material and the values recommended by Thirwall (2000). Mass fractionation and analytical errors were numerically propagated throughout all calculations and are presented at the 2σ level with results in Table 2.6.

Sr and Nd Isotope Results

Initial $^{87}Sr/^{86}Sr$ and epsilon Nd (εNd) values were corrected for an age of 100 Ma and range from 0.70853 to 0.72243 and from –6.0 to –17.5 respectively (Table 2.5). Sr and Nd results are shown plotted against silica content (Fig. 2.11 A and B) and against each other (Fig. 2.11 C). All of the intrusions have initial $^{87}Sr/^{86}Sr$ and εNd values that indicate dominantly crustal source rocks for these magmas. Nd and Sr values show a progressive shift across the study area. The lowest εNd values (~ -17.0) and corresponding high initial $^{87}Sr/^{86}Sr$ (~ 0.720) occur in the northwest portion of the field area. Moving to the southeast, the isotopic compositions shift toward the 'least-evolved' values, with the highest εNd values (~ -6.0) and corresponding low initial $^{87}Sr/^{86}Sr$ (~ 0.708).

Depleted mantle model ages (T_{DM}) after Goldstein et al. (1984) range from 1.36 to 2.72 Ga with an average of 1.77 Ga (Table 2.5). Fifteen out of the seventeen samples yield Mesoproterozoic ages between 1.36 and 1.96 Ga. The remaining two samples (SH-011E from the Mt. Billings Batholith and 98-Z-C028 from the Rudi Pluton) have significantly higher $^{147}Sm/^{144}Nd$ ratios and produce Archean model ages of 2.65 and 2.72 Ga, respectively.

Pb Isotope Results

All three plutonic suites have very similar and highly radiogenic Pb isotope compositions. Collectively, the $^{206}Pb/^{204}Pb$ ratios range from 19.397 to 19.772, the $^{207}Pb/^{204}Pb$ ratios range from 15.697 to 15.829, the $^{208}Pb/^{204}Pb$ ratios range from 39.461 to 39.883, the $^{207}Pb/^{206}Pb$ ratios range from 0.79962 to 0.81076, and the $^{208}Pb/^{206}Pb$ ratios range from 2.01221 to 2.03658. The results are plotted with reference to the upper-crustal Pb evolution model (Shale Curve) of Godwin and Sinclair (1982) (Fig. 2.12 A – C). The Shale Curve is of particular relevance to this study as it is based on the Pb isotope compositions of shale-hosted Zn-Pb deposits located within the Canadian Cordillera miogeocline and is interpreted to reflect the Pb isotopic evolution of average upper crustal Pb within the miogeocline.

Discussion

The observed spatial trends in isotopic data mirror the results of Lang (2000), who studied mid-Cretaceous plutons to the northwest of the study area. The remarkable constancy of major and trace element data suggest that isotopic variation does not reflect differences in the proportions of source components but instead reflect distinct isotopic differences of the underlying continental crust (Pitcher, 1997; Lang, 2000). The location of the strongly peraluminous two-mica WPS (Fig. 2.5) coincides with the most evolved isotopic signatures.

Nature of Magma Sources

The high initial $^{87}Sr/^{86}Sr$, low εNd, relatively radiogenic Pb isotopic compositions, Mesoproterozoic to Archean T_{DM} ages, and the common presence of inherited zircon of Precambrian ages indicate a dominantly crustal source for these magmas. The wide variation in Sr and Nd values with SiO_2 content excludes the possibility that these magmas formed from a single common source over time (Figs. 2.11 A and B). The curvilinear array on the εNd versus initial $^{87}Sr/^{86}Sr$ plot (Fig. 2.11 C) is characteristic of magmas generated by the mixing of two compositionally and isotopically distinct magmas and/or the assimilation of ancient crustal material by mantle-derived magmas (DePaolo et al., 1992). The absence of field evidence for magma mixing or mingling is supportive of the latter, however, no samples with primitive isotopic signatures were identified during the course of this study, nor have they been previously documented in the study area or elsewhere in this region. This information points toward the possibility of an entirely crustal derivation for these intrusions; however, the involvement of at least a minor isotopically juvenile or mantle-derived contribution cannot be completely ruled out.

The Sm-Nd characteristics of rocks that both host and underlie southeastern TGP intrusions have been documented from a variety of sedimentary provenance studies (Ross et al., 1997; Creaser and Erdmer, 1997; Garzione et al., 1997; Ross et al., 2001) and from limited dating and isotopic studies of the Paleoproterozoic crystalline rocks of the Fort Simpson arc (Villeneuve and Theriault, 1991). In light of these data, a significant contribution of lower crustal rocks (e.g., Muskwa Assemblage, Ross 1999 and Nahanni Terrane, Villeneuve and Theriault, 1991), with average εNd_{100} values of ~ -25, cannot account for the higher εNd values (-10 to -6) observed in the plutonic suites without contribution of a significant isotopically primitive component. Mafic volcanic rocks do occur within the Proterozoic stratigraphy of the Selwyn Basin but are volumetrically minor (at least at the present level of exposure) and therefore are unlikely to have formed a significant contribution to these magmas. This suggests one of two possibilities: first, that the intrusions are mainly of middle to upper crustal origin, where the range of εNd values more closely resembles those of the intrusions; or secondly, that mantle-derived magmas were extensively contaminated by a component of crustal material and have either not yet been identified or did not reach the present level of exposure.

Unlike the wide range of Nd and Sr compositions, lead isotopic compositions of the plutons in the study area show relatively minor variation (Fig. 2.12), suggesting that these magmas were derived from a homogenous Pb isotopic reservoir, or from multiple reservoirs that were well homogenized over time. The elevated $^{207}Pb/^{204}Pb$ ratios are indicative of rocks of old upper crustal origin (Tosdal, 1999) with high time-integrated U/Pb ratios that are similar to, and higher than those used in the Shale Curve model (μ = 12.16). Feldspar lead isotopic compositions from mid-Cretaceous intrusions measured in this study are among the most radiogenic signatures recognized from mid-Cretaceous intrusions in the northern Cordillera thus far (Fig. 2.13). In general, these data are consistent with the Pb in these magmas having been derived entirely from partial melting of model upper crustal rocks or from mantle derived melts that have been extensively contaminated by, and well homogenized with significant upper crustal material.

Crustal residence ages (T_{DM}) provide a qualitative approach to constraining the age(s) of source materials for magmas. The positive correlation between T_{DM} and εNd suggests that differences may be in part related to the ages of source materials. The dominantly Mesoproterozoic model ages (1.36 to 1.96 Ga) overlap with those reported from sedimentary rocks of the northern Cordillera miogeocline, and in particular, Paleozoic rocks of the Selwyn Basin (Garzione et al., 1997). The two Archean model ages (2.65 and 2.72 Ga) are from intrusions on the western side of the study area and more closely resemble the model ages of Proterozoic miogeoclinal sedimentary rocks (Garzione et al., 1997; Ross et al., 2001) and inferred crystalline basement (?) rocks of the Nahanni Terrane (Villeneuve and Theriault, 1991).

The presence of abundant inherited and/or xenocrystic zircon further substantiates the derivation of these magmas from crustal or crustally contaminated sources. Several samples (e.g., 99SH-023, 98-HAS-02, 98-HAS-12) consistently yield calculated upper intercept ages between ~1.8 and ~1.9 Ga (see earlier discussion). Another sample (99SH-001) gives an older, albeit poorly constrained, upper intercept age of 2.12 Ga. This range of ages is consistent with ca. 1850 Ma magmatism in the contemporaneous Fort Simpson and Great Bear magmatic arcs (Hoffman and Bowring, 1984; Villenueve and Theriault, 1991; Cook et al., 1999). However provenance studies report detrital zircons of this age in miogeoclinal sedimentary rocks throughout the entire Canadian Cordillera, from Mesoproterozoic (Ross et al., 2001) through to Mesozoic (Boghossian et al., 1996) times. As such, the ~1.8 to ~1.9 Ga inherited zircon component offers little intra-crustal constraint on the source of isotopically evolved materials in these magmas other than to confirm its presence.

Tectonic Setting of mid-Cretaceous Magmatism

The spatial and geochemical characteristics of the ~112 to ~99 Ma plutonic suites are consistent with magmatism in a southwest facing magmatic arc and back-arc region, respectively represented by the WCCS and the APS and CPS suites (Mortensen et al., 2000). Assessment of the tectonic setting within which younger (~99 to ~89 Ma) TRPS, WPS, and TPS magmatism occurred is more problematic. The contribution, if any, from a subduction-related source is unclear because the geochemical and isotopic systematics are consistent with a largely crustal origin (Mortensen et al., 2000; Driver et al., 2000; Lang, 2000).

Common characteristics of subduction related granitic batholiths include the association with coeval mafic magmatism (Ducea, 1992) and the presence of primitive isotopic signatures, even in areas underlain by extremely thick crust (Ducea, 1992; Rollinson, 1993). All of these characteristics are noticeably absent in the plutons in the study area, although mafic and even ultramafic phases are recognized locally within the TPS further to the northwest (e.g., Lang, 2000) . This suggests that subduction may not have played a significant role in magma genesis in this region. Furthermore, the reconstruction of Plafker and Berg (1994) suggests that an arc-trench gap between ~500 and ~700 km would have existed in mid-Cretaceous time. This would have required an extremely low angle of subduction (between ~12° and ~8°) for which there is little evidence. Indeed the trace element characteristics (LILE- and LREE-enrichment, and negative Nb, Ti, and Eu anomalies) are the only indication that these magmas might be subduction-related (Hildreth and Moorbath, 1988; Hawkesworth et al., 1993; Christiansen and Keith, 1996). The possibility that the subduction-related trace element signature was inherited remains to be tested.

Inherent to all models of crustally derived magmatism is a mechanism by which significant heat is introduced into the crust to induce partial melting (Pitcher, 1997). Given the current knowledge of the crustal structure in the northern Cordillera and our understanding of mid-Cretaceous magmatism, three plausible scenarios can be envisaged for the initiation of crustal anatexis in the area.

The first possibility is that the intrusions formed from decompression or dehydration melting of overthickened crust depressed into the mantle, implying a purely crustal origin (Patino Douce et al., 1990; Thompson, 1999; Patino Douce, 1999), and indeed the region has been subject to significant crustal thickening in early and middle Mesozoic time (see earlier discussion). There are however volumetric concerns with this model, specifically, could dehydration melting alone account for the nearly 5000 km^2 of granitic rocks within the study area?

The other two possibilities involve the upwelling or underplating of hot asthenospheric mantle due to either crustal extension (Pitcher, 1997; Thompson, 1999) or crust/mantle delamination (Bird, 1979; Kay and Kay, 1993; Houseman and Molnar, 2001). Cretaceous and younger extension is well documented in some parts of the northern Cordillera (Tempelman-Kluit et al., 1991; Murphy, 1997; de Keijzer and Williams, 1999) and Snyder et al. (2002) suggest a mid- to lower crustal detachment if the high crustal temperatures observed today

(Lewis et al., 2002) were present during orogenic evolution. Progressive delamination from west to east could account for the younging of magmatism from west to the east.

Similar studies of mid-Cretaceous magmatism elsewhere within the TGP (Selby et al., 1999; Driver et al., 2000; Lang et al., 2000) and of granitoids emplaced within the Omineca Belt in the southern Cordillera (Brandon and Lambert, 1993; Brandon and Smith, 1994; Logan, 2001) all invoke or suggest that these intrusions were entirely derived from the continental crust due to the partial melting of overthickened crust. However none of these studies can completely preclude the involvement of a subduction-related component.

Where does the Tintina Gold Province go?

With the ~425 km of dextral displacement along the Tintina Fault restored (see Fig. 2.14), plutonic suites of the TGP are seemingly truncated to the south of the study area. Two equally plausible scenarios that may account for the apparent truncation are presented here but remain to be fully tested.

The first explanation is that the plutonic suites continue to the south in a manner similar to that outlined herein (i.e., linear and non-overlapping suites) and are simply not exposed at current levels of erosion. Mineral deposits such as the Sa Dena Hes Zn-Pb-Ag skarn, and replacement deposits such as Quartz Lake (Pb, Zn, Ag) and Hyland (Au, Ba) are known to be associated with small volumes of felsic intrusives. These mineral deposits are all thought to be genetically related to buried intrusions of presumably mid-Cretaceous age although none have been dated directly. Indirect dating of mineralization from the past-producing Sa Dena Hes skarn indicate a mid-Cretaceous age (see Chapter 3). Geophysical evidence (e.g., regional aeromag surveys) for large volumes of buried intrusions to the south of the study area is uncertain and requires further investigation.

Alternatively, it is possible that the plutonic suites coalesce, swinging to the southwest around the basement promontory roughly demarcated by the location of the Liard Line (Fig. 2.14). If so, this scenario further emphasizes the strong control that the geometry of the latest Proterozoic rifting had on the distribution of Paleozoic sedimentation, Mesozoic deformation and suggests direct links to the genesis of TGP magmatism. Geochronologic, geochemical and isotopic data from the region is insufficient to permit comparison with currently exposed intrusions that may represent the southward continuation of the TGP.

Conclusions

The primary goal of this study was to investigate the southeastern extent of plutonic suites within the TGP. The combination of geochronological and geochemical data indicates that the known plutonic suites of the western and northern portions of the TGP do continue into southeastern Yukon and southwestern Northwest Territories. Within the study area, APS magmatism is for the most part limited to the westernmost Mt. Billings Batholith. The majority of intrusions, including the large Coal River and Hole-in-the-Wall batholiths, are considered part of the TRPS. The strongly peraluminous two-mica WPS does not appear to extend south of the Cantung area. The WPS suite seems restricted to a region that shows the most evolved isotopic signatures suggesting a direct correlation with the nature of the underlying basement rocks. The economically significant TPS continues to the extreme southeast, including the Big Charlie and McLeod plutons, appearing to occur discontinuously along the eastern limits of the belt.

Without contemporaneous mafic volcanism, it is difficult to conclusively identify the paleotectonic setting of mid-Cretaceous magmatism. However the data presented here provide some insight into the nature of the tectonic setting. Any tectonic model developed for the region must account for the following salient features: 1) trace element signatures consistent with volcanic arc or subduction-related magmatism; 2) the decidedly crustal isotopic signatures, including the highly variable Sr and Nd, and restricted Pb compositions; and 3) the progressive decrease in age from west to east that is now recognized over an incredible strike length (>1000 km).

References

Anderson, R.G. 1983. Selwyn plutonic suite and its relationship to tungsten mineralization, southeastern Yukon and District of Mackenzie. Canada Geological Survey, Current Research Paper 83-1B: 151-163.

Anderson, R.G. 1987. Plutonic rocks in the Dawson map area, Yukon Territory. Canada Geological Survey, Current Research Paper 87-1A: 689-697.

Anderson, R.G. 1988. An overview of some Mesozoic and Tertiary plutonic suites and their associated mineralization in the northern Canadian Cordillera. Canadian Institute of Mining and Metallurgy Special Volume **39:** 96-113.

Aitken, J.D. and McMechan, M.E. 1991. Middle Proterozoic assemblages, Chapter 5. *In:* Gabrielse, H. and Yorath, C.J. (eds.); Geology of the Cordilleran Orogen in Canada, Geological Survey of Canada, no. 4: 97-124.

Bird, P. 1979. Continental delamination and the Colorado Plateau. Journal of Geophysical Research **84:** 7561-7571.

Boghossian, N.D., Patchett, P.J., Ross, G.M. and Gehrels, G.E. 1996. Nd isotopes and the source of sediments in the miogeocline of the Canadian Cordillera. Journal of Geology **104:** 259-277.

Brandon, A.D. and Lambert, R.St.J. 1993. Geochemical characterization of mid-Cretaceous granitoids of the Kootenay Arc in the southern Canadian Cordillera. Canadian Journal of Earth Sciences **30:** 1076-1090.

Brandon, A.D. and Smith, A.D. 1994. Mesozoic granitoid magmatism in southeast British Columbia: Implications for the origin of granitoid belts in the North American Cordillera. Journal of Geophysical Research **99:** 11879-11896.

Cecile, M.P., Morrow, D.W. and Williams, G.K. 1997. Early Paleozoic (Cambrian to Early Devonian) tectonic framework, Canadian Cordillera. Bulletin of Canadian Petroleum Geology **45:** 54-74.

Christiansen, E.H. and Keith, J.D. 1996. Trace element systematics in silicic magmas: a metallogenic perspective. *In:* Wyman, D.A. (ed.), Trace element geochemistry of volcanic rocks: Applications for massive sulphide exploration: Geological Association of Canada, Short Course Notes **12:** 51-77.

Cook, F.A., van der Velden, A.J. and Hall, K.W. 1999. Frozen subduction in Canada's Northwest Territories: Lithoprobe deep lithospheric reflection profiling of the western Canada Shield. Tectonics **18:** 1-24.

Creaser, R.A. and Erdmer, P. 1997. Mixed signals from the Mioegeocline: Geochemical and Nd isotopic constraints from the Selwyn Basin. *In:* Cook, F. and Erdmer, P. (compilers); Slave-Northern Cordillera Lithospheric Evolution (SNORCLE) and Cordilleran Tectonics Workshop (March 7-9), University of Calgary, Lithoprobe Report No. 56, p.74-75.

Creaser, R.A., Erdmer, P., Stevens, R.A. Grant, S.L., 1997. Tectonic affinity of Nisutlin and Anvil assemblage strata from the Teslin tectonic zone, northern Canadian Cordillera: Constraints from neodymium and geochemical evidence. Tectonics **16:** 107-121.

De Keijzer, M. and Williams, P.F. 1999. Cretaceous extension and regional calcic metasomatism in the south of the d'Abbadie pluton, south-central Yukon. *In:* Cook, F. and Erdmer, P. compilers); Slave-Northern Cordillera Lithospheric Evolution (SNORCLE) and Cordilleran Tectonics Workshop (March 5-7), University of Calgary, Lithoprobe Report No. 69, p.122-129.

DePaolo, D.J., Perry, F.V. and Baldridge, W.S. 1992. Crustal versus mantle sources of granitic magmas: A two-parameter model based on Nd isotopic studies. *In:* Brown , P.E. and Chappel, B.W. (eds.), Second Hutton Symposium on the Origin of Granites and Related Rocks, Geological Society of America Special Paper 272, p.439-446.

Driver, L.A., Creaser, R.A., Chacko, T. and Erdmer, P. 2000. Petrogenesis of the Cretaceous Cassiar batholith, Yukon-British Columbia, Canada: Implications for magmatism in the North American Cordilleran Interior. Geological Society of America Bulletin **112:** 1119-1133.

Ducea, M. 2001. The California Arc: Thick granitic batholiths, eclogitic residues, lithosphere-scale thrusting, and magmatic flare-ups. GSA Today **11:** 4-10

Frost, B.R, Barnes, C.G., Collins, W.J., Arculus, R.J., Ellis, D.J. and Frost, C.D. 2001. A geochemical classification for granitic rocks. Journal of Petrology **42:** 2033-2048.

Gabrielse, H. and Yorath, C.J. 1991. Tectonic synthesis, Chapter 18. *In:* Gabrielse, H. and Yorath, C.J. (eds.); Geology of the Cordilleran Orogen in Canada, Geological Survey of Canada, no. 4: 677-705.

Gabrielse, H. and Yorath, C.J. 1991. Outstanding problems, Chapter 22. *In:* Gabrielse, H. and Yorath, C.J. (eds.); Geology of the Cordilleran Orogen in Canada, Geological Survey of Canada, no. 4: 819-823.

Gabrielse, H., Monger, J.W.H., Wheeler, J.O. and Yorath, C.J. 1991. *In:* Gabrielse, H. and Yorath, C.J. (eds.); Tectonic framework, Chapter 2. Geology of the Cordilleran Orogen in Canada, Geological Survey of Canada, no. 4: 15-28.

Garzione, C.N., Patchett, P.J., Ross, G.M. and Nelson, J. 1997. Provenance of Paleozoic sedimentary rocks in the Canadian Cordilleran miogeocline: a Nd isotopic study. Canadian Journal of Earth Sciences **34:** 1603-1618.

Godwin, C.I. and Sinclair, A.J. 1982. Average lead isotope growth curves for shale-hosted zinc-lead deposits, Canadian Cordillera. Economic Geology **77:** 208-211.

Goldstein, S.L., Onion, R.K. and Hamilton, P.J. 1984. A Sm-Nd study of atmospheric dusts and particulates from major river systems. Earth and Planetary Science Letters **70:** 221-236.

Gordey, S.P. and Anderson, R.G. 1993. Evolution of the northern Cordillera Miogeocline, Nahanni Map Area (105I), Yukon and Northwest Territories. Geological Survey of Canada Memoir 428, 214 p.

Gordey, S.P. and Makepeace, A.J. 1999. Yukon Digital Geology, S.P. Gordey and A.J. Makepeace (comp.); Geological Survey of Canada, Open File D3826, and Exploration and Geological Services Division, Yukon, Indian and Northern Affairs Canada, Open File 1999-1(D).

Gordey, S.P. 1988. The South Fork Volcanics: mid-Cretaceous caldera fill tuffs in east-central Yukon. Current Research, Part E, Geological Survey of Canada, Paper 88-1E: 13-18.

Green, T.H. 1995. Significance of Nb/Ta as an indicator of geochemical processes in the crust-mantle system. Chemical Geology **120:** 347-359.

Hawkesworth, C.J., Gallagher, K., Hergt, J.M. and McDermott, F. 1993. Mantle and slab contributions in arc magmas. Annual Reviews of Earth and Planetary Science **21:** 175-204.

Hoffman, P.F. and Bowring, S.A. 1984. Short-lived 1.9 Ga continental margin and its destruction, Wopmay orogen, northwest Canada. Geology **12:** 68-72.

Houseman, G. and Molnar, P. 2001. Mechanisms of lithospheric rejuvenation associated with continental orogeny. *In:* Miller, J.A., Holdsworth, R.E., Buick, I.S. and Hand, M. (eds.), Continental Reactivation and Reworking, Geological Society, London, Special Publications **184:** 13-38.

Harris, N.B.W., Pearce, J.A. and Tindle, A.G. 1986. Geochemical characteristics of collision-zone magmatism. *In:* Coward, M.P. and Reis, A.C. (eds.), Collision Tectonics, Geological Society, Special Publication **19:** 67-81.

Hildreth, W. and Moorbath, S. 1988. Crustal contributions to arc magmatism in the Andes of central Chile. Contributions to Mineralogy and Petrology **98:** 455-489.

Irvine, T.N. and Baragar, W.R.A. 1971. A guide to the chemical classification of the common volcanic rocks. Canadian Journal of Earth Sciences **8:** 523-548.

Jenner, G.A. 1996. Trace element geochemistry of igneous rocks: geochemical nomenclature and analytical geochemistry. *In:* Wyman, D.A. (ed.), Trace element geochemistry of volcanic rocks: Applications for massive sulphide exploration: Geological Association of Canada, Short Course Notes **12:** 51-77.

Joyce, N.L. (née M[ac]Donald), 2002. Geologic setting , nature, and structural evolution of intrusion-hosted Au-bearing quartz veins at the Longline occurrence, Moosehorn Range area, west-central Yukon Territory. Unpublished Master's thesis, University of British Columbia, 196 p.

Kay, R.W. and Mahlburg Kay, S. 1993. Delamination and delamination magmatism. Tectonophysics **219:** 177-189.

Keskin, M., Pearce, J.A. and Mitchell, J.G. 1998. Volcano-stratigraphy and geochemistry of collision-related volcanism on the Erzurum-Kars Plateau, northeastern Turkey. Journal of Volcanology and Geothermal Research **85:** 355-404.

Krogh, T.E. 1982. Improved accuracy of U-Pb zircon ages by the creation of more concordant systems using an air abrasion technique. Geochimica et Cosmochimica Acta **46:** 637-649.

Lang, J.R., Thompson, J.F., Mortensen, J.K., Baker, C.J.R., Coulsen, I.M., Duncan, R. and Maloof, T. 2001. Tombstone-Tungsten Belt. *In:* Lang, J. (ed.), Regional and System-scale controls on the formation of copper and/or gold magmatic-hydrothermal mineralization. Mineral Deposit research Unit, Special Publication Number 2, January 2001, 115p.

Le Bas, M.J., Le Maitre, R.W., Streckeisen, A. and Zanettin, B. 1986. A chemical classification of volcanic rocks based on the total alkali-silica diagram. Journal of Petrology **27:** 745-750.

Le Maitre, R.W. 1989. A classification of igneous rocks and glossary of terms. Blackwell, Oxford, 193 p.

Lewis, T., Hyndman, R.D. and Flueck, P. 2001. Thermal controls on present tectonics in the northern Canadian Cordillera. *In:* Cook, F. and Erdmer, P. (compilers); Slave-Northern Cordillera Lithospheric Evolution (SNORCLE) and Cordilleran Tectonics Workshop, Pacific Geoscience Centre, Lithoprobe Report No. 79, p.28-29.

Logan, J.M. 2001. Prospective areas for intrusion-related gold-quartz veins in southern BC. British Columbia Ministry of Energy and Mines, Paper 2001-1: 231-252.

Maniar, P.D. and Piccoli, P.M. 1989. Tectonic discrimination of granitoids. Geological Society of America Bulletin **101:** 635-643.

Miyashiro, A. 1970. Volcanic rock series in island arcs and active continental margins. American Journal of Science **274:** 321-355.

Monger, J.W.H. and Price, R.A. 1979. Geodynamic evolution of the Canadian Cordillera – progress and problems. Canadian Journal of Earth Sciences **16:** 770-791.

Morris, G.A., Larson, P.B. and Hooper, P.R. 2000. 'Subduction style' magmatism in a non-subduction setting: the Colville igneous complex, NE Washington State, USA. Journal of Petrology **41:** 43-67.

Mortensen, J.K., Hart, C.J.R., Murphy, D.C. and Heffernan, S. 2000. Temporal evolution of Early and mid-Cretaceous magmatism in the Tintina Gold Belt. *In:* The Tintina Gold Belt: Concepts, Exploration and Discoveries, British Columbia and Yukon Chamber of Mines, Special Volume 2, p. 49-58.

Murphy, D.C. 1997. Geology of the McQuesten River region, northern McQuesten and Mayo map areas, Yukon Territory. Exploration and Geological services Division, Yukon Region, Indian and Northern Affairs Canada, Bulletin 6, 95 p.

Parrish, R., Roddick, J.C., Loveridge, W.D. and Sullivan, R.W. 1987. Uranium-Lead analytical techniques at the geochronology laboratory, Geological Survey of Canada. Radiogenic Age and Isotopic Studies, Report 1, Geological Survey of Canada, Paper 87-2: 3-7.

Parrish, R. 1990. U-Pb dating of monazite and its application to geological problems. Canadian Journal of Earth Science **27:** 1431-1450.

Patino Douce, A.E. 1999. What do experiments tell us about the relative contributions of crust and mantle to the origin of granitic magmas? *In:* Castro, A., Fernandez, C. and Vigneresse, J.L. (eds.); Understanding granites: Integrating new and classical techniques, Geological Society, London, Special Publications **168:** 55-75.

Peacock, M.A. 1931. Classification of igneous rock series. Journal of Geology **39:** 54-67.

Pearce, J.A., Harris, N.B.W. and Tindle, A.G. 1984. Trace element discrimination diagrams for the tectonic interpretation of granitic rocks. Journal of Petrology **25:** 956-983.

Pigage, L.C. and Anderson, R.G., 1985. The Anvil plutonic suite, Faro, Yukon Territory. Canadian Journal of Earth Science **22:** 1204-1216.

Pitcher, W.S. 1997. The nature and origin of granite, Second Edition. Chapman and Hall, London, England, 387p.

Plafker, G. and Berg, H.C. 1994. Overview of the geology and tectonic evolution of Alaska. *In:* Plafker, G. and Berg, H.C. (eds.), The geology of Alaska: Boulder, Colorado, Geological Society of America, The geology of North America, v. G-1: 989-1021.

Roddick, J.C. 1987. Generalized numerical error analysis with application to geochronology and thermodynamics. Geochimica et Cosmochimica Acta **51:** 2129-2135.

Rollinson, H.R. 1993. Using geochemical data: evaluation, presentation, interpretation. Longman Group Limited, Essex, England, 352 p.

Ross, G.M., Villenueuve, M.E. and Theriault R.J. 2001. Isotopic provenance of the lower Muskwa assemblage (Mesoproterozoic, Rocky Mountains, British Columbia): new clues to correlation and source areas. Precambrian Research **111:** 57-77.

Ross, G.M., Gehrels, G.E. and Patchett, P.J. 1997. Provenance of Triassic strata in the Cordilleran miogeocline, western Canada. Bulletin of Canadian Petroleum Geology **45:** 461-473.

Selby, D., Creaser, R.A. and Nesbitt, B.E. 1999. Major and trace element compositions and Sr-Nd-Pb systematics of crystalline rocks from the Dawson Range, Yukon, Canada. Canadian Journal of Earth Sciences **36:** 1463-1481.

Snyder, D.B., Clowes, R.M., Cook, F.A., Erdmer, P., Evenchick, C.A., van der Velden, A.J., and Hall, K.W. 2002. Proterozoic prism arrests suspect terranes: Insights into the ancient Cordilleran margin from seismic reflection data. GSA Today **12:** 4-10.

Sun, S.S. and McDonough, W.F. 1989. Chemical and isotope systematics of oceanic basalts: implications for mantle compositions and processes. In: Saunders, A.D., Norry, M.J. (eds), Magmatism in ocean basins. Geological Society, London, Special Publications **42:** 313-345.

Tempelman-Kluit, D.J., Gabrielse, H., Evenchick, C.A., Mansy, J.L., Brown, R.L., Journeay, J.M., Lane, L.S., Struik, L.C., Murphy, D.C., Rees, C.J., Simony, P.S., Fyles, J.T., Hoy, T., Gordey, S.P., Thompson, R.I., McMechan, M.E. and Harms, T.A., 1991. Structural styles, Chapter 17; Omineca Belt. *In:* Gabrielse, H. and Yorath, C.J. (eds.); Geology of the Cordilleran Orogen in Canada, Geological Survey of Canada, no. 4: 571-675.

Thirwall, M.F. 2000. Inter-laboratory and other errors in Pb isotope analyses investigated using a ^{207}Pb-^{204}Pb double spike. Chemical Geology **163:** 299-322.

Thompson, A.B. 1999. Some time-space relationships for crustal melting and granitic intrusion at various depths. *In:* Castro, A., Fernandez, C. and Vigneresse, J.L. (eds.) Understanding granites: Integrating new and classical techniques, Geological Society, London, Special Publications **168:** 7-25.

Todt, W., Cliff, R.A., Hanser, A. and Hofman, A.W. 1996. Evaluation of a ^{202}Pb-^{205}Pb double spike for high-precision lead isotope analysis. Geophysical Monograph **95:** 429-437.

Villeneuve, M.E. and Theriault, R.J. 1991. U-Pb ages and m-Nd signature of two subsurface granites from the Fort Simpson magnetic high, northwest Canada. Canadian Journal of Earth Sciences **28:** 1003-1008.

Watson, E.B. and Harrison M.T. 1983. Zircon saturation revisited: temperature and composition effects in a variety of crustal magma types. Earth and Planetary Science Letters **64:** 295-304.

Welford, J.K, Clowes, R.M., Ellis, R.M., Spence, G.D., Asudeh, I. And Hajnal, Z. 2001. Lithospheric structure across the craton-Cordilleran transition of northeastern British Columbia. Canadian Journal of Earth Sciences **38:** 1169-1189.

Whalen, J.B., Jenner, G.A., Currie, K.L., Barr, S.M., Longstaffe, F.J. and Hegner, E. 1994. Geochemical and isotopic characteristics of granitoids of the Avalon Zone, southern New Brunswick: Possible evidence for repeated delamination events. Journal of Geology **102:** 269-282.

Wheeler, J.O. and McFeely, P. (comp.) 1991. Tectonic assemblage map of the Canadian Cordillera and adjacent parts of the United States of America. Geological Survey of Canada, Map 1712A, 1:2 000 000 scale.

Table 2.1. U-Pb Geochronology samples, intrusive bodies, locations, and rock types.

Sample Number	Intrusive Body	UTM Location*		Rock Type
1 - *99-SH-022*	Mt. Billings Batholith	6757200N	507300E	biotite granodiorite
2 - *00-SH-001*	Mt. Billings Batholith	6852852N	499996E	biotite granodiorite
3 - *SH-073*	Mt. Billings Batholith	6853027N	499680E	biotite monzogranite
4 - *SH-070*	Mt. Billings Batholith	6844586N	518400E	biotite monzogranite
5 - *99-SH-008*	Coal River Batholith	6803635N	574000E	hornblende biotite granodiorite
6 - *99-SH-006*	Coal River Batholith	6796900N	569700E	hornblende biotite granodiorite
7 - *99-SH-013*	Caesar Lakes Pluton	6799200N	559500E	biotite granodiorite
8 - *99-SH-016*	Tuna Stock	6855058N	541644E	biotite monzogranite
9 - *98-HAS-06*	Mulholland Pluton	6886772N	570080E	hornblende biotite granodiorite
10 - *98-Z-C028*	Rudi Pluton	6912513N	525353E	biotite monzogranite
11 - *98-HAS-12*	Patterson Stock	6751424N	631698E	biotite granodiorite
12 - *98-HAS-12a*	Patterson Stock	6751424N	631698E	felsic porphyry dyke
13 - *99-SH-001*	Shannon Creek Pluton	6860975N	511410E	biotite granodiorite
14 - *98-HAS-02*	Mt. Appler Pluton	6900544N	552576E	biotite monzogranite
15 - *98-HAS-14*	McLeod Pluton	6775408N	632194E	biotite monzogranite
16 - *99-SH-011*	Big Charlie Pluton	6789175N	624400E	biotite monzogranite

* NAD 27, Zone 9

Table 2.2. U-Pb analytical data for intrusive samples used in this study.

Fraction[1]	Wt. (mg)	U[2] (ppm)	Pb*[3] (ppm)	$^{206}Pb/^{204}Pb$[4]	Pb[5] (pg)	^{208}Pb[3] %	Isotopic Ratios (1σ%)[6] $^{206}Pb/^{238}U$	$^{207}Pb/^{235}U$	$^{207}Pb/^{206}Pb$	Apparent Age (2σ Ma)[6] $^{206}Pb/^{238}U$	$^{207}Pb/^{235}U$	$^{207}Pb/^{206}Pb$	Th/U
1. *Sample 99SH-022 - Mt.Billings Batholith (southern)*													
A,c,n2,el	0.032	176	3.1	1031	6	13.6	0.016881 (0.28)	0.114374 (0.52)	0.049138 (0.47)	107.9 (0.6)	110.0 (1.1)	154.4 (22.3)	0.518
B,c,n2,el	0.024	472	11	3001	5	17.0	0.021063 (0.15)	0.182404 (0.21)	0.062809 (0.13)	134.4 (0.4)	170.1 (0.7)	701.8 (5.4)	0.699
C,c,n2,sp	0.036	*	13	7550	4	5.5	0.017891 (0.12)	0.130763 (0.17)	0.053010 (0.11)	114.3 (0.3)	124.8 (0.4)	329.2 (4.9)	0.195
2. *Sample 00SH-001 - Mt.Billings Batholith (north)*													
M4,m,m,eu	0.011	1829	186	607	34	85.4	0.016363 (0.17)	0.106946 (0.43)	0.047403 (0.34)	104.6 (0.4)	103.2 (0.8)	69.5 (16.1)	19.1
M6,c,m,eu	0.017	2286	261	748	54	86.9	0.016425 (0.12)	0.107767 (0.29)	0.047587 (0.21)	105.0 (0.2)	103.9 (0.6)	78.8 (10.1)	21.8
3. *Sample SH-073 - Mt.Billings Batholith (north) - Tia Occurrence*													
M4,m,m,su	0.008	6262	374	488	105	75.5	0.016141 (0.20)	0.105621 (0.59)	0.047459 (0.52)	103.2 (0.4)	102.0 (1.1)	72.4 (25.1)	10.1
M6,m,m,su	0.011	4708	421	160	359	83.8	0.015940 (0.16)	0.103605 (0.83)	0.047140 (0.70)	101.9 (0.3)	100.1 (1.6)	56.3 (33.7)	17.0
4. *Sample SH-070 - Mt.Billings Batholith (north) - Cali Occurrence*													
M4,c,m,sp	0.010	4643	250	174	306	72.1	0.016516 (0.16)	0.110348 (0.81)	0.048458 (0.69)	105.6 (0.3)	106.3 (1.6)	121.7 (32.8)	8.5
M5,m,m,sp	0.008	4969	203	702	58	63.4	0.016390 (0.10)	0.108521 (0.28)	0.048021 (0.19)	104.8 (0.2)	104.6 (0.5)	100.3 (9.2)	5.7
M6,c,m,sp	0.009	2963	220	463	61	79.9	0.016435 (0.17)	0.108321 (0.38)	0.047802 (0.27)	105.1 (0.3)	104.4 (0.8)	89.5 (13.0)	13
5. *Sample 99SH-008 - Coal River Batholith*													
B,m,n2,ta	0.032	277	4.4	1325	6	15.4	0.014942 (0.15)	0.098645 (0.35)	0.047881 (0.28)	95.6 (0.3)	95.5 (0.6)	93.4 (13.5)	0.597
C,m,n2,ta	0.048	408	6.5	1797	10	15.8	0.014848 (0.12)	0.098136 (0.24)	0.047935 (0.16)	95.0 (0.2)	95.1 (0.4)	96.0 (7.7)	0.615
D,m,n2,el	0.105	614	9.8	4398	14	14.5	0.014912 (0.12)	0.099153 (0.19)	0.048224 (0.13)	95.4 (0.2)	96.0 (0.3)	110.3 (5.9)	0.557
6. *Sample 99SH-006 - Coal River Batholith*													
A,c,n2,el	0.043	339	5.7	2310	6	18.4	0.015179 (0.12)	0.100376 (0.22)	0.047962 (0.16)	97.1 (0.2)	97.1 (0.4)	97.4 (7.5)	0.740
B,c,n2,ta	0.012	533	9	933	7	19.1	0.015146 (0.18)	0.100228 (0.53)	0.047995 (0.47)	96.9 (0.3)	97.0 (1.0)	99.0 (22.6)	0.775
C,c,n2,sp	0.063	239	3.9	1872	8	16.4	0.015038 (0.14)	0.099893 (0.23)	0.048177 (0.14)	96.2 (0.3)	96.7 (0.4)	108.0 (6.8)	0.644
7. *Sample 99SH-013 - Caesar Lakes Pluton*													
F#,f,m2,su	0.039	1159	18	2040	21	11.4	0.015185 (0.19)	0.100652 (0.26)	0.048074 (0.14)	97.2 (0.4)	97.4 (0.5)	102.9 (6.8)	0.422
H#,f,m5,su	0.039	1036	16	1670	22	12.2	0.014786 (0.11)	0.098589 (0.22)	0.048359 (0.15)	94.6 (0.2)	95.5 (0.4)	116.9 (6.9)	0.455
I#,f,m5,su	0.026	985	15	1634	15	12.9	0.014970 (0.14)	0.099648 (0.31)	0.048279 (0.25)	95.8 (0.3)	96.5 (0.6)	112.9 (11.6)	0.486
M4,c,m,eu	0.010	1806	389	1134	15	93.5	0.015373 (0.11)	0.100349 (0.28)	0.047342 (0.22)	98.3 (0.2)	97.1 (0.5)	66.5 (10.5)	47.3
8. *Sample 99SH-016 - Tuna Stock*													
M3,f,m,eu	0.024	2820	342	197	354	88.6	0.015221 (0.15)	0.099789 (0.79)	0.047550 (0.68)	97.4 (0.3)	96.6 (1.5)	76.9 (32.5)	25.5
M4,m,m,eu	0.018	1765	241	342	93	89.8	0.015377 (0.12)	0.099847 (0.42)	0.047094 (0.33)	98.4 (0.2)	96.6 (0.8)	54.0 (15.9)	28.8
M5,m,m,su	0.009	3402	399	613	48	88.1	0.015318 (0.10)	0.100474 (0.30)	0.047573 (0.22)	98.0 (0.2)	97.2 (0.6)	78.1 (10.4)	24.3
M6,m,m,su	0.005	2409	267	279	44	87.4	0.015348 (0.13)	0.101397 (0.55)	0.047917 (0.47)	98.2 (0.2)	98.1 (1.0)	95.1 (22.2)	22.3

Table 2.2. U-Pb analytical data continued.

Fraction[1]	Wt. (mg)	U[2] (ppm)	Pb*[3] (ppm)	$^{206}Pb/^{204}Pb$[4]	Pb[5] (pg)	^{208}Pb[3] %	Isotopic Ratios (1σ%)[6] $^{206}Pb/^{238}U$	$^{207}Pb/^{235}U$	$^{207}Pb/^{206}Pb$	Apparent Age (2σ Ma)[6] $^{206}Pb/^{238}U$	$^{207}Pb/^{235}U$	$^{207}Pb/^{206}Pb$	Th/U
9. *Sample 98HAS-06 - Mulholland (Cirque) Pluton*													
A,vc,n1,el	0.058	691	11	3191	12	13.1	0.015264 (0.12)	0.101251 (0.21)	0.048110 (0.12)	97.7 (0.2)	97.9 (0.4)	104.7 (5.6)	0.494
B,c,n1,eq	0.025	445	13	2567	8	9.6	0.029197 (0.12)	0.322451 (0.20)	0.080097 (0.11)	185.5 (0.4)	283.8 (1.0)	1199.4 (4.4)	0.382
C#,c,n1,el	0.032	1012	15	2187	14	11.1	0.015007 (0.09)	0.099874 (0.20)	0.048268 (0.13)	96.0 (0.2)	96.7 (0.4)	112.4 (6.1)	0.408
10. *Sample 98Z-C028 - Rudi Pluton*													
M2,m,m,eu	0.011	6699	435	362	199	78.7	0.015185 (0.12)	0.100795 (0.40)	0.048141 (0.31)	97.2 (0.2)	97.5 (0.7)	106.2 (14.7)	12.2
M3,m,m,eu	0.010	4991	379	367	133	81.8	0.015212 (0.11)	0.101027 (0.42)	0.048167 (0.34)	97.3 (0.2)	97.7 (0.8)	107.5 (16.1)	14.8
M4,m,m,eu	0.026	5175	699	393	336	89.7	0.015299 (0.25)	0.101415 (0.51)	0.048076 (0.35)	97.9 (0.5)	98.1 (1.0)	103.0 (16.6)	28.6
11. *Sample 98HAS-12 - Patterson Stock(?)*													
A,m,n1,ta	0.009	373	5.6	544	6	8.2	0.015319 (0.28)	0.102627 (1.49)	0.048589 (1.39)	98.0 (0.6)	99.2 (2.8)	129.1 (66.8)	0.291
B,m,n1,el	0.005	803	13	616	6	14.0	0.015329 (0.16)	0.104891 (0.65)	0.049628 (0.60)	98.1 (0.3)	101.3 (1.2)	177.6 (28.0)	0.538
C,m,n1,el	0.018	424	6	927	8	9.2	0.015223 (0.14)	0.100387 (0.40)	0.047797 (0.34)	97.5 (0.3)	97.1 (0.7)	89.2 (16.1)	0.330
D,m,n1,eq	0.002	6115	278	2887	11	10.2	0.042758 (0.11)	0.653597 (0.18)	0.110865 (0.10)	269.9 (0.6)	510.7 (1.5)	1813.6 (3.6)	0.432
12. *Sample 98HAS-12a - Patterson Stock (late stage dyke)*													
M4,m,m,eu	0.007	452	134	875	4	95.2	0.015543 (0.17)	0.101718 (0.82)	0.047464 (0.76)	99.4 (0.3)	98.4 (1.5)	72.6 (36.5)	65.6
M6,vc,m,su	0.012	2990	253	426	82	83.6	0.015233 (0.10)	0.100775 (0.36)	0.047980 (0.27)	97.5 (0.2)	97.5 (0.7)	98.3 (13.0)	16.8
13. *Sample 99SH-001 - Shannon Creek Pluton*													
AA,c,n2,sp	0.030	800	13	1543	16	9.1	0.016156 (0.10)	0.128501 (0.21)	0.057685 (0.15)	103.3 (0.2)	122.8 (0.5)	517.8 (6.3)	0.339
B,c,n2,sp	0.031	77	1.3	366	7	16.1	0.015163 (0.22)	0.100053 (0.75)	0.047857 (0.65)	97.0 (0.4)	96.8 (1.4)	92.2 (30.5)	0.627
C,m,n2,el	0.062	317	5.1	1332	14	15.0	0.015160 (0.11)	0.105366 (0.25)	0.050408 (0.17)	97.0 (0.2)	101.7 (0.5)	213.9 (7.8)	0.583
DA,c,n2,ti	0.016	5888	84	2303	37	8.4	0.014511 (0.13)	0.096291 (0.22)	0.048127 (0.13)	92.9 (0.2)	93.3 (0.4)	105.5 (6.3)	0.300
DB,c,n2,ti	0.009	5565	80	11120	4	10.1	0.014300 (0.11)	0.095307 (0.17)	0.048337 (0.08)	91.5 (0.2)	92.4 (0.3)	115.8 (3.9)	0.370
14. *Sample 98HAS-02 - Mt.Appler Pluton*													
D,m,n2,ta	0.027	1521	21	3537	11	3.8	0.014717 (0.14)	0.097648 (0.22)	0.048122 (0.13)	94.2 (0.3)	94.6 (0.4)	105.3 (6.2)	0.130
E#,m,n2,ta	0.034	1407	19	2774	16	4.1	0.014708 (0.14)	0.097900 (0.22)	0.048276 (0.15)	94.1 (0.3)	94.8 (0.4)	112.8 (7.2)	0.140
F#,m,n2,el	0.013	1542	21	436	43	5.3	0.014602 (0.10)	0.097919 (0.37)	0.048636 (0.29)	93.4 (0.2)	94.9 (0.7)	130.3 (13.7)	0.185
M1,m,m,an	0.022	1076	123	375	60	88.2	0.014791 (0.11)	0.096923 (0.45)	0.047527 (0.38)	94.6 (0.2)	93.9 (0.8)	75.8 (18.1)	24.5
M2,m,m,eu	0.020	2273	235	426	99	87.2	0.014573 (0.13)	0.096392 (0.43)	0.047971 (0.34)	93.3 (0.2)	93.4 (0.8)	97.8 (16.1)	22.3
M7,c,m,eu	0.040	2029	245	604	126	88.6	0.014891 (0.09)	0.097144 (0.29)	0.047314 (0.21)	95.3 (0.2)	94.1 (0.5)	65.1 (9.8)	25.6
M8,c,m,eu	0.042	2079	263	722	113	89.3	0.014910 (0.10)	0.097096 (0.27)	0.047230 (0.20)	95.4 (0.2)	94.1 (0.5)	60.9 (9.3)	27.4
M10,c,m,eu	0.022	1888	186	105	445	86.2	0.014974 (0.14)	0.098657 (1.05)	0.047784 (0.94)	95.8 (0.3)	95.5 (1.9)	88.6 (45.1)	20.5

Table 2.2. U-Pb analytical data continued.

Fraction[1]	Wt. (mg)	U^{2} (ppm)	Pb*[3] (ppm)	$^{206}Pb/^{204}Pb$[4]	Pb[5] (pg)	^{208}Pb[3] %	Isotopic Ratios (1σ%)[6] $^{206}Pb/^{238}U$	$^{207}Pb/^{235}U$	$^{207}Pb/^{206}Pb$	Apparent Age (2σ, Ma)[6] $^{206}Pb/^{238}U$	$^{207}Pb/^{235}U$	$^{207}Pb/^{206}Pb$	Th/U
15. *Sample 98HAS-14 - McLeod Pluton (aka Skinboat South, Bennett Creek S)*													
A,vc,n1,el	0.078	1139	17	3369	24	11.3	0.014589 (0.12)	0.096875 (0.19)	0.048160 (0.11)	93.4 (0.2)	93.9 (0.3)	107.1 (5.3)	0.418
B,vc,n1,el	0.055	847	13	2439	17	10.7	0.014674 (0.11)	0.097178 (0.21)	0.048029 (0.13)	93.9 (0.2)	94.2 (0.4)	100.7 (6.2)	0.394
C,vc,n1,ta	0.059	1388	20	724	104	8.1	0.014702 (0.10)	0.097599 (0.26)	0.048148 (0.18)	94.1 (0.2)	94.6 (0.5)	106.5 (8.7)	0.288
T1,vc,m5,an	0.357	359	5.8	128	1040	18.9	0.014492 (0.12)	0.095583 (0.90)	0.047834 (0.80)	92.8 (0.2)	92.7 (1.6)	91.1 (38.2)	0.765
16. *Sample 99SH-011 - Big Charlie Pluton (aka Skinboat North, Bennett Creek N)*													
AA,c,n2,el	0.055	1740	24	616	142	7.8	0.014196 (0.15)	0.093759 (0.40)	0.047903 (0.30)	90.9 (0.3)	91.0 (0.7)	94.5 (14.3)	0.276
AB,c,n2,el	0.037	1387	20	1473	32	8.9	0.014347 (0.12)	0.095593 (0.25)	0.048323 (0.16)	91.8 (0.2)	92.7 (0.4)	115.1 (7.5)	0.319
B,c,n2,sp	0.063	1409	20	839	96	8.6	0.014286 (0.14)	0.094925 (0.32)	0.048192 (0.23)	91.4 (0.2)	92.1 (0.6)	108.7 (10.7)	0.308
CA,c,n2,ti	0.020	1070	15	2183	9	6.5	0.014308 (0.20)	0.095338 (0.30)	0.048328 (0.19)	91.6 (0.4)	92.5 (0.5)	115.4 (9.0)	0.229

[1]Upper case letter = zircon fraction identifier (titanite fractions are T1, T2, etc. and monazite fractions are M1, M2, etc.); zircon fractions air abraided unless marked with #.
Grain size: vc=>150 μm, c=<150 μm and >134 μm, m=<134 μm and >104 μm, f=<104 μm.
Titanite and monazite were recovered from magnetic fractions (m) whereas all zircons are non-magnetic on a Frantz magnetic separator at field strength of 1.8-2.0A with a 20° front slope; m5=magnetic at side slope of 5°, m2=magnetic at side slope of 2°, n2=non-magnetic at side slope of 2°, n1=non-magnetic at side slope of 1°.
Grain shape: el=elongate, eq=equant, eu=euhedral, p=prismatic, s=stubby, su=subhedral, an=anhedral, ta=tabular, ti=tips, fr=fragments.
[2]U blank correction of 1pg +/-20%; U fractionation corrections were measured for each run with a double ^{233}U-^{235}U spike (about 0.005/amu).
[3]Radiogenic Pb.
[4]Measured ratio corrected for spike and Pb fractionation of 0.0035/amu +/-20% (Daly collector) and 0.0012/amu +/-7% and laboratory blank Pb of 1-3pg +/-20%. Laboratory blank Pb concentrations and isotopic compositions based on total procedural blanks analyzed.
[5]Total common Pb in analysis based on blank isotopic composition.
[6]Corrected for blank Pb, U, and common Pb. Common Pb corrections based on Pb isotopic compositions of feldspars from individual rock samples or the $^{207}Pb/^{206}Pb$ age of the fraction.

Table 2.3. Locations and descriptions for geochemical samples.

Sample	Intrusive Body	Plutonic Suite	Northing*	Easting*	Description
99-SH-022	Mt. Billings Batholith	Anvil	6757200	507300	massive med-gr Bt granodiorite
00-SH-001	Mt. Billings Batholith	Anvil	6852852	499996	massive med-gr Bt granodiorite
00-SH-002	Mt. Billings Batholith	Anvil	6853027	499680	weakly-foliated med-gr Bt granite
00-SH-003	Mt. Billings Batholith	Anvil	6853027	499680	fine-gr Bt-Pl dioritic enclave
SH-005	Mt. Billings Batholith	Anvil	6778227	517998	altered med-gr Bt granodiorite
SH-008	Mt. Billings Batholith	Anvil	6792026	525509	med-gr Bt granodiorite
SH-011E	Mt. Billings Batholith	Anvil	6792830	515480	massive fine-gr Bt granite
SH-024	Mt. Billings Batholith	Anvil	6789456	532946	altered Pl-Bt porphyry (dioritic)
SH-028a	Mt. Billings Batholith	Anvil	6803467	533040	altered Pl-Bt porphyry (dioritic)
SH-028b	Mt. Billings Batholith	Anvil	6801832	531635	altered fine-gr diorite
SH-029	Mt. Billings Batholith	Anvil	6809731	529105	meg-gr Bt granodiorite
SH-070	Mt. Billings Batholith	Anvil	6844586	518400	altered fine-gr Bt granite
99-SH-001	Shannon Creek pluton	Tay River	6860975	511410	weakly foliated med-gr Bt granite
99-SH-002	Shannon Creek pluton	Tay River	6861110	510575	weakly foliated med-gr Bt granite
99-SH-006	Coal River Batholith	Tay River	6796900	569700	massive med-gr Hbl-Bt granodiorite
99-SH-007	Coal River Batholith	Tay River	6798125	571000	massive med-gr Bt granodiorite
99-SH-008	Coal River Batholith	Tay River	6803635	574000	massive med-gr Bt granodiorite
99-SH-009	Coal River Batholith	Tay River	6824250	581700	massive med-gr Bt granodiorite
98-HAS-02	Mt. Appler Pluton	Tay River	6900544	552576	massive med-gr Bt granite
98-HAS-03	Faille pluton	Tay River	6896228	569674	megacrystic Bt granodiorite
98-HAS-06	Mulholland (Cirque) pluton	Tay River	6886772	570080	megacrystic Hbl-Bt granodiorite
98-Z-C028	Rudi Pluton	Tay River	6912514	525354	megacrystic Bt granite
98-HAS-07	Jorgensen pluton	Tay River	6751093	645902	Hbl-Pl-Bt porphyry (dioritic)
98-HAS-12	Patterson pluton	Tay River	6751425	631699	massive Bt granodiorite
98-HAS-12a	Patterson pluton	Tay River	6751425	631699	Pl-Bt porphyritic dyke (granitic)
98-HAS-12b	Patterson pluton	Tay River	6751425	631699	aplite dyke (granitic)
98-Z-12	Powers pluton	Tay River	6743796	659038	Pl-Hbl-Bt porphyry (dioritic)
99-SH-013	Caesar Lakes pluton	Tay River	6799200	559500	massive fine-gr Bt granite
99-SH-014	Caesar Lakes pluton	Tay River	6802500	556750	massive med-gr Bt granodiorite
99-SH-015	Caesar Lakes pluton	Tay River	6800680	555870	Pl phyric diorite dyke
99-SH-016	Tuna stock	Tay River	6855058	541644	megacrystic Bt granite
99-SH-010	Big Charlie pluton	Tombstone	6799292	628757	megacrystic Bt granite
99-SH-011	Big Charlie pluton	Tombstone	6789175	624400	megacrystic Bt granite
99-SH-012	Big Charlie pluton	Tombstone	6794800	621528	coarse-gr Bt granite
98-HAS-15	Big Charlie pluton	Tombstone	6799598	627564	megacrystic Bt granodiorite
98-HAS-14	McLeod pluton	Tombstone	6775409	632194	megacrystic Bt granite
98-HAS-14a	McLeod pluton	Tombstone	6775409	632196	megacrystic Bt monzonite

* NAD 27, Zone 9

Abbreviations used in descriptions: fine-gr = fine-grained, med-gr = medium grained

Mineral abbreviations: Bt = biotite, Pl = plagioclase, Hbl = hornblende

Table 2.4. Major, trace, and REE data from samples analyzed for this study.[1]

Sample	Major elements (wt. %)[2]													
	SiO_2	TiO_2	Al_2O_3	Fe_2O_3T[4]	Fe_2O_3	FeO	MnO	MgO	CaO	Na_2O	K_2O	P_2O_5	Cr_2O_3	LOI	TOTAL
SH-99-001	76.26	0.08	12.83	1.17	0.43	0.67	0.05	<0.01	0.62	3.33	4.76	0.02	<0.01	0.55	99.67
SH-99-002	73.90	0.13	13.25	1.54	0.22	1.19	0.06	0.11	0.78	3.40	4.88	0.05	<0.01	0.54	98.64
SH-99-006	66.69	0.53	15.29	4.04	1.12	2.63	0.08	1.85	3.79	2.87	3.64	0.13	<0.01	0.52	99.43
SH-99-007	66.23	0.49	14.83	3.59	1.00	2.33	0.07	1.68	2.87	2.49	3.59	0.10	<0.01	3.46	99.40
SH-99-008	67.54	0.45	15.25	3.42	1.04	2.14	0.07	1.56	3.38	2.87	3.92	0.11	<0.01	0.72	99.29
SH-99-009	65.78	0.57	14.95	3.93	0.76	2.85	0.08	1.47	2.58	2.38	4.19	0.16	<0.01	3.23	99.32
SH-99-010	71.05	0.51	14.35	3.00	0.59	2.17	0.06	0.75	2.22	3.08	4.11	0.17	<0.01	0.44	99.74
SH-99-011	71.25	0.38	14.52	2.37	0.30	1.86	0.06	0.55	1.64	3.31	4.95	0.12	<0.01	0.52	99.67
SH-99-012	69.65	0.46	14.53	3.00	0.53	2.22	0.06	0.81	2.02	3.19	4.62	0.16	<0.01	0.69	99.19
SH-99-013	72.49	0.29	14.02	2.52	0.68	1.66	0.06	0.81	2.16	3.02	3.67	0.09	<0.01	0.69	99.82
SH-99-014	69.28	0.39	14.93	3.16	0.34	2.54	0.06	0.98	2.71	3.11	3.73	0.10	<0.01	0.77	99.22
SH-99-015	52.69	0.78	15.98	6.93	1.63	4.77	0.11	6.67	6.65	2.78	1.43	0.16	<0.01	5.26	99.44
SH-99-016	69.68	0.30	15.51	2.52	0.16	2.12	0.05	0.71	2.08	3.28	4.46	0.10	<0.01	0.68	99.37
SH-99-022	68.36	0.41	15.40	3.18	0.99	1.97	0.07	1.04	2.81	3.37	3.62	0.16	<0.01	1.32	99.74
98-HAS-14	69.30	0.37	14.88	2.43	0.74	1.52	0.06	0.64	1.69	3.48	5.07	0.13	<0.01	0.43	98.48
98-HAS-14a	57.03	1.43	16.50	7.08	2.35	4.26	0.13	3.16	4.00	3.58	4.09	0.55	<0.01	1.15	98.70
98-HAS-12a	72.37	0.09	14.99	1.33	0.22	1.00	0.06	0.20	1.64	4.00	3.59	0.10	<0.01	0.41	98.78
98-HAS-12b	73.16	0.05	14.95	0.16	0.05	0.10	0.01	0.09	0.53	3.44	4.89	0.10	<0.01	1.18	98.56
98-HAS-12	65.61	0.43	15.76	3.84	0.97	2.58	0.06	1.98	4.07	2.98	3.05	0.12	<0.01	0.82	98.72
98-HAS-02	69.76	0.36	14.99	2.39	0.08	2.08	0.05	0.68	1.91	2.93	5.10	0.14	<0.01	0.55	98.86
98-Z-C-028	72.23	0.24	13.87	1.94	0.17	1.59	0.05	0.44	1.69	2.78	4.65	0.10	<0.01	0.68	98.67
98-Z-12	60.80	0.59	16.53	5.08	1.17	3.52	0.10	2.24	4.20	3.92	2.45	0.13	<0.01	2.62	98.66
SH-00-001	68.83	0.47	15.08	3.30	0.21	2.78	0.06	0.80	1.68	3.03	3.26	0.16	<0.01	1.36	98.03
SH-00-002	73.05	0.15	14.10	1.03	-0.04	0.96	0.04	0.22	1.27	3.11	5.04	0.06	<0.01	0.48	98.55
SH-00-003	57.40	0.79	18.03	7.42	0.45	6.27	0.15	3.31	4.96	2.00	3.08	0.18	<0.01	1.25	98.57
SH-070	72.49	0.07	14.54	0.84	0.61	0.21	0.07	0.05	0.67	3.58	5.24	0.14	<0.01	0.74	98.43
SH-028	58.99	0.69	16.95	5.96	1.31	4.18	0.10	3.28	6.14	2.79	1.39	0.16	<0.01	2.36	98.81
SH-028a	71.87	0.13	13.11	1.00	0.16	0.76	0.10	0.19	2.35	1.84	5.16	0.14	<0.01	2.66	98.55
SH-024	58.50	0.70	15.80	5.53	0.22	4.78	0.10	2.61	4.80	2.73	2.72	0.16	<0.01	4.93	98.58
SH-008	67.94	0.37	15.27	2.70	-1.56	3.83	0.07	0.92	3.55	2.89	3.82	0.17	<0.01	1.09	98.79
SH-005	65.99	0.50	14.99	4.45	2.03	2.18	0.24	1.29	2.81	2.94	2.52	0.15	<0.01	2.67	98.55
SH-029	65.75	0.24	17.82	2.14	0.33	1.63	0.20	0.56	4.87	3.78	1.38	0.35	<0.01	1.55	98.64
SH-011E	72.20	0.15	14.45	1.39	0.10	1.16	0.06	0.17	0.97	3.88	4.28	0.13	<0.01	0.67	98.35
98-HAS-03	66.72	0.43	15.52	3.57	0.54	2.73	0.08	1.01	2.57	2.58	5.04	0.17	<0.01	0.90	98.59
98-HAS-06	67.23	0.45	14.98	3.48	0.70	2.50	0.07	1.27	3.11	2.86	4.28	0.20	<0.01	0.40	98.33
98-HAS-07	61.09	0.53	16.18	4.84	2.22	2.36	0.11	2.60	3.66	3.69	2.72	0.14	<0.01	3.14	98.70
98-HAS-015	67.24	0.59	14.90	3.74	0.81	2.64	0.08	1.11	2.60	3.25	4.24	0.19	<0.01	0.61	98.55

[1] All analyses conducted by Chemex Labs Ltd. in Vancouver, BC.

[2] Major element analyses performed by X-ray diffraction (XRF).

[3] Trace and REE element analyses performed by inductively coupled plasma mass spectrometry (ICP-MS).

[4] All Fe reported as Fe_2O_3.

[5] $Eu/Eu^* = Eu_N/(Sm_N * Gd_N)^{1/2}$ (Taylor and McLennan, 1985).

[6] $Nb/Nb^* = 0.5 * Nb_{pm}/(Th_{pm}+La_{pm})$; $Ti/Ti^* = 0.5 * Ti_{pm}/(Gd_{pm}+La_{pm})$, pm = primitive mantle normalized (values from Sun and Mcdonough, 1989).

[7] Subscript "N" denotes values normalized to chondrite values of Sun and McDonough (1989).

[8] Zircon saturation temperatures after Watson and Harrison (1983).

Table 2.4. Continued

Sample	Trace and rare earth elements (ppm)[3]																
	Ba	Ce	Cs	Co	Cu	Dy	Er	Eu	Gd	Ga	Hf	Ho	La	Pb	Lu	Nd	Ni
SH-99-001	222	51	2.7	20	<5	6.5	3.9	0.1	6.9	17	4	1.1	22.5	20	0.3	24	<5
SH-99-002	461	63.5	1.7	18.5	<5	7.1	4	0.3	7.2	18	4	1.1	30	25	0.3	29	<5
SH-99-006	794	83	3.2	22	<5	3.3	1.4	0.8	4.8	16	5	0.5	46	5	0.1	28	5
SH-99-007	588	59.5	3.9	16.5	<5	2.6	1.7	0.6	4	17	5	0.4	33.5	10	<0.1	21.5	5
SH-99-008	763	60	3	23.5	<5	2.3	1.4	0.5	3.4	16	4	0.4	33.5	10	<0.1	22	5
SH-99-009	741	87.5	5.3	16	<5	4	2.5	0.9	5.2	17	6	0.7	48.5	10	0.1	30.5	<5
SH-99-010	519	101.5	3.9	20.5	<5	3.4	1.7	1	5.5	18	5	0.5	51	25	<0.1	33.5	<5
SH-99-011	318	57.5	10.3	22	<5	3.2	1.9	0.6	4	17	5	0.5	29	30	<0.1	20.5	<5
SH-99-012	545	74.5	8	29.5	<5	2.8	1.4	0.7	4.8	19	5	0.4	40	25	<0.1	24.5	<5
SH-99-013	469	57	5.3	23.5	<5	3.9	2.5	0.4	4.2	17	4	0.7	30	15	0.2	21.5	<5
SH-99-014	691	62.5	6.3	21.5	<5	3.7	2.2	0.7	4.5	17	4	0.6	32	10	<0.1	25.5	<5
SH-99-015	717	44	2.1	29.5	<5	3.1	2.3	1	4	16	3	0.4	21.5	5	<0.1	19	85
SH-99-016	872	71.5	11.8	16	<5	3.2	1.4	0.8	4.9	19	4	0.5	37.5	35	<0.1	29	<5
SH-99-022	925	61	3.8	15.5	<5	3.2	1.4	0.6	4.7	19	4	0.4	30.5	20	<0.1	25	<5
98-HAS-14	492	82	7.6	15	<5	3.1	1.9	1	3.5	20	4	0.6	42.5	20	0.3	27.5	<5
98-HAS-14a	672	245	18.2	19.5	15	4.8	2.7	1.9	8.9	29	11	0.9	135.5	5	0.4	87	20
98-HAS-12a	712	61.5	3	12.5	<5	2.2	1.2	1	2.8	18	2	0.4	33.5	30	0.1	23	<5
98-HAS-12b	902	23.5	2.2	13	<5	2	1.2	0.6	2	17	1	0.4	12.5	20	0.1	8.5	5
98-HAS-12	769	89.5	2.7	16.5	5	3.2	1.8	1.4	4.4	20	6	0.6	47	5	0.3	34.5	15
98-HAS-02	476	92	10.3	15.5	<5	3	1.6	1	4.7	22	4	0.5	46	25	0.1	36.5	5
98-Z-C-028	273	62.5	9.8	15	<5	5.8	3.6	0.8	5.9	17	5	1.2	32	45	0.6	29	<5
98-Z-12	1000	56.5	1.6	217	5	3.1	2	1.3	3.7	22	4	0.6	30.5	10	0.3	24	15
SH-00-001	1010	88.5	3.5	8	<5	4.6	2.3	1.2	6.3	22	6	0.8	43.5	15	0.3	39	<5
SH-00-002	733	52.5	5	14.5	<5	3.3	1.8	0.8	3.6	18	2	0.6	26.5	20	0.3	22.5	<5
SH-00-003	567	51	14	16.5	5	3.8	2.4	1	4.3	27	3	0.8	25	<5	0.3	23.5	5
SH-070	223	15.5	5.6	26	15	1.8	0.9	0.2	1.6	16	1	0.3	8.5	20	0.1	6.5	<5
SH-028	356	52.5	8	15.5	<5	3.9	2.4	1.2	4.3	20	3	0.8	25.5	<5	0.3	24.5	15
SH-028a	552	47.5	4	11	<5	3	1.3	0.7	4	18	2	0.5	22.5	20	0.1	20	<5
SH-024	1260	64	4.1	12.5	10	3.9	2.2	1.3	4.4	19	3	0.8	33	5	0.3	27.5	<5
SH-008	1220	73.5	4.7	16	<5	3.1	1.6	1.2	4.6	21	4	0.6	36.5	35	0.2	31.5	<5
SH-005	845	82	3.9	13	<5	3.6	2.2	1.2	4.7	19	4	0.7	43.5	90	0.3	32.5	5
SH-029	328	31.5	2	9	30	5.6	2.5	0.8	5	24	2	1	15	455	0.3	15.5	<5
SH-011E	436	34.5	5	14	<5	2.7	1.4	0.5	2.8	21	3	0.5	17	25	0.2	14.5	<5
98-HAS-03	1295	154.5	6.9	15	500	4.8	2.6	2	6.8	22	7	0.9	84	40	0.4	56.5	<5
98-HAS-06	929	110.5	6.9	15.5	<5	3.3	1.7	1.4	4.9	19	5	0.6	61	25	0.2	40	<5
98-HAS-07	812	63	4.3	12.5	110	3	1.8	1.2	3.8	20	3	0.7	34	5	0.2	25	25
98-HAS-015	513	97.5	7.4	13	135	3.9	2	1.3	5.2	22	5	0.7	51.5	20	0.3	35.5	5

Table 2.4. Continued

Sample	Nb	Pr	Rb	Sm	Ag	Sr	Ta	Tb	Tl	Th	Tm	Sn	W	U	V	Yb	Y	Zn
SH-99-001	28	6.1	224	5.6	<1	46.2	10	0.9	<0.5	27	0.4	4	183	8.5	<5	3.8	36	10
SH-99-002	22	6.9	218	5.4	<1	78	8	1	0.5	21	0.4	2	171	4.5	5	3.7	38	20
SH-99-006	14	7.8	136	4.7	<1	305	6	0.4	<0.5	19	<0.1	2	137	2	75	1.5	17	30
SH-99-007	13	6.1	128.5	3.6	<1	241	4	0.4	<0.5	21	<0.1	3	94	3.5	65	1.8	16	40
SH-99-008	14	5.8	136	3.7	<1	279	7.5	0.3	<0.5	20	<0.1	4	171	2	60	1.8	15.5	30
SH-99-009	23	9.1	153	5.3	<1	272	4.5	0.6	0.5	22	0.1	2	91	2.5	65	2.7	22	35
SH-99-010	26	9.7	159.5	5.1	<1	211	7.5	0.7	<0.5	25	<0.1	4	163	3.5	30	1.8	18.5	45
SH-99-011	32	5.7	229	3.3	<1	134.5	10	0.4	0.5	23	<0.1	7	195	7.5	25	1.6	18.5	40
SH-99-012	34	6.6	207	4.2	<1	193.5	12	0.4	0.5	24	<0.1	5	248	3	30	2.1	17	55
SH-99-013	15	6.2	162	4.2	<1	184	10	0.6	<0.5	23	0.1	3	207	8	30	2.8	26.5	25
SH-99-014	16	6.9	150	4.7	<1	264	7	0.4	<0.5	13	0.1	1	169	2	45	1.7	21.5	35
SH-99-015	10	5.1	38	3.7	<1	453	1	0.5	<0.5	7	0.1	1	26	1	160	1.6	19	50
SH-99-016	10	7.7	189.5	5.2	<1	277	6	0.6	0.5	18	<0.1	4	122	3.5	25	1.6	18	20
SH-99-022	15	6.8	147	4.5	<1	459	5	0.4	<0.5	14	<0.1	3	103	2.5	50	1.6	17.5	45
98-HAS-14	37	8.6	215	4.7	<1	186.5	9	0.6	0.5	22	0.3	7	131	5	35	2.1	16.5	50
98-HAS-14a	55	26.2	301	13.3	<1	357	7	1.2	0.5	31	0.4	8	66	9	120	2.2	23.5	130
98-HAS-12a	16	6.7	136	3.6	<1	295	6.5	0.4	<0.5	13	0.1	2	122	4	10	1.3	11.5	25
98-HAS-12b	16	2.7	154	1.9	<1	177	7	0.3	<0.5	5	0.1	1	127	1.5	<5	1.3	13	15
98-HAS-12	21	9.9	111.5	6.1	<1	458	12.5	0.7	<0.5	21	0.3	13	112	3.5	75	1.8	15.5	30
98-HAS-02	25	10.6	227	6.5	<1	164	9.5	0.7	0.5	22	0.1	9	148	3	25	1.3	14.5	55
98-Z-C-028	24	7.6	230	6.3	<1	166	16.5	1	0.5	23	0.6	14	162	14.5	25	4.2	34	40
98-Z-12	41	6.6	73.6	4.7	<1	673	69	0.6	<0.5	9	0.3	2	1290	3	105	1.9	16.5	65
SH-00-001	17	10.5	147	7.7	<1	312	4	0.9	0.5	22	0.3	3	75	2.5	40	1.8	21.5	60
SH-00-002	11	6.3	195	4.6	<1	170.5	7.5	0.6	<0.5	13	0.3	3	155	4.5	5	1.5	17.5	15
SH-00-003	11	6.3	230	4.8	<1	345	2.5	0.7	0.5	9	0.4	6	52	2.5	145	2	21	120
SH-070	11	1.9	229	1.7	<1	80.4	14.5	0.3	0.5	4	0.1	3	278	13.5	<5	1.1	10	5
SH-028	9	6.4	118	4.9	<1	398	2.5	0.8	0.5	8	0.3	2	46	2.5	130	2	21	65
SH-028a	15	5.6	216	4.6	<1	195	6.5	0.7	0.5	11	0.1	6	128	4	<5	1	14	45
SH-024	11	7.4	94.4	5	<1	331	2	0.7	<0.5	14	0.4	1	29	3.5	135	2.2	21	60
SH-008	16	8.4	155.5	5.8	<1	413	7	0.6	0.5	15	0.2	2	143	3.5	50	1.4	15.5	60
SH-005	13	9.3	104	5.3	<1	271	4.5	0.7	0.5	17	0.3	4	90	2	70	1.9	18.5	290
SH-029	17	4	48.2	4.5	<1	654	5	1	<0.5	4	0.3	3	86	3	20	2	26	2670
SH-011E	28	4.1	228	3.1	<1	205	10	0.5	0.5	7	0.2	7	146	7	5	1.7	13.5	50
98-HAS-03	20	16.9	188	9.2	1	407	7	0.9	0.5	33	0.4	4	130	4	55	2.5	22	85
98-HAS-06	18	11.7	163	6.2	<1	408	7	0.7	0.5	33	0.2	3	137	6.5	60	1.5	15.5	45
98-HAS-07	12	7.2	94.8	4.8	<1	601	2.5	0.6	<0.5	12	0.3	1	40	3.5	105	1.7	16	55
98-HAS-015	25	10.4	180.5	6.3	<1	215	6	0.7	0.5	22	0.3	5	105	4	55	1.9	18.5	60

Table 2.4. Continued

Sample	Calculated ratios							
	Zr	Eu/Eu*[5]	Nb/Nb*[6]	Ti/Ti*[6]	La_N/Yb_N[7]	Nb/Ta	Fe_2O_3/FeO	T (°C)$_{Zr\text{-}Sat}$[8]
SH-99-001	108	0.05	0.06	0.02	4.2	2.8	0.63	N/A
SH-99-002	110	0.15	0.05	0.04	5.8	2.8	0.18	759.5
SH-99-006	144.5	0.51	0.03	0.19	22.0	2.3	0.42	760.3
SH-99-007	152	0.48	0.03	0.23	13.3	3.3	0.43	782.1
SH-99-008	144	0.43	0.03	0.21	13.3	1.9	0.49	765.1
SH-99-009	212	0.52	0.05	0.18	12.9	5.1	0.27	811.8
SH-99-010	189	0.58	0.05	0.17	20.3	3.5	0.27	799.0
SH-99-011	167.5	0.50	0.07	0.20	13.0	3.2	0.16	787.9
SH-99-012	204	0.48	0.07	0.19	13.7	2.8	0.24	802.3
SH-99-013	115	0.29	0.03	0.12	7.7	1.5	0.41	761.8
SH-99-014	135	0.46	0.06	0.14	13.5	2.3	0.13	767.6
SH-99-015	99	0.79	0.06	0.36	9.6	10.0	0.34	689.0
SH-99-016	119.5	0.48	0.03	0.10	16.8	1.7	0.08	762.1
SH-99-022	119.5	0.40	0.05	0.16	13.7	3.0	0.50	756.1
98-HAS-14	145	0.75	0.08	0.13	14.5	4.1	0.49	772.1
98-HAS-14a	417	0.53	0.07	0.18	44.2	7.9	0.55	824.7
98-HAS-12a	63.5	0.96	0.06	0.04	18.5	2.5	0.22	716.5
98-HAS-12b	26.5	0.94	0.15	0.04	6.9	2.3	0.49	664.5
98-HAS-12	150.5	0.82	0.05	0.12	18.7	1.7	0.38	765.6
98-HAS-02	139	0.55	0.05	0.09	25.4	2.6	0.04	773.3
98-Z-C-028	101.5	0.40	0.05	0.07	5.5	1.5	0.11	752.3
98-Z-12	146.5	0.95	0.19	0.21	11.5	0.6	0.33	752.1
SH-00-001	179.5	0.53	0.04	0.10	17.3	4.3	0.08	813.4
SH-00-002	69.5	0.60	0.04	0.06	12.7	1.5	0.04	723.2
SH-00-003	92	0.67	0.05	0.28	9.0	4.4	0.07	724.0
SH-070	24	0.37	0.13	0.07	5.5	0.8	2.89	650.2
SH-028	103	0.80	0.05	0.24	9.1	3.6	0.31	720.0
SH-028a	49.5	0.50	0.06	0.05	16.1	2.3	0.20	693.2
SH-024	109.5	0.84	0.04	0.24	10.8	5.5	0.05	725.9
SH-008	116	0.71	0.05	0.11	18.7	2.3	0.41	745.8
SH-005	116	0.73	0.03	0.16	16.4	2.9	0.93	764.0
SH-029	74	0.51	0.17	0.09	5.4	3.4	0.20	716.9
SH-011E	65.5	0.52	0.18	0.08	7.2	2.8	0.09	720.2
98-HAS-03	223	0.77	0.03	0.08	24.1	2.9	0.20	809.8
98-HAS-06	157.5	0.77	0.03	0.12	29.2	2.6	0.28	771.1
98-HAS-07	113	0.86	0.04	0.19	14.3	4.8	0.94	738.6
98-HAS-015	177	0.69	0.05	0.16	19.4	4.2	0.31	782.8

Table 2.5. Rb-Sr and Sm-Nd isotope data from samples analyzed for this study.†

Sample	Rb ppm	Sr ppm	$^{87}Rb/^{86}Sr$	$^{87}Sr/^{86}Sr$	2σ	Initial $^{87}Sr/^{86}Sr$*	Sm ppm	Nd ppm	$^{147}Sm/^{144}Nd$	$^{143}Nd/^{144}Nd$	2σ	εNd*	T_{DM}**
98-HAS-02	603.8	439.0	3.9877	0.726343	0.000016	0.72068	6.01	33.85	0.1074	0.511963	0.000009	-12.0	1.72
98-HAS-03	253.0	545.5	1.3433	0.717537	0.000013	0.71563	8.53	51.63	0.0999	0.511949	0.000009	-12.2	1.62
98-HAS-06	253.5	620.5	1.1833	0.715915	0.000011	0.71423	6.37	37.15	0.1038	0.511954	0.000010	-12.2	1.67
98-HAS-07	108.2	689.5	0.4542	0.710602	0.000012	0.70996	4.20	23.49	0.1081	0.512132	0.000009	-8.7	1.49
98-HAS-12	302.3	1232.0	0.7103	0.711740	0.000016	0.71073	3.56	20.37	0.1057	0.512105	0.000009	-9.2	1.49
98-HAS-14	291.1	259.4	3.2505	0.718500	0.000018	0.71388	4.57	25.40	0.1087	0.512126	0.000011	-8.9	1.50
99-SH-001	328.9	65.8	14.5030	0.735457	0.000014	0.71485	5.44	20.42	0.1611	0.511945	0.000010	-13.1	N.D.
SH-005	235.5	610.2	1.1180	0.718418	0.000014	0.71683	5.98	35.05	0.1032	0.511941	0.000006	-12.4	1.68
99-SH-006	192.1	429.0	1.2964	0.712964	0.000015	0.71112	4.52	27.37	0.0998	0.512042	0.000010	-10.4	1.50
99-SH-008	167.5	347.5	1.3953	0.712973	0.000015	0.71099	3.83	21.94	0.1056	0.512039	0.000006	-10.5	1.58
99-SH-009	149.0	264.4	1.6318	0.714283	0.000013	0.71196	5.73	34.42	0.1006	0.512018	0.000010	-10.9	1.54
99-SH-011	474.4	293.9	4.6770	0.719578	0.000013	0.71293	4.36	22.38	0.1179	0.512047	0.000012	-10.5	1.77
99-SH-013	350.0	381.7	2.6551	0.715160	0.000012	0.71139	4.43	21.78	0.1231	0.512021	0.000009	-11.1	1.92
99-SH-016	358.5	508.5	2.0435	0.724338	0.000015	0.72143	5.56	30.72	0.1094	0.511820	0.000009	-14.9	1.96
SH-011E	239.6	218.3	3.1819	0.726951	0.000011	0.72243	2.97	13.22	0.1357	0.511799	0.000010	-15.6	2.65
99-SH-022	136.5	408.6	0.9675	0.716164	0.000015	0.71479	4.80	25.64	0.1133	0.511902	0.000008	-13.3	1.91
SH-029	56.2	742.9	0.2191	0.719992	0.000015	0.71968	4.26	14.68	0.1754	0.511728	0.000007	-17.5	N.D.
SH-070	229.0	79.5	8.3549	0.730360	0.000018	0.71849	1.19	4.34	0.1665	0.511835	0.000008	-15.3	N.D.
98-Z-12	83.1	759.9	0.3166	0.708983	0.000012	0.70853	4.11	21.79	0.1140	0.512274	0.000007	-6.0	1.36
98-Z-C-028	488.9	349.0	4.0608	0.726249	0.000018	0.72048	5.31	23.76	0.1352	0.511752	0.000010	-16.5	2.72

† All analyses conducted at the Radiogenic Isotope Facility at the University of Alberta.

* Initial $^{87}Sr/^{86}Rb$ ratio and eNdT corrected for T=100 Ma.

** Model ages after Goldstein et al., 1984.

Note: N.D. - not determined

Table 2.6. Pb isotope data from feldspar separates analyzed for this study.[1]

Sample	$^{206}Pb/^{204}Pb$	2σ,%	$^{207}Pb/^{204}Pb$	2σ,%	$^{208}Pb/^{204}Pb$	2σ,%	$^{207}Pb/^{206}Pb$	2σ,%	$^{208}Pb/^{206}Pb$	2σ,%
98-HAS-02	19.490	0.032	15.757	0.045	39.541	0.064	0.80844	0.017	2.02878	0.032
98-HAS-03	19.440	0.032	15.731	0.045	39.480	0.064	0.80920	0.017	2.03090	0.032
98-HAS-06	19.487	0.037	15.751	0.048	39.578	0.069	0.80830	0.019	2.03103	0.036
98-HAS-07	19.560	0.044	15.754	0.054	39.673	0.071	0.80541	0.017	2.02830	0.032
98-HAS-12	19.534	0.081	15.771	0.079	39.757	0.102	0.80736	0.040	2.03530	0.044
98-HAS-14	19.594	0.032	15.772	0.045	39.577	0.064	0.80496	0.017	2.01991	0.032
98-Z-12	19.651	0.113	15.829	0.116	39.883	0.126	0.80553	0.022	2.02960	0.033
98-Z-C028	19.493	0.033	15.750	0.046	39.569	0.065	0.80797	0.017	2.02993	0.032
99-SH-001	19.404	0.032	15.732	0.045	39.461	0.064	0.81076	0.017	2.03365	0.032
99-SH-006	19.477	0.098	15.771	0.102	39.640	0.113	0.80975	0.022	2.03526	0.034
99-SH-008	19.460	0.087	15.741	0.092	39.596	0.103	0.80893	0.018	2.03480	0.033
99-SH-011	19.585	0.032	15.788	0.045	39.618	0.064	0.80612	0.017	2.02294	0.032
99-SH-022	19.447	0.040	15.749	0.049	39.598	0.071	0.80983	0.021	2.03621	0.039
SH-005	19.447	0.242	15.697	0.239	39.528	0.251	0.80718	0.053	2.03259	0.046
SH-073	19.473	0.033	15.762	0.046	39.591	0.064	0.80943	0.017	2.03317	0.032
99-SH-009	19.545	0.037	15.757	0.049	39.670	0.067	0.80621	0.017	2.02969	0.032
99-SH-013	19.397	0.034	15.713	0.047	39.469	0.065	0.81007	0.017	2.03484	0.032
99-SH-016	19.530	0.041	15.798	0.047	39.774	0.071	0.80890	0.027	2.03658	0.035
SH-011E	19.772	0.036	15.810	0.048	39.786	0.066	0.79962	0.017	2.01221	0.032
SH-029	19.444	0.034	15.730	0.047	39.467	0.065	0.80899	0.017	2.02983	0.032

[1]All analyses conducted by J. Gabites in the Pacific Centre for Geochemical and Isotopic Research at the University of British Columbia.

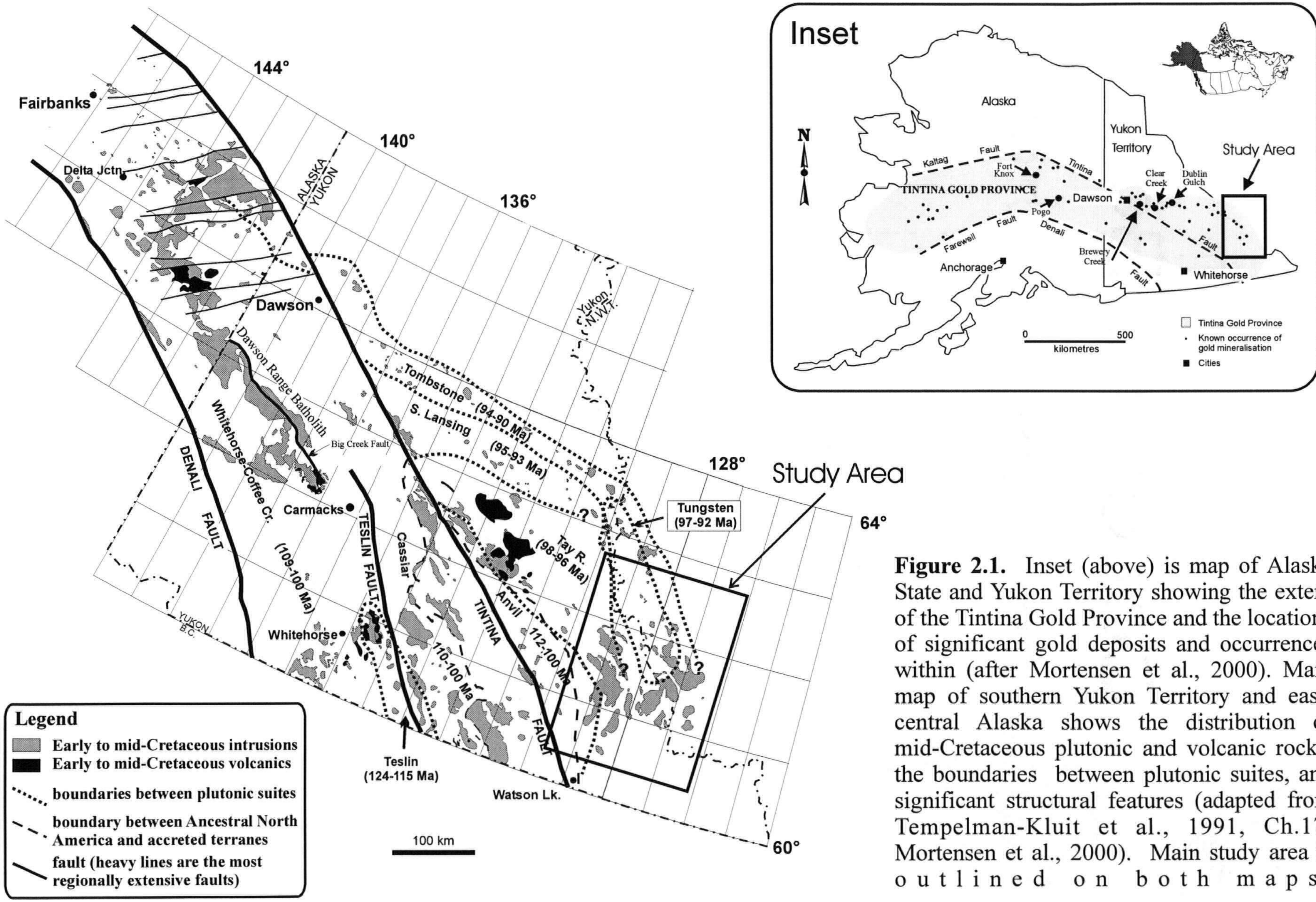

Figure 2.1. Inset (above) is map of Alaska State and Yukon Territory showing the extent of the Tintina Gold Province and the locations of significant gold deposits and occurrences within (after Mortensen et al., 2000). Main map of southern Yukon Territory and east-central Alaska shows the distribution of mid-Cretaceous plutonic and volcanic rocks, the boundaries between plutonic suites, and significant structural features (adapted from Tempelman-Kluit et al., 1991, Ch.17; Mortensen et al., 2000). Main study area is outlined on both maps.

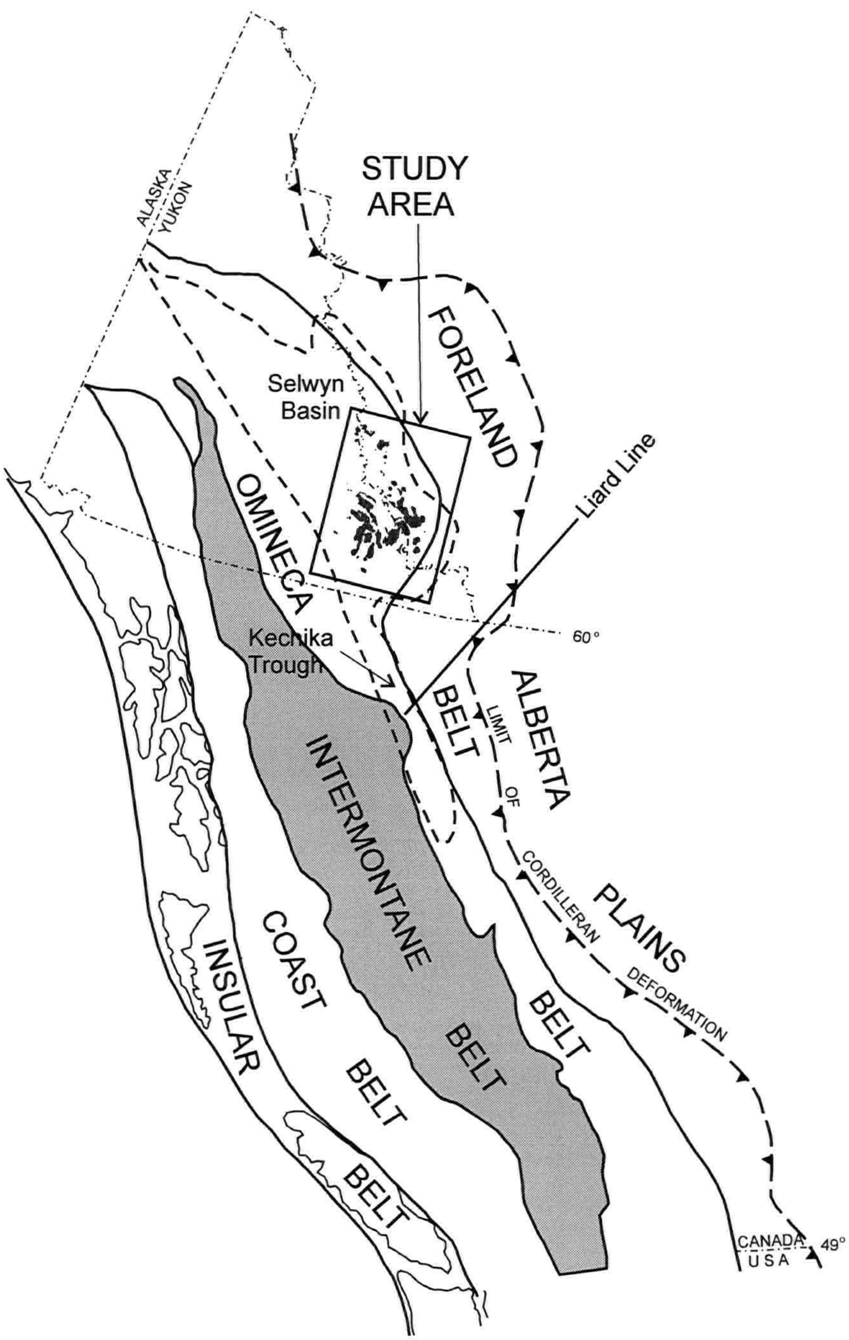

Figure 2.2. Map of the Canadian Cordillera showing the location of the study area with reference to morphogeological belts, the outline of the Selwyn Basin-Kechika Trough depositional system (dashed line), and the location of the Liard Line (after Wheeler and McFeely, 1991;Gabrielse et al., 1991; and Cecile et al., 1997).

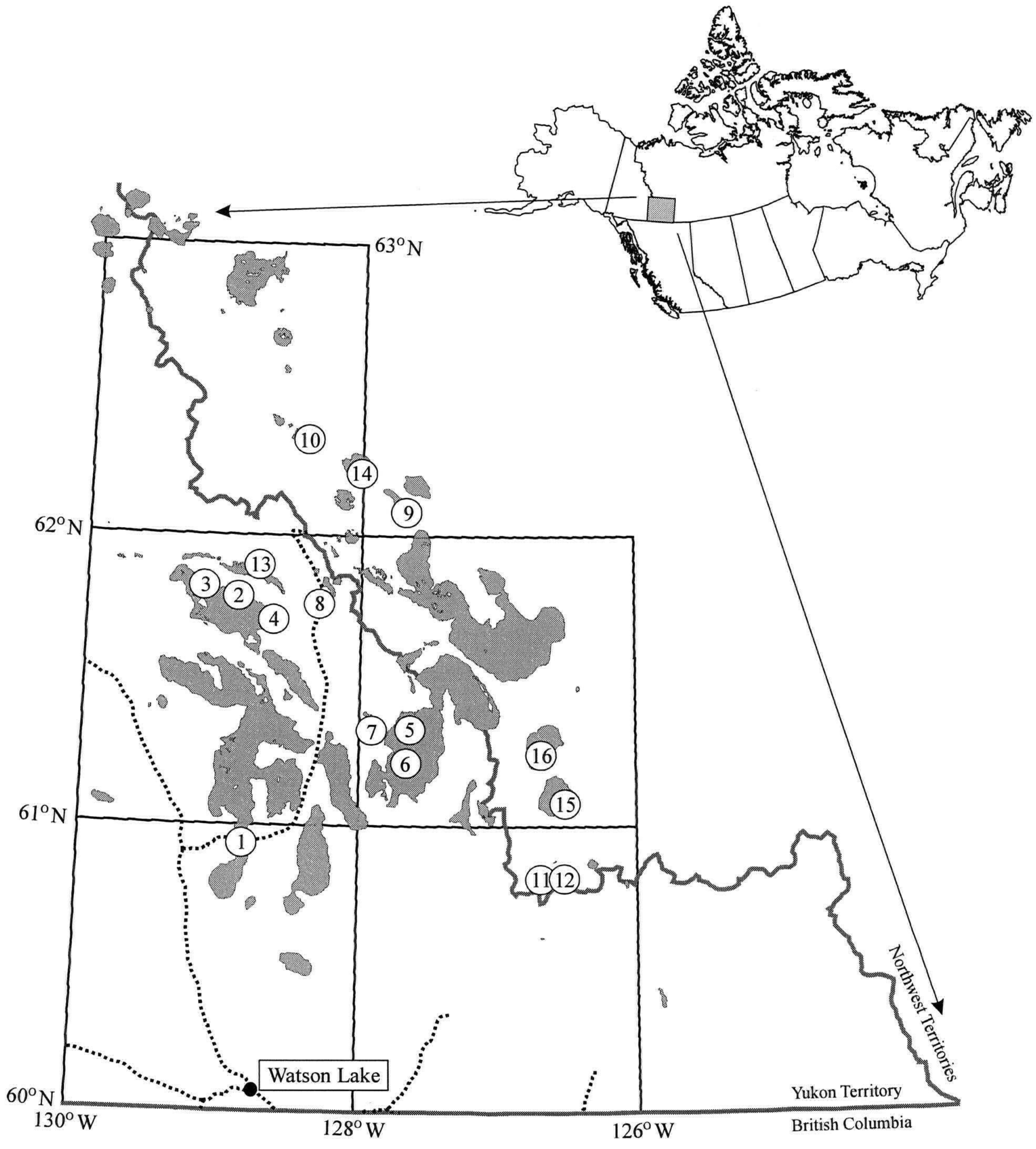

Figure 2.3. Map of study area showing distribution of early and mid-Cretaceous intrusions (shaded areas) and the location of U-Pb samples (circled numbers) as discussed in text. Dotted lines represent major roads. Map modified from Gordey and Makepeace, 1999.

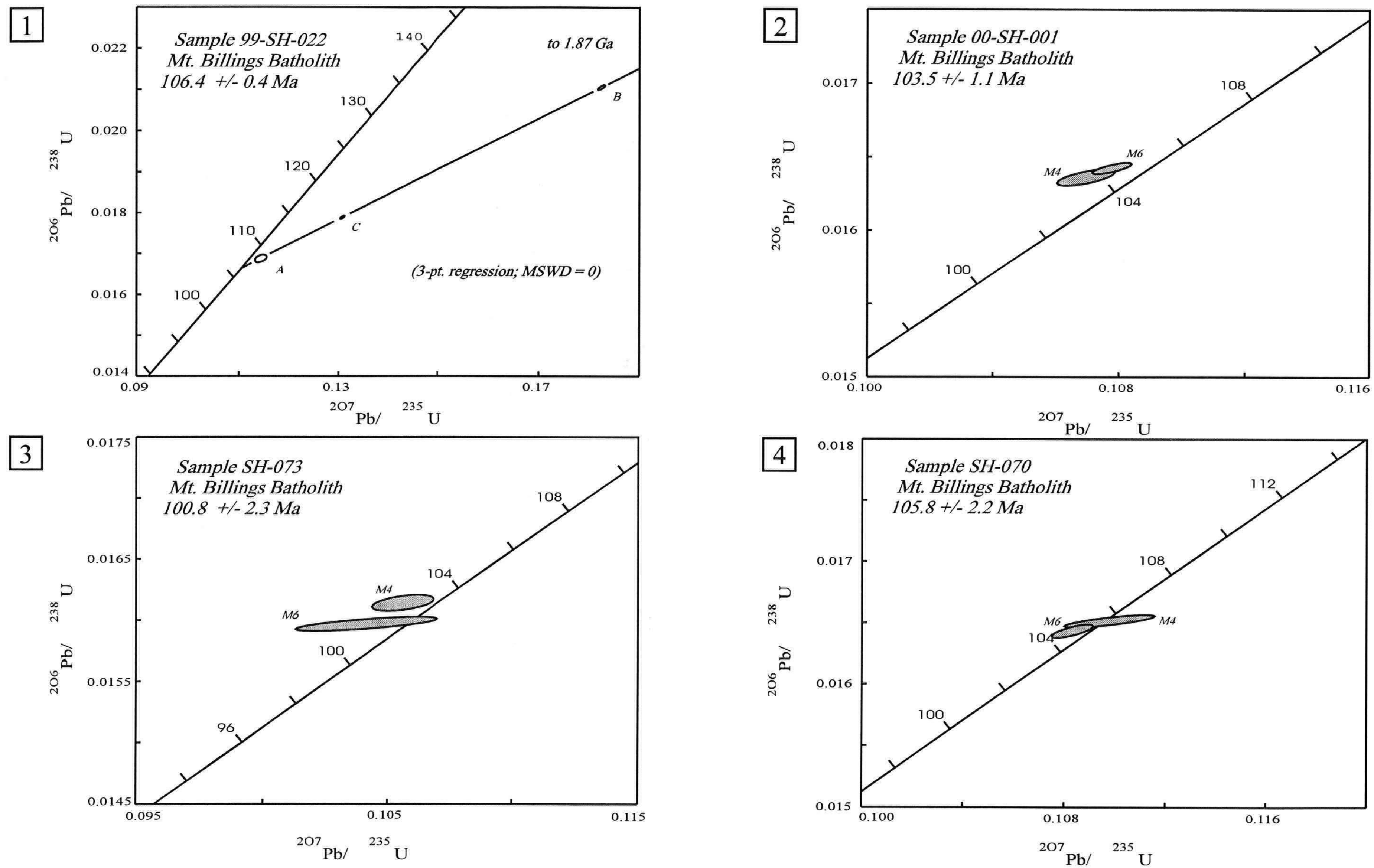

Figure 2.4. U-Pb conchordia plots for intrusions from southeast Yukon and southwest Northwest Territories used in this study. Open, shaded, and striped ellipses denote zircon, monazite, and titanite fractions, respectively. Results and interpretations are discussed in text.

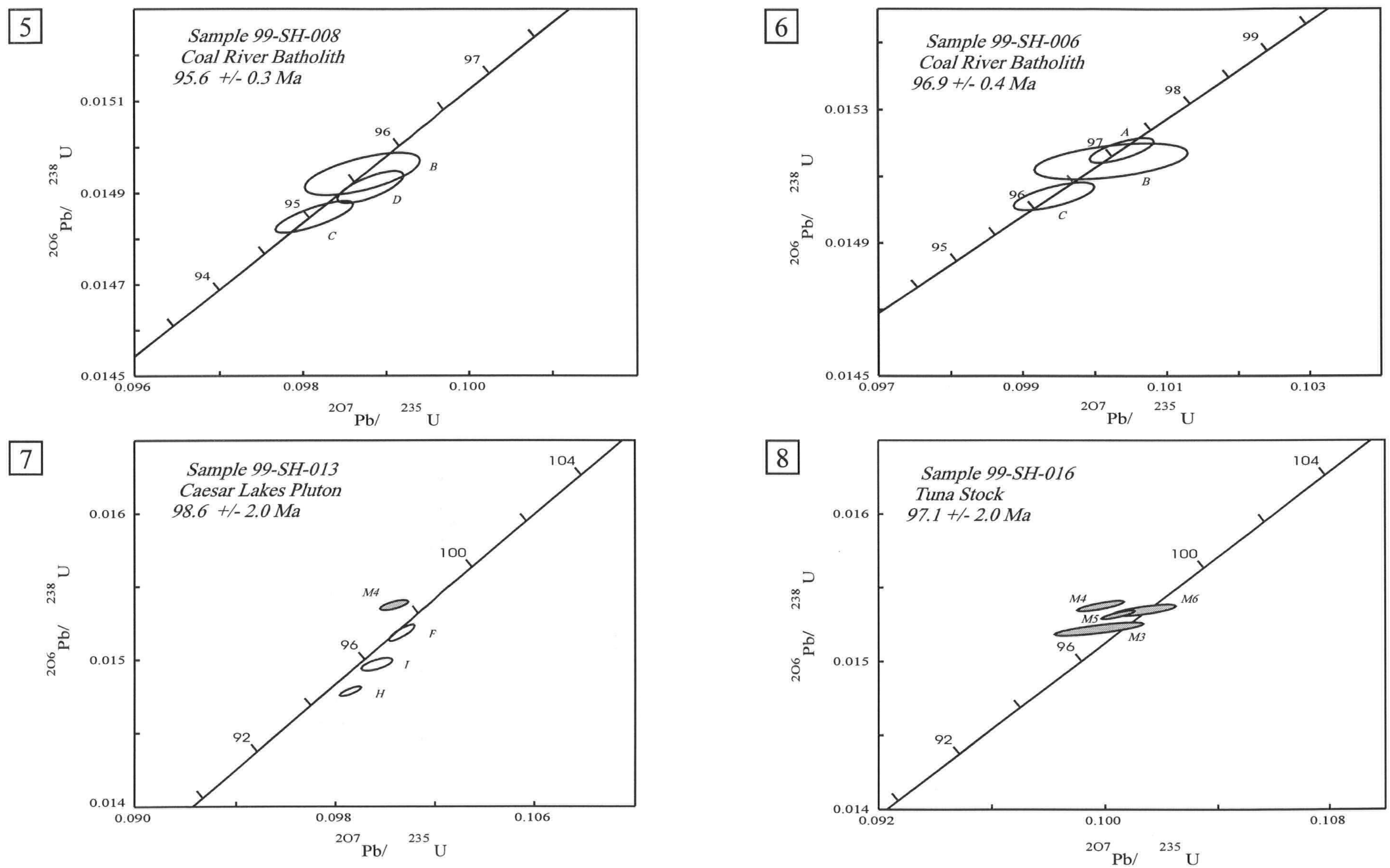

Figure 2.4. continued.

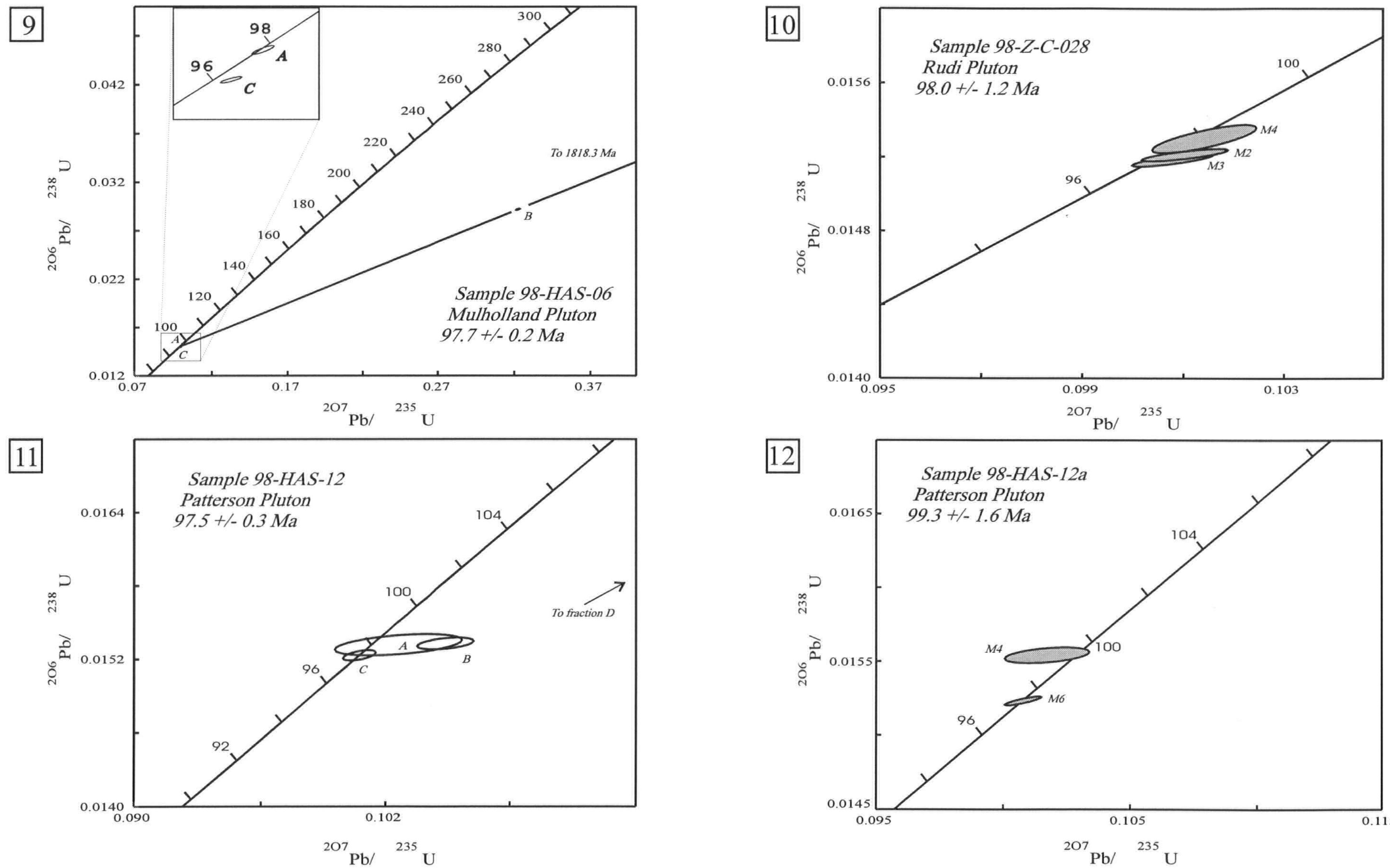

Figure 2.4. continued.

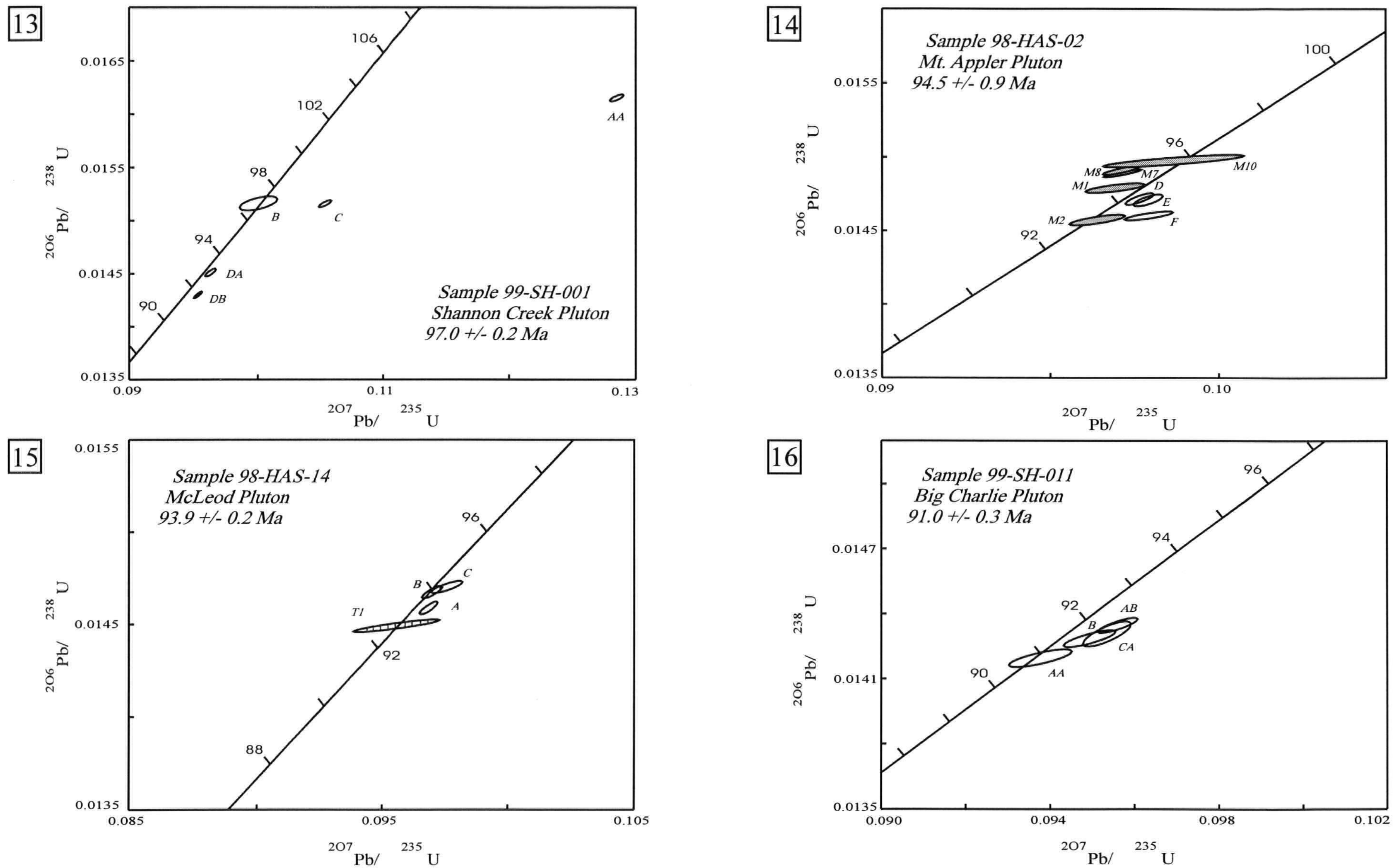

Figure 2.4. continued.

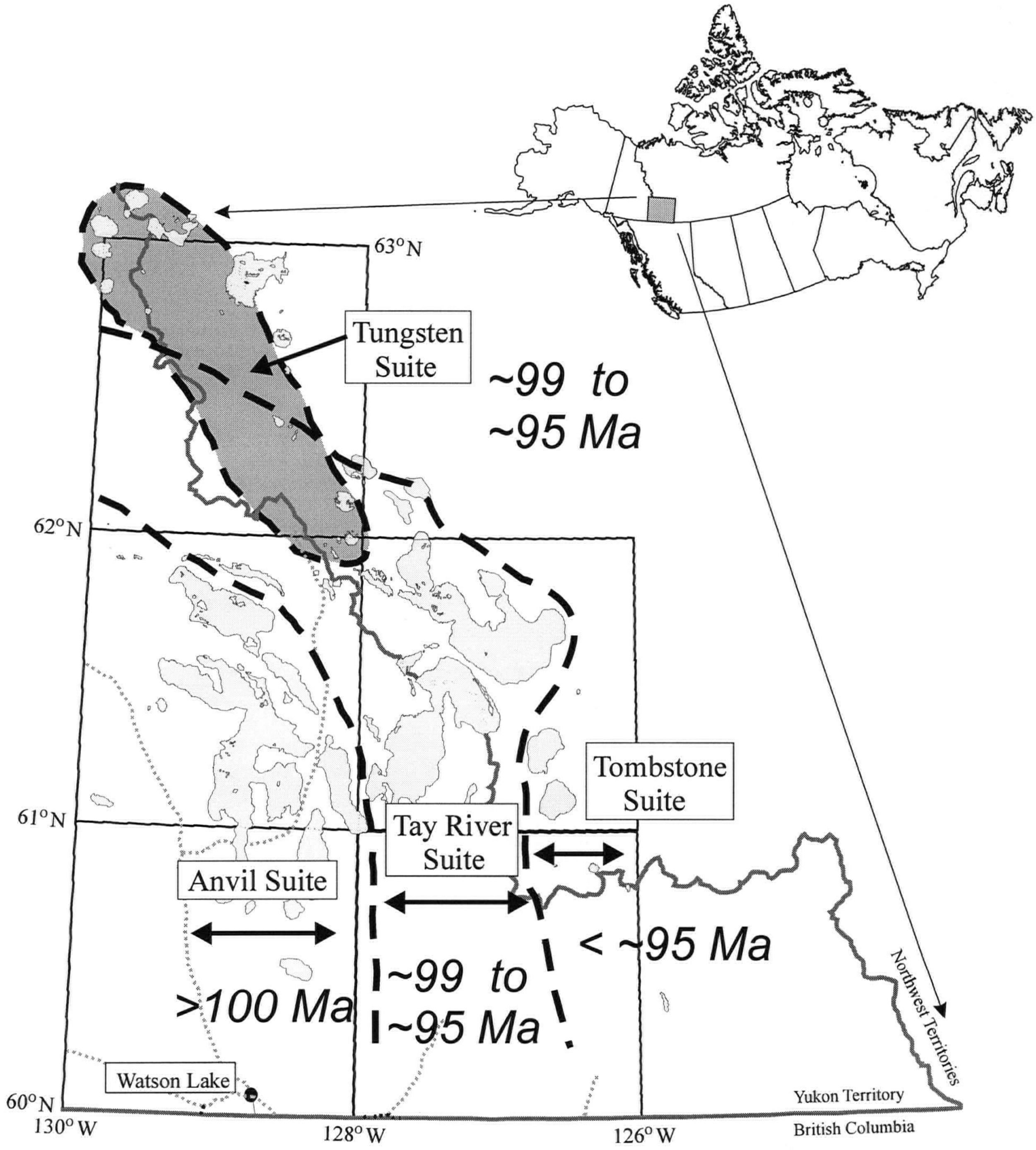

Figure 2.5. Map of study area showing distribution of early and mid-Cretaceous intrusions (light shaded areas). Dashed lines separate designated plutonic suites as discussed in text and the dark shaded area outlines the extent of the overlapping Tungsten suite. Dotted lines represent major roads. Map modified from Gordey and Makepeace, 1999.

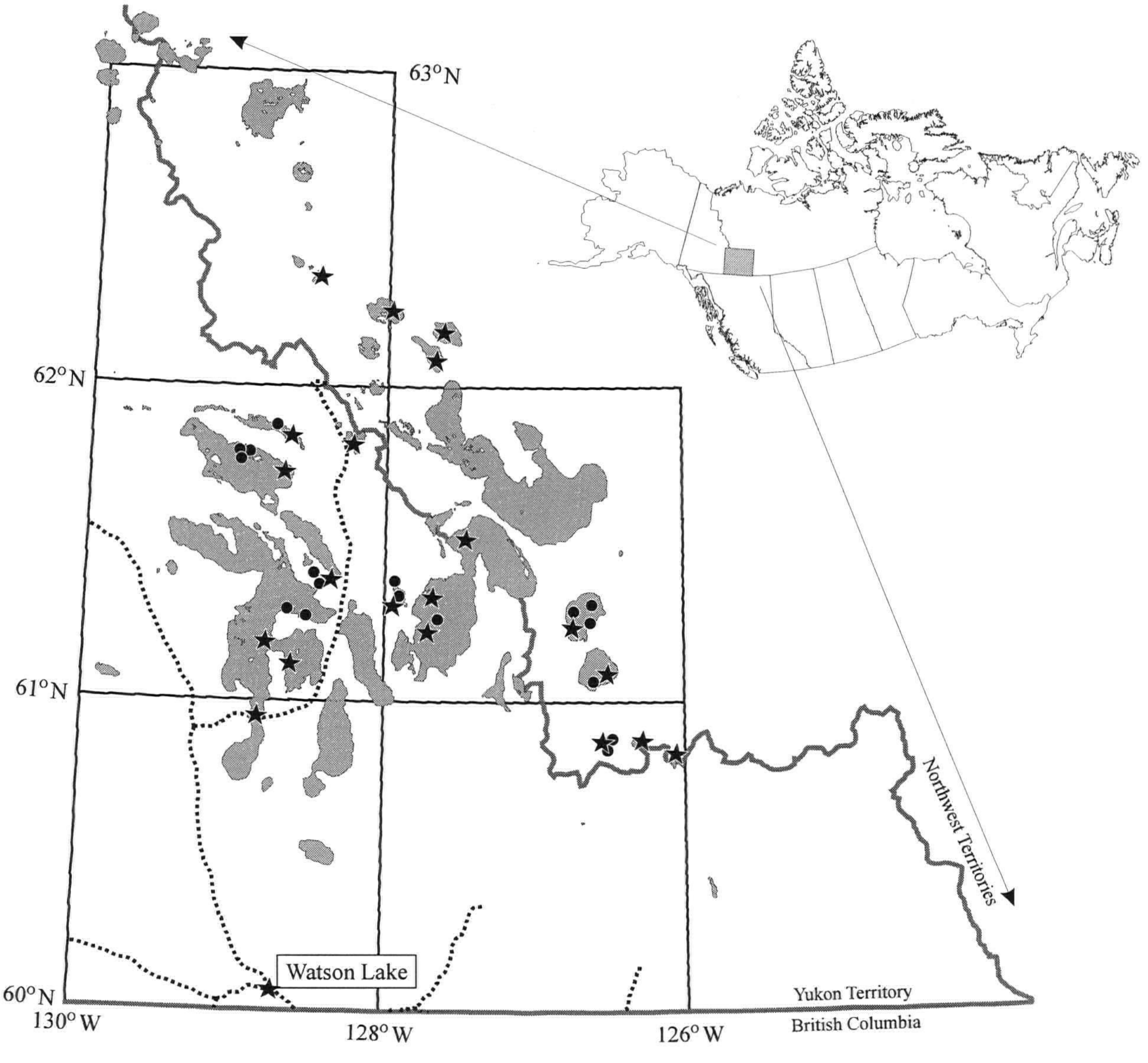

Figure 2.6. Map of study area showing distribution of early and mid-Cretaceous intrusions (shaded areas) and the location of geochem samples: circles denote wholerock analyses and stars denote wholerock plus Sr, Nd, and Pb analyses. Dotted lines represent major roads. Map modified from Gordey and Makepeace, 1999.

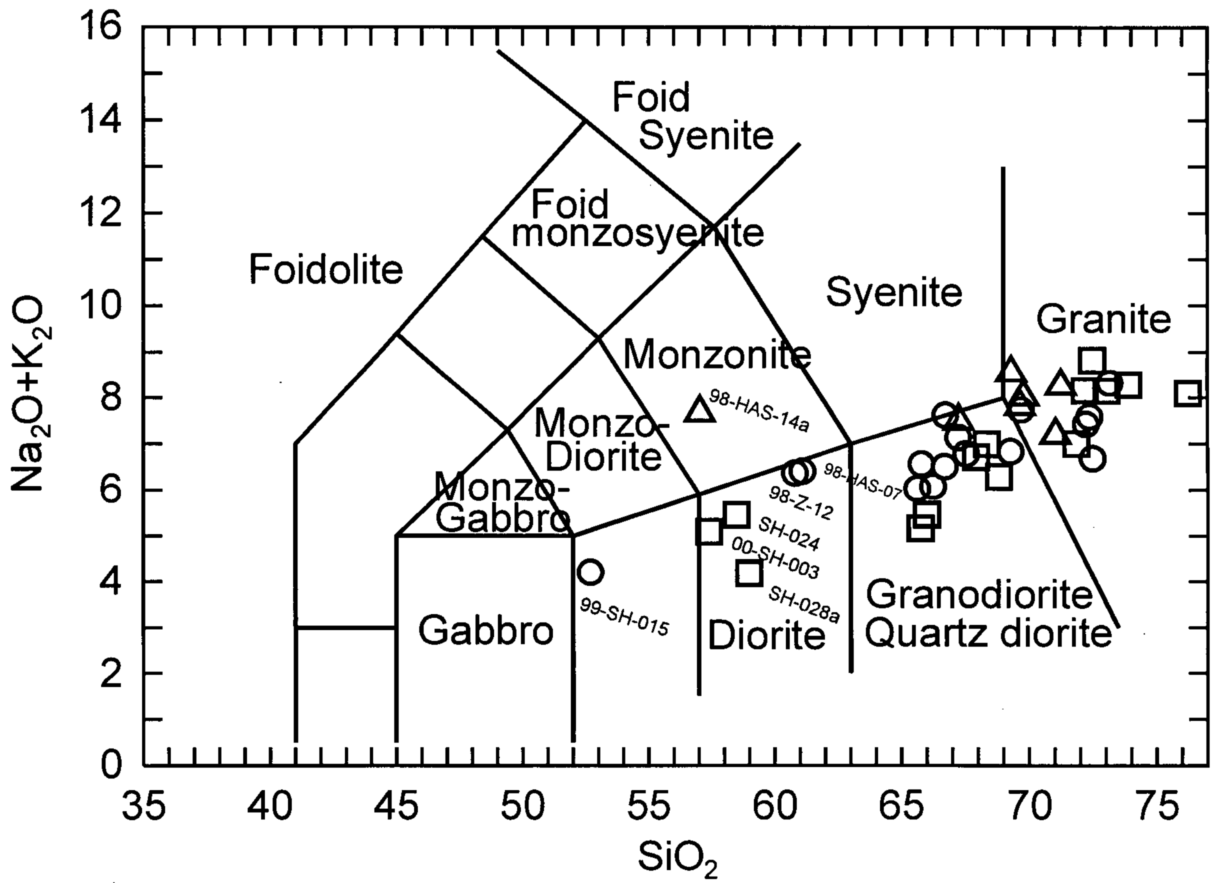

Figure 2.7. Total alkalis versus silica plot (Le Bas et al., 1986) showing range of rock types sampled during the course of this study. Symbols: □ - Anvil suite intrusions, ○ - Tay River suite intrusions, △ - Tombstone suite intrusions.

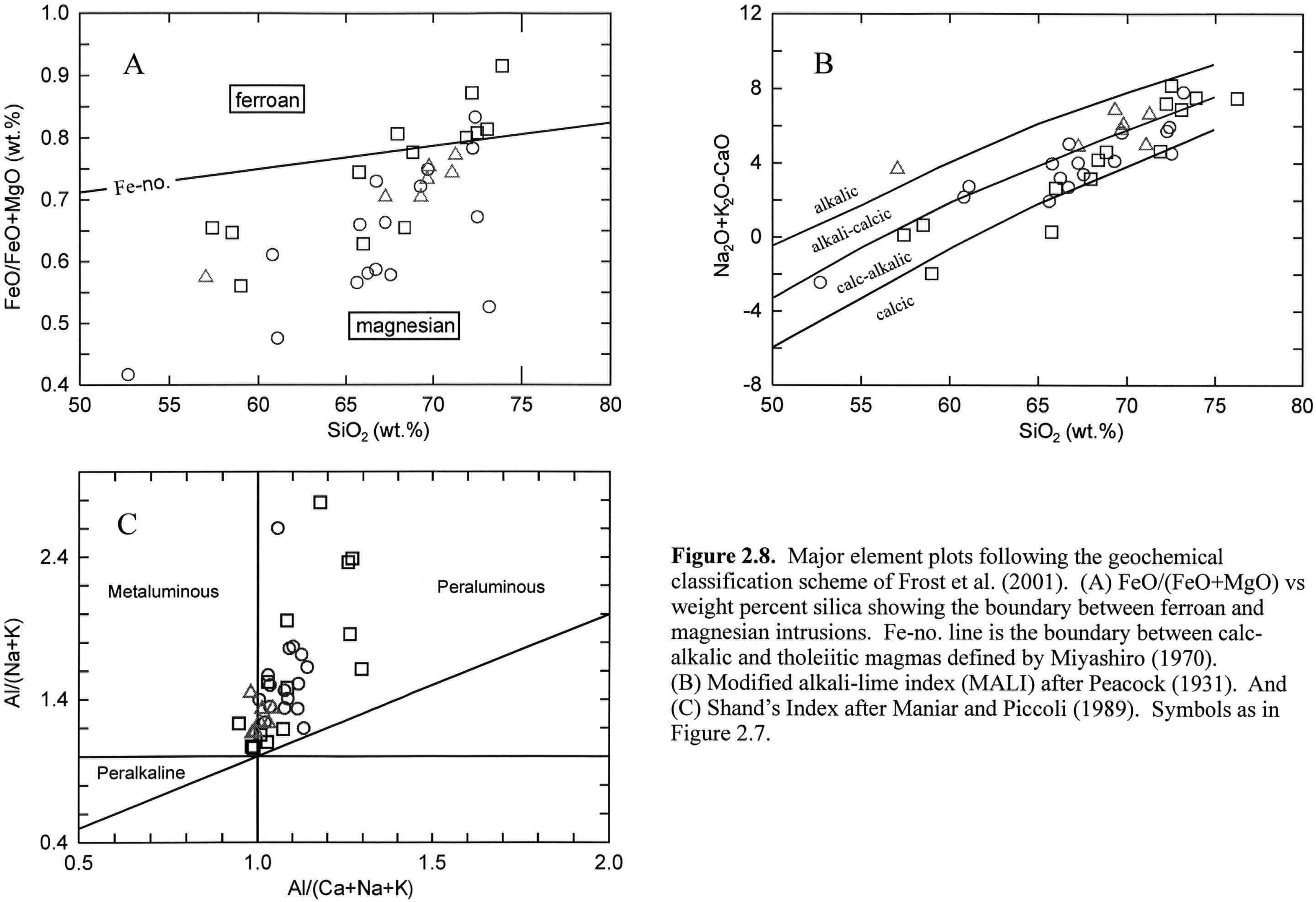

Figure 2.8. Major element plots following the geochemical classification scheme of Frost et al. (2001). (A) FeO/(FeO+MgO) vs weight percent silica showing the boundary between ferroan and magnesian intrusions. Fe-no. line is the boundary between calc-alkalic and tholeiitic magmas defined by Miyashiro (1970). (B) Modified alkali-lime index (MALI) after Peacock (1931). And (C) Shand's Index after Maniar and Piccoli (1989). Symbols as in Figure 2.7.

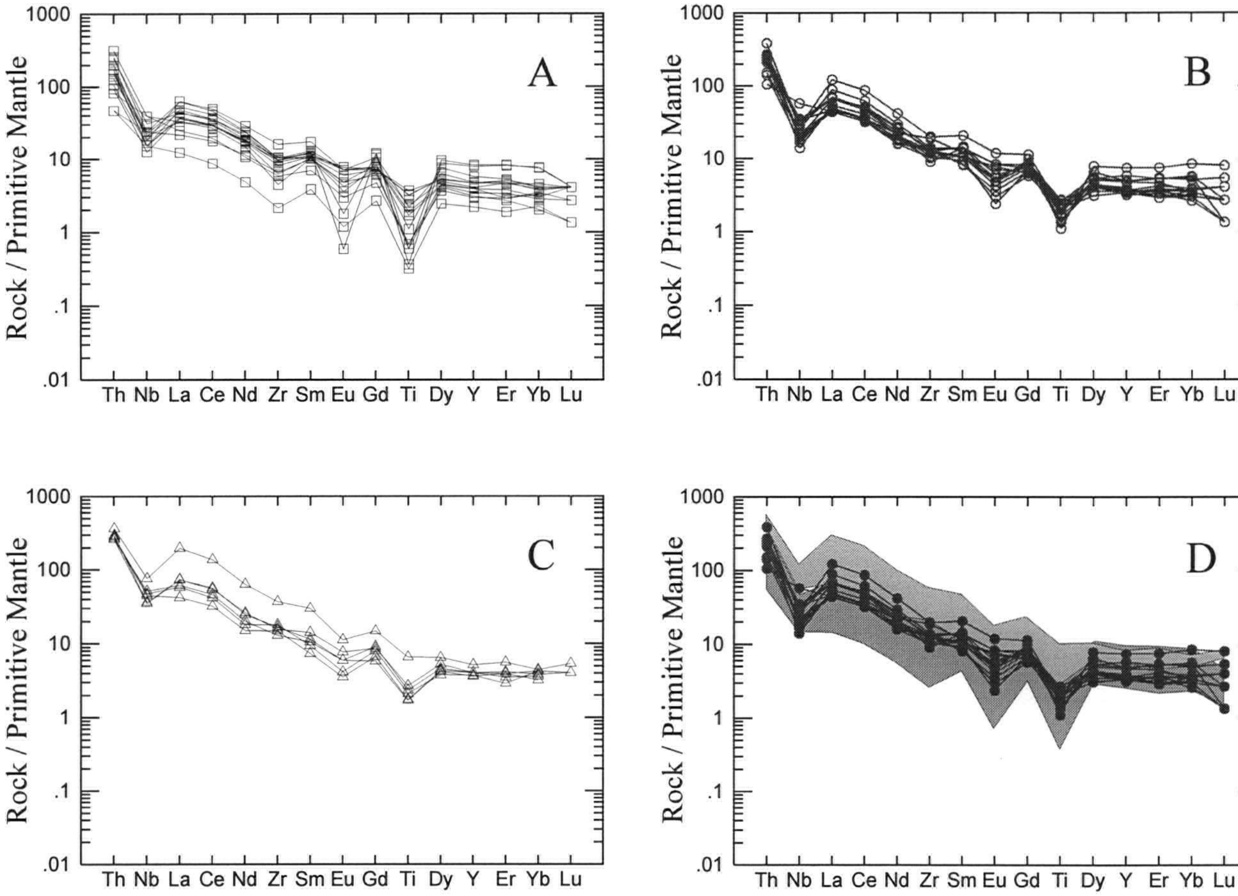

Figure 2.9. Primitive mantle-normallized rare earth element plots of (A) Anvil plutonic suite samples (n=12); (B) Tay River plutonic suite samples (n=19); (C) Tombstone plutonic suite samples (n=6); and (D) TayRiver suite samples with the compositional fields of the Anvil suite samples (dark shaded) and the Tombstone suite samples (light-shaded) in the background for comparison. Primitve mantle values from Sun and McDonough (1989).

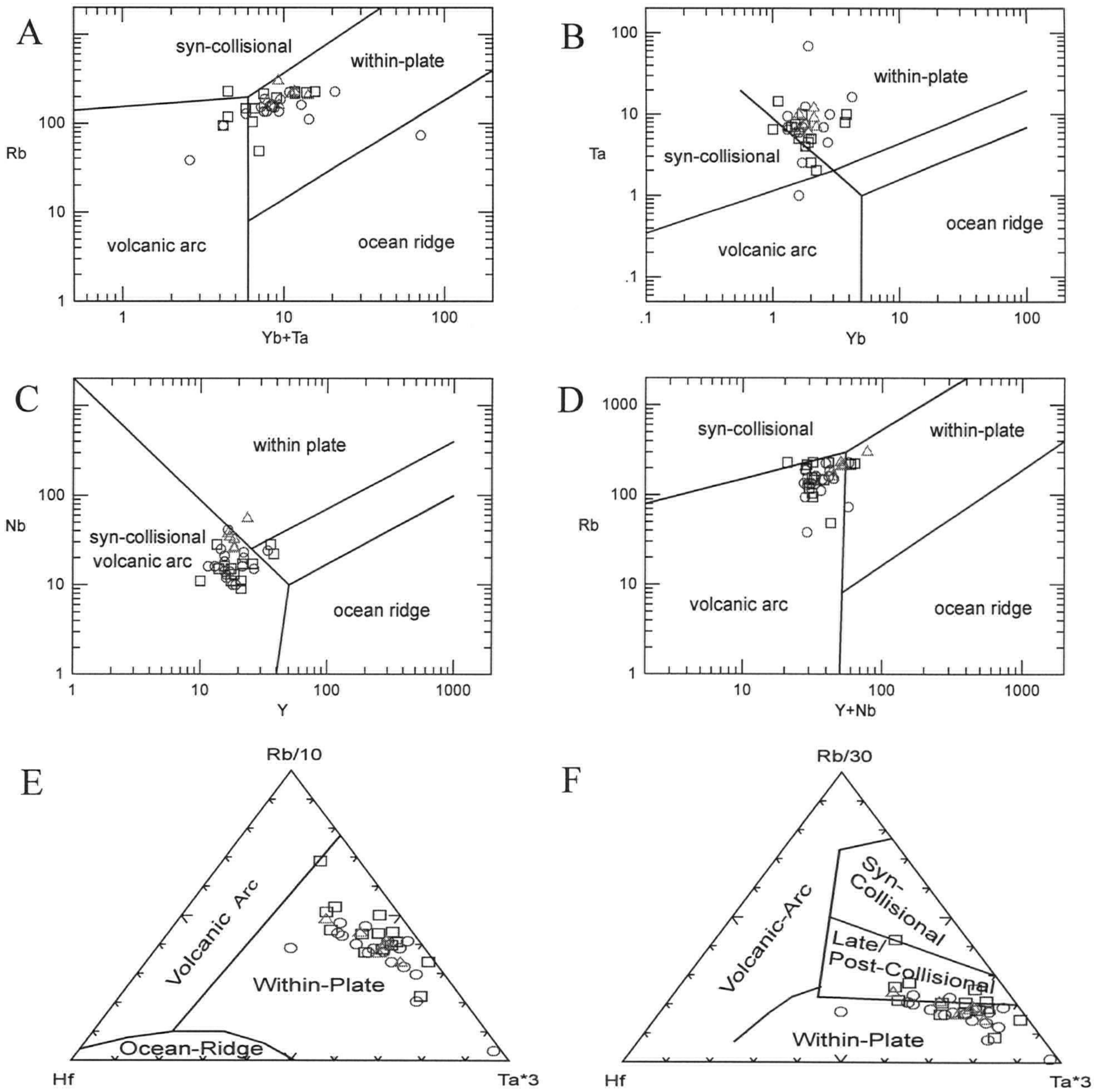

Figure 2.10. (A) Rb-Y, (B) Ta-Yb, (C) Nb-Y, and (D) Rb-Y+Nb discrimination diagrams of Pearce et al. (1984). (E) and (F) Hf-Rb-Ta discrimination diagrams of Harris et al. (1986). Symbols as in Figure 2.7.

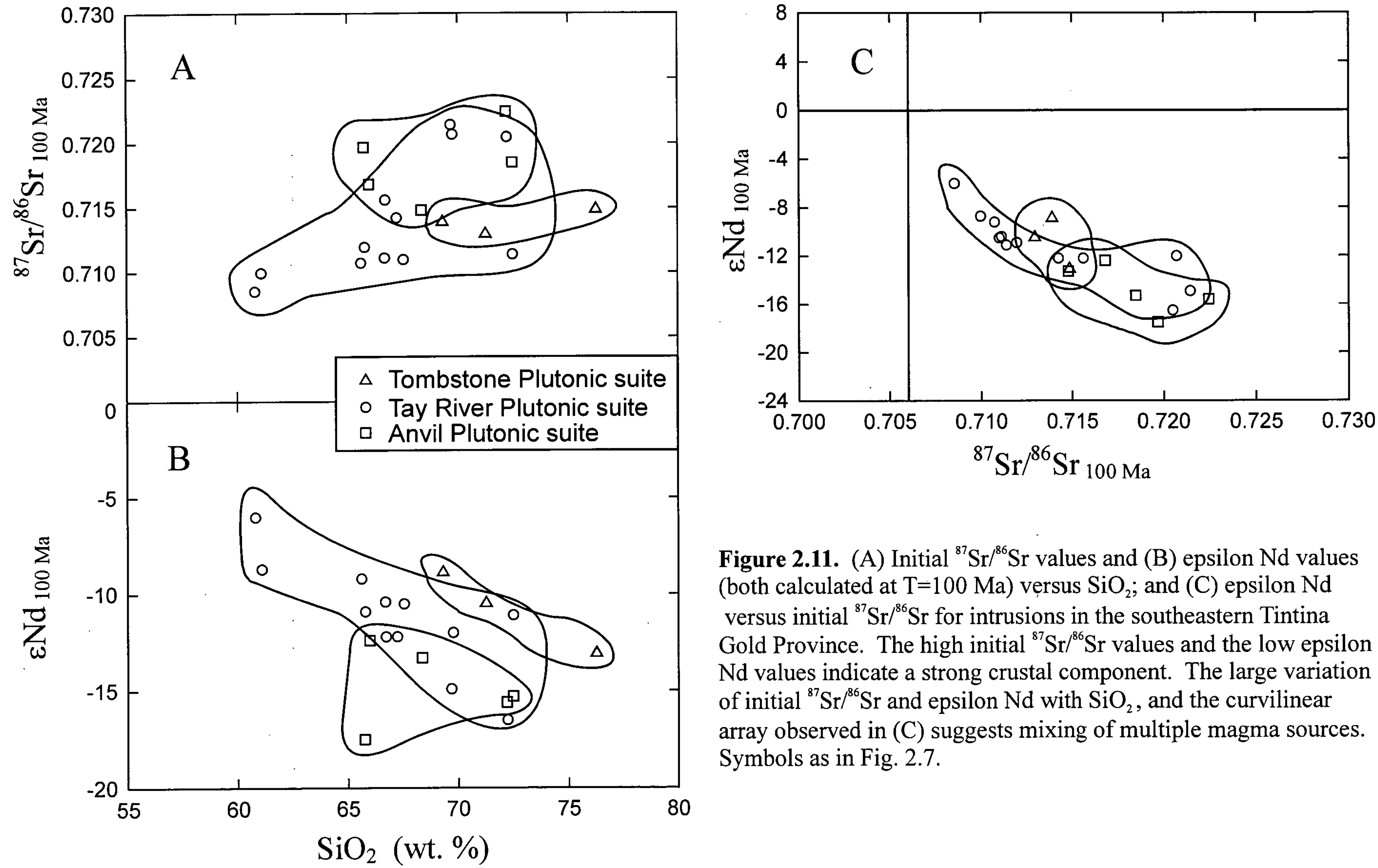

Figure 2.11. (A) Initial $^{87}Sr/^{86}Sr$ values and (B) epsilon Nd values (both calculated at T=100 Ma) versus SiO_2; and (C) epsilon Nd versus initial $^{87}Sr/^{86}Sr$ for intrusions in the southeastern Tintina Gold Province. The high initial $^{87}Sr/^{86}Sr$ values and the low epsilon Nd values indicate a strong crustal component. The large variation of initial $^{87}Sr/^{86}Sr$ and epsilon Nd with SiO_2, and the curvilinear array observed in (C) suggests mixing of multiple magma sources. Symbols as in Fig. 2.7.

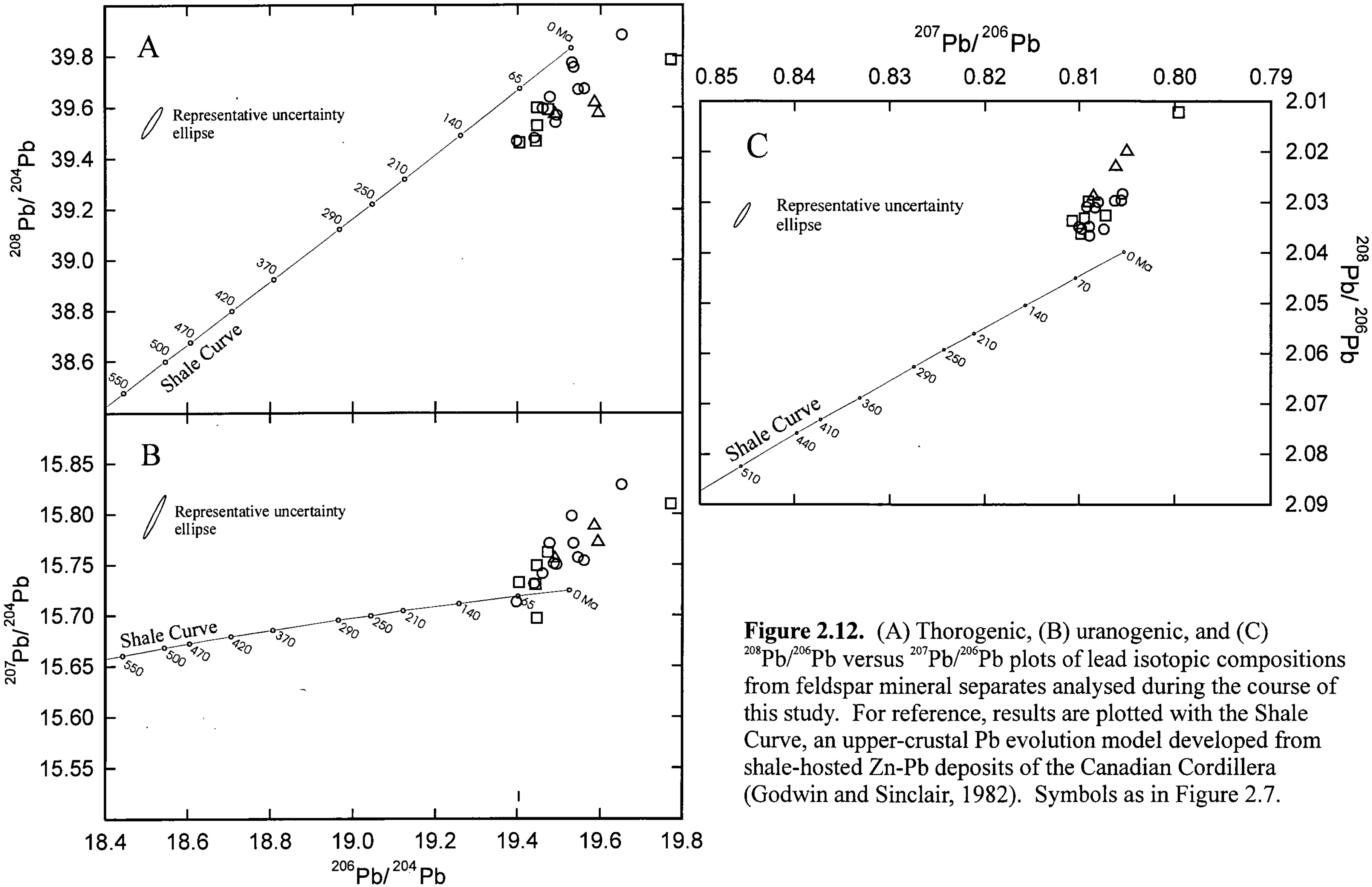

Figure 2.12. (A) Thorogenic, (B) uranogenic, and (C) $^{208}Pb/^{206}Pb$ versus $^{207}Pb/^{206}Pb$ plots of lead isotopic compositions from feldspar mineral separates analysed during the course of this study. For reference, results are plotted with the Shale Curve, an upper-crustal Pb evolution model developed from shale-hosted Zn-Pb deposits of the Canadian Cordillera (Godwin and Sinclair, 1982). Symbols as in Figure 2.7.

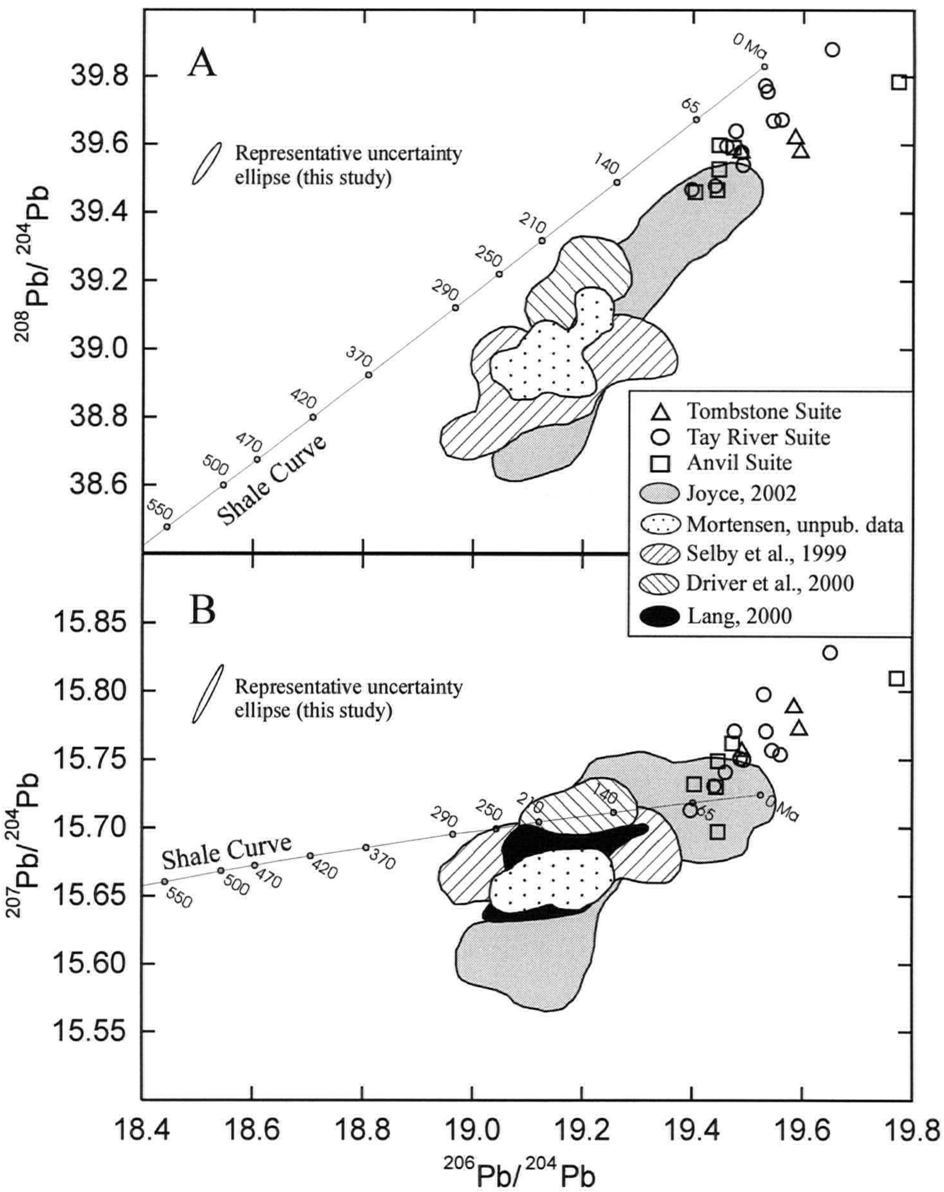

Figure 2.13. (A) Thorogenic and (B) uranogenic plots of feldspar lead isotope compositions from this study plotted against similar data from across the TGP. Shale Curve of Godwin and Sinclair (1982) is shown for reference. Data from Joyce (2002) - Dawson Range Batholith and Moosehorn Range intrusions; Selby et al. (1999) - Dawson Range Batholith; Mortensen unpub. data - Clear Creek area intrusions; Lang et al. (2000) - TPS intrusions; and Driver et al. (2000) - Cassiar Batholith.

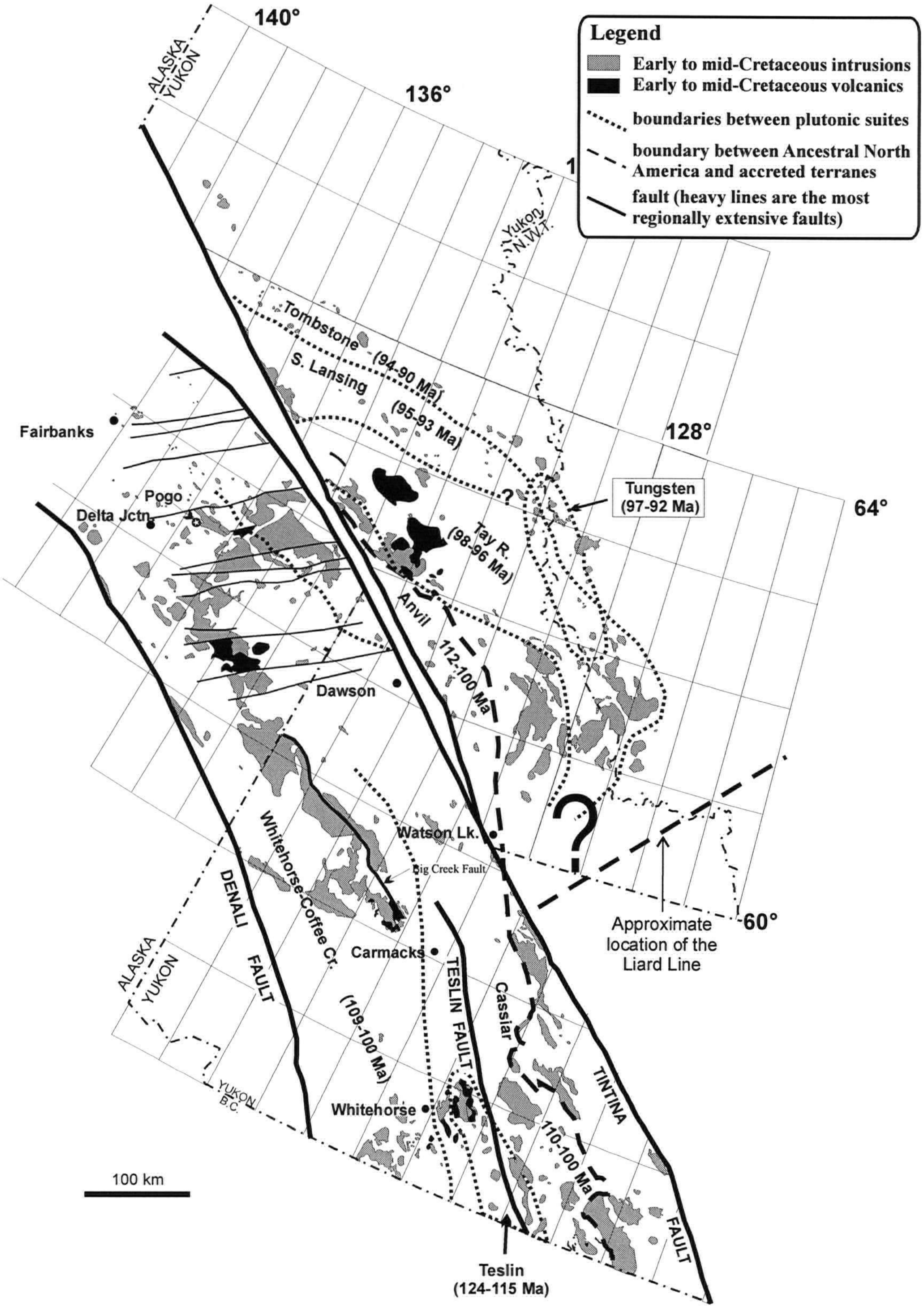

Figure 2.14. Map of study the area showing the distribution of TGP magmatism in mid-Cretaceous time with the ~425 km of dextral strike-slip displacement along the Tintina Fault restored. Dotted lines represent major roads. Map modified from Gordey and Makepeace, 1999.

Chapter 3

Lead isotope signatures of Tintina Gold Province intrusions and associated mineral deposits from southeastern Yukon and southwestern Northwest Territories: Implications for exploration in the southeastern Tintina Gold Province

Introduction

The Tintina Gold Province (TGP) in east-central Alaska, Yukon Territory, and southwestern Northwest Territories is host to numerous styles of precious- and base-metal mineralization thought to be genetically associated with widespread Early to Late Cretaceous magmatism (Fig. 3.1). Styles of mineralization in the TGP are highly variable and include sheeted quartz-feldspar veins, polymetallic replacement bodies, auriferous breccias, disseminated ores, and Au-rich skarns, as well as epithermal vein systems (especially associated with late Cretaceous intrusive and volcanic rocks). In the early 1990's, the discovery of gold deposits such as Fort Knox and Brewery Creek spurred exploration activity, leading to further discoveries at Pogo, Donlin Creek, True North, Dublin Gulch, Ryan Lode, and Scheelite Dome. The rush of exploration success was accompanied by significant research directed at the development genetic and exploration models. The resultant Intrusion-Related Gold Systems (IRGS) model has been continuously evolving since its inception (Thompson et al., 1999; Lang et al., 2000; Hart et al, 2000; and Mineralium Deposita Vol. 36, No. 6).

This paper presents new Pb isotope data from intrusive rocks and several mineral deposits and occurrences from the southeastern portion of the TGP. These data provide insight on metal sources within these systems and hence help to constrain possible relationships between magmatism and mineralization and resulting exploration models.

Regional Metallogeny

A variety of intrusion-hosted and (probably) intrusion-related deposits and occurrences are known in the eastern Selwyn Basin, including W (± base metal) skarns such as Mactung, Cantung, and Lened, Ag-rich base metal skarns and mantos such as Sa Dena Hes, gold-bearing sheeted quartz-feldspar veins (e.g., within the Mactung intrusion), distal, apparently structurally controlled deposits such as Hyland, and massive sulphide replacement deposits such as Quartz Lake (Macmillan) (Fig. 3.2). Indeed, at least 45% of the 325 MINFILE occurrences listed for the six map sheets that comprise the study area (105-A, -H, -I, and 95-D, -E, -L) are definitely or arguably intrusion-related. A discussion of the mineral potential of the eastern Selwyn Basin would not be complete without mention of the numerous SEDEX-type occurrences such as the Howards Pass deposit and the Matt Berry prospect. The combination of both syngenetic and epigenetic exploration targets has led to a considerable amount of interest from exploration companies in the mineral potential of this region for several decades.

Geologic Background

One of the most striking features of the southeastern portion of the TGP is the shear volume of granitic magmatism in the area. At current levels of exposure there is over 5000 km^2 of mid-Cretaceous intrusive rocks exposed within the study area. These intrusions comprise simple to complex, single to multi-phase stocks, plutons and batholiths (Fig. 3.2). Intrusions of the southeastern TGP were emplaced into Late Precambrian to Mesozoic strata of the Selwyn Basin. Stratigraphy of the Selwyn Basin consists mostly of turbiditic sandstones, deep water limestones, shale and chert which were deposited contemporaneously with shallow water carbonates and sandstones of the Mackenzie platform to the north and west (Gordey and Anderson, 1993). Results of geochronological, geochemical and isotopic investigations described in Chapter 2 indicate that the known plutonic suites of the western and northern portions of the TGP (Mortensen et al., 2000) do continue into southeastern Yukon and southwestern Northwest Territories. For further discussion on the regional geology see Chapter 2.

Lead Isotope Study

Lead isotope studies of feldspars separated from various mid-Cretaceous intrusions in the study area, and sulphides from a number of precious- and base metal deposits and occurrences have been carried out in order to investigate possible relationships between mineralization and magmatism.

Samples and Analytical Techniques

Sulphide samples were collected from numerous mineral deposits and occurrences that were examined during the course of this study. The names and brief descriptions of the sampld occurrences are presented in Table 3.1, and sample locations are shown in Figure 3.2. All sample preparation, geochemical separations, and isotopic measurements were done at Pacific Centre for Geochemical and Isotopic Research (PCIGR) at the University of British Columbia. A detailed discussion of samples and analytical techniques for feldspar mineral separates is presented in Chapter 2. For trace lead sulphide samples, approximately 10-50 milligrams of hand picked sulphides minerals were first leached in dilute hydrochloric acid to remove surface contamination and then dissolved in dilute nitric acid. Samples of galena required no leaching and were directly dissolved in dilute hydrochloric acid. Following ion exchange chemistry, approximately 10-25 nanograms of lead in chloride form was loaded on rhenium filaments using a phosphoric acid-silica gel emitter. Isotopic ratios were determined with a modified VG54R thermal ionization mass spectrometer in peak-switching mode on a Faraday detector. Measured ratios were corrected for instrumental mass fractionation of 0.12%/amu based repeated measurements of the NBS 981 standard and the values recommended by Thirwall (2000). Errors were numerically propagated throughout all calculations and are reported at the 2σ level (Table 3.2).

Results

Lead isotopic analyses of feldspar and sulphide mineral separates are presented in Table 3.2 and are plotted with reference to the upper-crustal Pb evolution model (Shale Curve) of Godwin and Sinclair (1982) in Figure 3.3. The Shale Curve is of particular relevance to this study as it is based on the Pb isotope compositions of shale-hosted Zn-Pb deposits located within the Canadian Cordillera miogeocline. The new data is plotted together with previously determined Pb isotopic compositions for other sulphide occurrences in the area (discussed later).

Analyses of feldspar from intrusions throughout the region generally yield quite consistent Pb isotopic compositions (Table 3.2), with the exception of one sample (SH-011E-INT) collected from the Mt. Billings, which returned significantly more radiogenic values. The Pb isotopic compositions (n=19) range from 19.397 to 19.651 for $^{206}Pb/^{204}Pb$, 15.697 to 15.829 for $^{207}Pb/^{204}Pb$, 39.461 to 39.883 for $^{208}Pb/^{204}Pb$, 0.805 to 0.811 for $^{207}Pb/^{206}Pb$, and 2.020 to 2.037 for $^{208}Pb/^{206}Pb$.

Analyses for sulphide samples collected from spatially associated mineral occurrences also yield similar Pb isotopic compositions (Table 3.2). Exceptions include three samples (SH-073-1, SH-070-1 and -2) from the Tai and Cali mineral occurrences at the north end of the Mt. Billings Batholith (Fig. 3.2), which returned the least radiogenic $^{207}Pb/^{206}Pb$, and $^{208}Pb/^{206}Pb$ ratios from this study. The majority of analyses (n=9) yield narrow ranges of $^{206}Pb/^{204}Pb$, $^{207}Pb/^{204}Pb$, $^{208}Pb/^{204}Pb$, $^{207}Pb/^{206}Pb$, and $^{208}Pb/^{206}Pb$ ratios with values of 19.396 to 19.615, 15.711 to 15.904, 39.391 to 40.039, 0.806 to 0.811, and 2.024 to 2.041, respectively.

Discussion

The feldspar Pb isotopic compositions are highly radiogenic, plotting above the Shale Curve of Godwin and Sinclair (1982), indicating the intrusions are largely, if not entirely, product of the partial melting of Selwyn Basin-like sedimentary rocks (see Chapter 2 for further discussion). Pb isotopic compositions of most sulphide occurrences proximal to the plutons are very similar to feldspar Pb isotopic compositions from the plutons themselves. This is consistent with the metals having been derived mainly from the plutons.

In the case of the past producing Sa Dena Hes Zn-Pb-Ag skarn, sulphide Pb compositions plot within the cluster of Cretaceous intrusion feldspars and associated sulphides. Rare felsic and andesitic dykes are known to be associated with, and possibly related to mineralization at the mine but have not been dated directly. The similarity in Pb ratios suggests that the deposit is also mid-Cretaceous in age.

Lead isotopic compositions from the Quartz Lake (Macmillan) occurrence in the southeastern part of the study area (Fig. 3.2) are much more radiogenic than any of the other sulphides or feldspars from the area. The implications of this are uncertain. It could indicate that the metals in the Quartz Lake deposit were derived from an intrusive phase that is much more radiogenic than any recognized thus far in the study area, that the metals were derived mainly from sedimentary sources and are completely unrelated to the plutons, or possibly represent a mixture of igneous and sedimentary Pb.

Lead isotopic compositions of sulphides from the Hyland Gold occurrence, a gold-rich, base-metal poor deposit located near the Quartz Lake occurrence, are not yet available. This occurrence has been suggested to represent a proximal style of intrusion-related mineralization. If this model is correct, the Hyland gold mineralization would be expected to yield Pb isotopic compositions intermediate between the Quartz Lake values and the cluster of Cretaceous intrusive feldspars and associated sulphides.

The sulphide Pb isotopic compositions are very different from typical SEDEX-type Pb-Zn occurrences in the Selwyn Basin (Fig. 3.3), indicating that none of the occurrences represent remobilized SEDEX-type mineralization.

Conclusions

The primary goal of this study was to compare and contrast the Pb isotope compositions of feldspars from various intrusions and sulphides from associated precious- and base metal deposits and occurrences within the southeastern TGP in order to investigate possible linkages between magmatism and mineralization. Results from this study indicate that the metals in many mineral deposits (and prospects) in the region are mostly derived from the mid-Cretaceous TGP intrusions. In an area with such voluminous magmatism, these results also serve to highlight the exploration potential throughout the study area.

References

Deklerk, R. (compiler) 2003. Yukon MINFILE – A database of mineral occurrences. Yukon Geology Survey, CD-ROM.

Godwin, C.I. and Sinclair, A.J. 1982. Average lead isotope growth curves for shale-hosted zinc-lead deposits, Canadian Cordillera. Economic Geology **77:** 208-211.

Godwin C.I., Gabites, J.E. and Andrew, A. 1988. Leadtable: A galena lead isotope database for the Canadian Cordillera. *In:* British Columbia Ministry of Energy and Mines and Petroleum Resources Paper 1988-4, 214.

Gordey, S.P. and Anderson, R.G. 1993. Evolution of the northern Cordillera Miogeocline, Nahanni Map Area (105I), Yukon and Northwest Territories. Geological Survey of Canada Memoir 428, 214 p.

Gordey, S.P. and Makepeace, A.J. 1999. Yukon Digital Geology, S.P. Gordey and A.J. Makepeace (comp.); Geological Survey of Canada, Open File D3826, and Exploration and Geological Services Division, Yukon, Indian and Northern Affairs Canada, Open File 1999-1(D).

Gordey, S.P. and Makepeace, A.J. (compilers) 2001. Bedrock Geology, Yukon Territory. *In:* Geological Survey of Canada, Open File 3754 and Exploration and Geological Services Division, Yukon Indian and Northern Affairs Canada, Open File 2001-1, scale 1:1 000 000.

Hart, C.J.R., McCoy, D.T., Goldfarb, R.J., Smith, M., Roberts, P., Hulstein, R., Bakke, A.A. and Bundtzen, T.K. 2002. Geology, exploration and discovery in the Tintina Gold Province, Alaska and Yukon. *In:* Society of Economic Geologists Special Publication 9, Integrated Methods for Discovery: Global Exploration in the 21st Century, p.241-274.

Krogh, T.E. 1982. Improved accuracy of U-Pb zircon ages by the creation of more concordant systems using an air abrasion technique. Geochimica et Cosmochimica Acta **46:** 637-649.

Lang, J.R., Thompson, J.F., Mortensen, J.K., Baker, C.J.R., Coulsen, I.M., Duncan, R. and Maloof, T. 2001. Tombstone-Tungsten Belt. *In:* Lang, J. (ed.), Regional and System-scale controls on the formation of copper and/or gold magmatic-hydrothermal mineralization. Mineral Deposit research Unit, Special Publication Number 2, January 2001, 115p.

Mortensen, J.K., Hart, C.J.R., Murphy, D.C. and Heffernan, S. 2000. Temporal evolution of Early and mid-Cretaceous magmatism in the Tintina Gold Belt. *In:* The Tintina Gold Belt: Concepts, Exploration and Discoveries, British Columbia and Yukon Chamber of Mines, Special Volume 2, p. 49-58.

Thompson, J.F.H., Sillitoe, R.H., Baker, T., Lang, J.R. and Mortensen, J.K. 1999. Intrusion-related gold deposits associated with tungsten-tin provinces. Mineralium Deposita **34** No.4:323-334.

Thirwall, M.F. 2000. Inter-laboratory and other errors in Pb isotope analyses investigated using a ^{207}Pb-^{204}Pb double spike. Chemical Geology **163:** 299-322.

Table 3.1. Location and basic descriptions of skarn deposits and occurrences examined during this study.

Occurrence/ Deposit	Minfile Reference	Commodities	Location* Northing	Easting	Status	Samples
Tai	#105H 073	W, Cu, Zn, Mo	6854191	497966	drilled prospect	SH-073-1, SH-073-2
Cali	#105H 070	W, Cu, Ag	6845327	518253	drilled prospect	SH-070, SH-070s
Flip	#105H 005	Ag, Pb, Zn, W, Cu	6778677	518322	prospect	SH-005-1
Max	#105H 011	Pb, Zn, Ag, W, Cu	6795031	515542	drilled prospect	SH-011E-1 to -4
Fir Tree	#105H 029	Pb, Zn, Ag, Cu, W	6808645	529674	drilled prospect	SH-028-1, SH-029-2
Sa Dena Hes (Mt. Hundere)	#105A 012	Zn, Pb, Ag	6709115	506817	past underground producer	SH-SDH (this study), 10138-001, -002, 501

Note: Italicized samples refer to data compiled from Godwin et al. (1988).

Table 3.2. Pb isotope data from feldspar and sulphide mineral separates analyzed during this study.*

Sample	Mineral	$^{206}Pb/^{204}Pb$	2σ,%	$^{207}Pb/^{204}Pb$	2σ,%	$^{208}Pb/^{204}Pb$	2σ,%	$^{207}Pb/^{206}Pb$	2σ,%	$^{208}Pb/^{206}Pb$	2σ,%
98-HAS-02	fs	19.490	0.032	15.757	0.045	39.541	0.064	0.80844	0.017	2.02878	0.032
98-HAS-03	fs	19.440	0.032	15.731	0.045	39.480	0.064	0.80920	0.017	2.03090	0.032
98-HAS-06	fs	19.487	0.037	15.751	0.048	39.578	0.069	0.80830	0.019	2.03103	0.036
98-HAS-07	fs	19.560	0.044	15.754	0.054	39.673	0.071	0.80541	0.017	2.02830	0.032
98-HAS-12	fs	19.534	0.081	15.771	0.079	39.757	0.102	0.80736	0.040	2.03530	0.044
98-HAS-14	fs	19.594	0.032	15.772	0.045	39.577	0.064	0.80496	0.017	2.01991	0.032
98-Z-12	fs	19.651	0.113	15.829	0.116	39.883	0.126	0.80553	0.022	2.02960	0.033
98-Z-C028	fs	19.493	0.033	15.750	0.046	39.569	0.065	0.80797	0.017	2.02993	0.032
99SH-001	fs	19.404	0.032	15.732	0.045	39.461	0.064	0.81076	0.017	2.03365	0.032
99SH-006	fs	19.477	0.098	15.771	0.102	39.640	0.113	0.80975	0.022	2.03526	0.034
99SH-008	fs	19.460	0.087	15.741	0.092	39.596	0.103	0.80893	0.018	2.03480	0.033
99SH-011	fs	19.585	0.032	15.788	0.045	39.618	0.064	0.80612	0.017	2.02294	0.032
99SH-023	fs	19.447	0.040	15.749	0.049	39.598	0.071	0.80983	0.021	2.03621	0.039
SH-005-INT	fs	19.447	0.242	15.697	0.239	39.528	0.251	0.80718	0.053	2.03259	0.046
SH-073-INT	fs	19.473	0.033	15.762	0.046	39.591	0.064	0.80943	0.017	2.03317	0.032
99SH-009	fs	19.545	0.037	15.757	0.049	39.670	0.067	0.80621	0.017	2.02969	0.032
99SH-013	fs	19.397	0.034	15.713	0.047	39.469	0.065	0.81007	0.017	2.03484	0.032
99SH-016	fs	19.530	0.041	15.798	0.047	39.774	0.071	0.80890	0.027	2.03658	0.035
SH-011E-INT	fs	19.772	0.036	15.810	0.048	39.786	0.066	0.79962	0.017	2.01221	0.032
SH-029-INT	fs	19.444	0.034	15.730	0.047	39.467	0.065	0.80899	0.017	2.02983	0.032
SH-005-1	po	19.579	0.047	15.775	0.057	39.750	0.073	0.80569	0.017	2.03022	0.033
SH-011E-1	gl	19.473	0.032	15.731	0.045	39.482	0.064	0.80787	0.017	2.02757	0.032
SH-011E-2	gl	19.491	0.033	15.752	0.046	39.545	0.064	0.80817	0.017	2.02888	0.032
SH-011E-3	cp	19.615	0.040	15.904	0.049	40.039	0.069	0.81080	0.021	2.04126	0.033
SH-011E-4	py	19.494	0.034	15.758	0.046	39.594	0.065	0.80832	0.017	2.03107	0.033
SH-029-1	gl	19.396	0.036	15.728	0.047	39.445	0.066	0.81092	0.019	2.03373	0.033
SH-029-2	po	19.467	0.033	15.795	0.046	39.709	0.065	0.81136	0.017	2.03979	0.032
SH-070	po	20.550	0.045	15.702	0.049	40.003	0.074	0.76406	0.031	1.94663	0.037
SH-070s	po	21.106	0.146	15.843	0.212	42.657	0.281	0.75066	0.070	2.02121	0.139
SH-073-1	po	19.915	0.150	15.797	0.214	39.648	0.283	0.79325	0.072	1.99101	0.139
SH-073-2	po	19.513	0.104	15.780	0.109	39.500	0.118	0.80873	0.017	2.02436	0.032
SH-SDH	gl	19.397	0.033	15.711	0.045	39.391	0.067	0.80998	0.019	2.03081	0.036

* All analyses conducted in the Pacific Centre for Geochemical and Isotopic Research at the University of British Columbia.

Mineral abbreviations: fs - feldspar; po - pyrrhotite; gl - galena; cp - chalcopyrite; py - pyrite

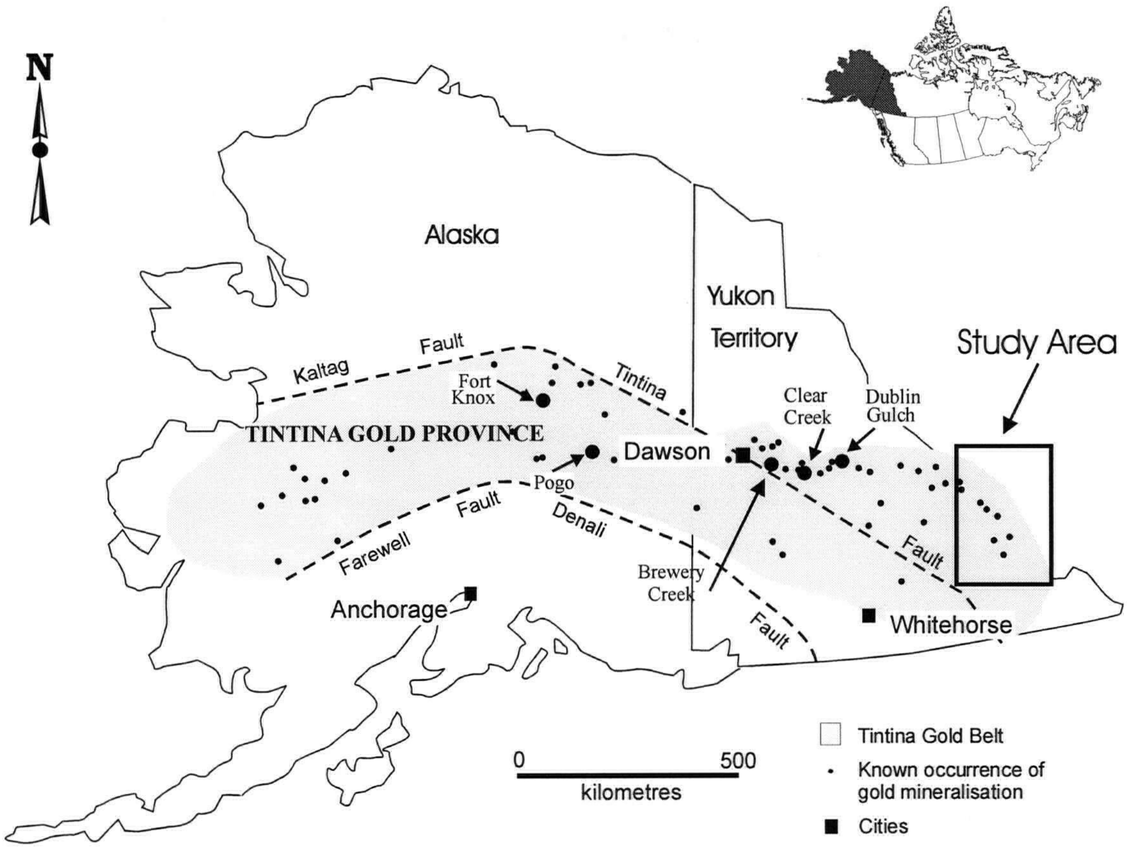

Figure 3.1. Map of Alaska State and Yukon Territory showing the extent of the Tintina Gold Province and the locations of significant gold deposits and occurrences within (after Mortensen et al., 2000). The main study area is outlined at right.

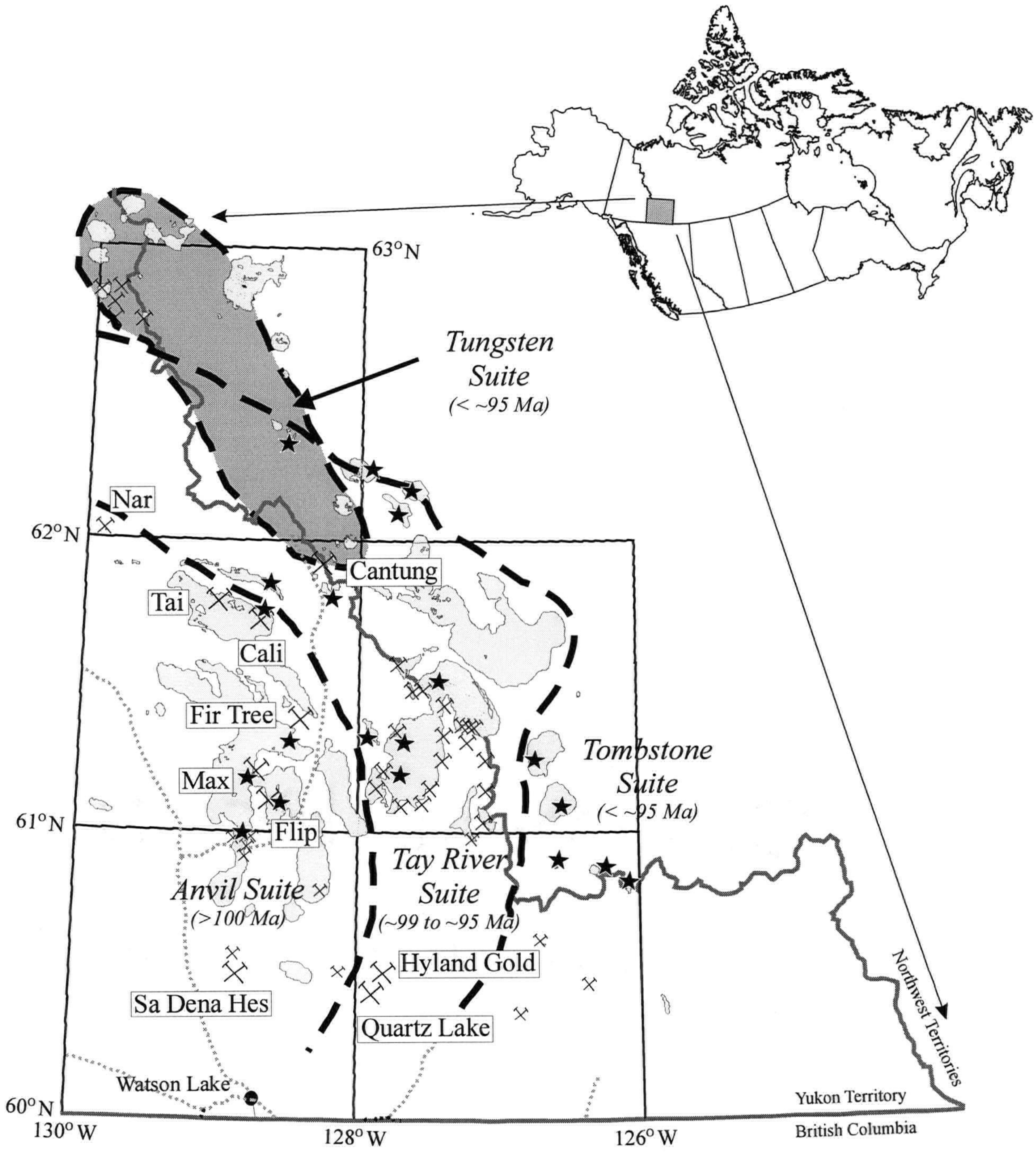

Figure 3.2. Map of study area showing the location of intrusion-related deposits discussed in text and occurrences and the distribution of early and mid-Cretaceous intrusions (light shaded areas). Stars denote the location of feldspar (mineral separates) samples used in this study. Dashed lines separate designated plutonic suites as discussed in text and the dark shaded area outlines the extent of the overlapping Tungsten suite. Dotted lines represent major roads. Map modified from Gordey and Makepeace, 1999.

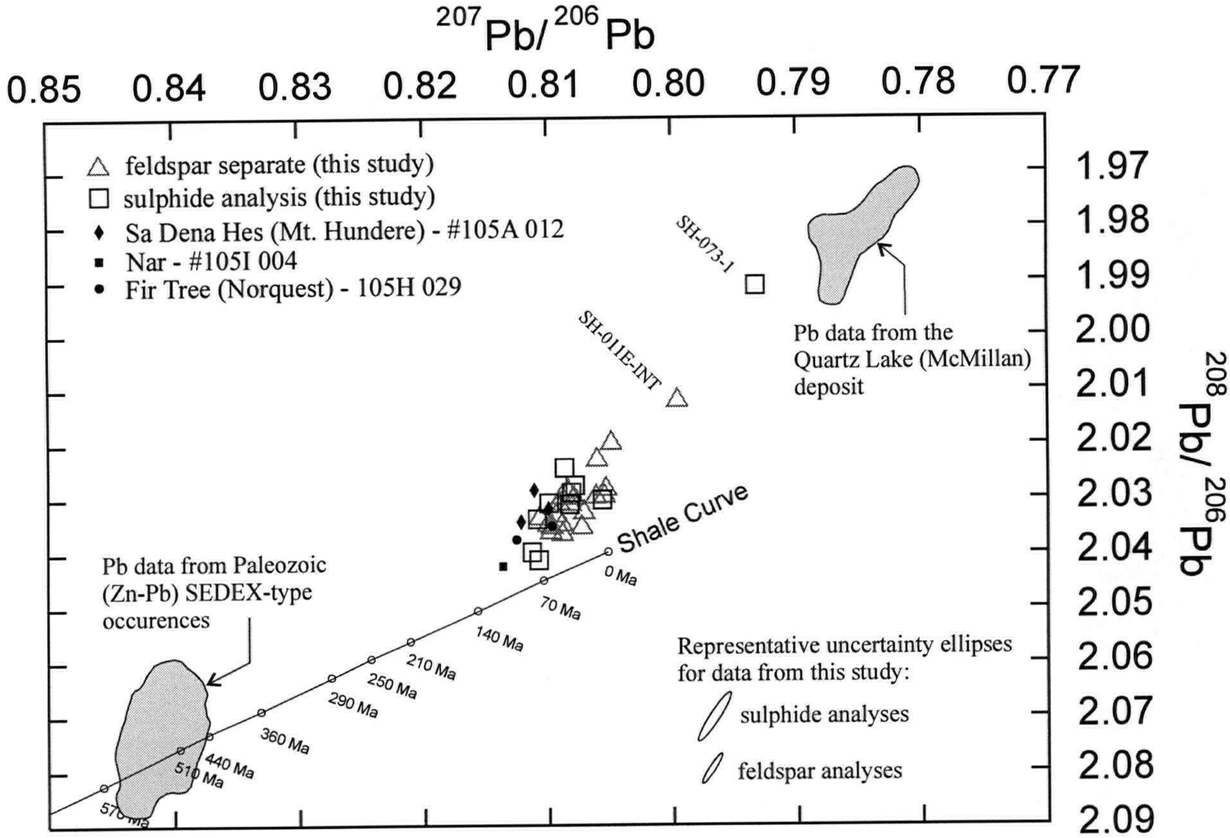

Figure 3.3. $^{207}Pb/^{206}Pb$ versus $^{208}Pb/^{206}Pb$ plot of Pb data from this study plotted and similar data compiled from Godwin et al. (1988) for other mineral occurrences and deposits from within the study area. Pb data for the Paleozoic SEDEX-type occurrences includes data from the Howards Pass, Matt Berry, Mel-Hoser, Maxi, and Pas occurrences. Shale Curve of Godwin and Sinclair (1982) is shown for reference.

Chapter 4

Summary and Directions for Future Research

Summary

Mid-Cretaceous magmatism in the Tintina Gold Province (TGP) of southeastern Yukon and southwestern Northwest Territories represents some of the most prolific, yet poorly studied granitic magmatism of the northern Canadian Cordillera. Geochronological, lithogeochemical, and isotopic data produced during the course of this study provides a temporal and geochemical framework for mid-Cretaceous magmatism in the southeastern TGP. The data confirm the continuation of known plutonic suites from the northern and western portions of the TGP, and provide new insights into the overall tectonomagmatic evolution of the region. These results will also bear directly on genetic and exploration models developed for associated precious- and base-metal mineralization.

U-Pb geochronology identified the same 'inboard younging' pattern of magmatism that was previously recognized in the northern and western portions of the TGP (Mortensen et al., 2000). Within the study area, Anvil plutonic suite (APS; >100 Ma) magmatism is for the most part limited to the westernmost Mt. Billings Batholith. The majority of intrusions, including the large Coal River and Hole-in-the-Wall batholiths, are considered part of the Tay River plutonic suite (TRPS; ~99 to ~95 Ma). The strongly peraluminous two-mica Tungsten plutonic suite (WPS; ~99 to ~95 Ma) does not appear to extend south of the Cantung area. The Tungsten plutonic suite seems restricted to a region that shows the most evolved isotopic signatures, possibly suggesting a direct correlation with the nature of the underlying basement rocks. The economically significant Tombstone plutonic suite (TPS; <~95 Ma) continues to the extreme southeast end of the TGP, including the Big Charlie and McLeod plutons.

The dominantly granitic and granodioritic intrusions are high-K calc-alkaline in nature with mixed I- and S-type characteristics. The intrusions tend to become less peraluminous with decreasing age. Primitive mantle normalized REE patterns are virtually identical for the APS, TRPS and TPS, displaying steep profiles with negative Nb, Eu, and Ti anomalies. These characteristics are generally ascribed to I-type volcanic arc or subduction-related granitoids, however this signature is probably partially, if not entirely, inherited from the partial melting or assimilation of crustal material previously formed in a subduction setting. TPS intrusions show more pronounced LREE-enrichment and less prominent Eu anomalies. There is an increase in overall REE abundance with decreasing age (APS → TRPS→ TPS) which also correlates with a general increase from ~700° to ~800°C in calculated zircon saturation temperatures

The high initial $^{87}Sr/^{86}Sr$, low εNd, radiogenic Pb compositions, Mesoproterozoic to Archean T_{DM} ages, and the peraluminous nature of the granitoids indicate a dominantly crustal source for these magmas.

Without contemporaneous mafic volcanism, it is difficult to conclusively constrain the paleotectonic setting in which the mid-Cretaceous magmatism occurred. The data presented here provide some insight into the nature of the tectonic setting; however for such large region, it can provide little more than generalities.

Lead isotope compositions of feldspars separated from various mid-Cretaceous intrusions and of sulphides from a number of precious- and base metal deposits are very similar and indicate that the metals in many mineral deposits (and prospects) throughout the region are mostly derived from the mid-Cretaceous TGP intrusions.

Directions for Future Research

Although this thesis has contributed to the understanding of the magmatic, tectonic, and metallogenic understanding of the TGP in the eastern Selwyn Basin, numerous questions remain unanswered and provide directions for future research.

Perhaps the most obvious question to emerge from this study is: What happens to the plutonic suites south of the study area? The three most obvious answers are: 1) the TGP, including the plutonic suites recognized in the study area, terminates or is truncated; 2) the TGP continues to the south in a similar fashion and intrusions are not exposed at current levels of erosion; and 3) plutonic suites within the TGP converge, swing to the southwest, and wrap around the basement promontory where the narrow margin has focused the locus magmatism. Indeed this is not a trivial question to answer. Studies similar to this one on intrusions that may be the southward continuation of the TGP (currently those west of the Tintina Fault in south-central Yukon) will be required to resolve this.

The shear volume of magmatism suggests that this portion of the crust remained hot for a significant period of time. The combination of expanded U-Pb dating, particularly for the larger batholiths, and regional Ar-Ar dating would be able to provide insight into whether the magmatism was essentially a continuum or was sharply episodic, as appears to have been the case further to the northwest (Mortensen et al., 2000).

One of the most challenging directions for future research will be to address the change in geochemistry and isotopic compositions with age, and geographic location. In particular, the question of whether the shift towards higher REE content and generally 'less-evolved' isotopic signatures reflects differences in the nature of underlying crust, a tectonic process whereby intrusions incorporate larger amounts of primitive material or if it represents a shift in the melt dissolution-kinetics (i.e., more wholesale melting of crustal material). This problem will require integrating new geochemical and geochronological studies on the regional scale with detailed mineralogical studies.

Additional geothermobarometry, geochemical, and isotopic studies, including Hf and $\delta^{18}O$, on both intrusive rocks and potential source rocks will provide the best means to further constrain the question of magma sources. The combination of these studies with detailed mapping to examine issues such as the nature of emplacement will ultimately lead to the development of a robust tectonomagmatic model for the region

Tracing the economically important Tombstone plutonic suite (TPS) is a challenge left for the exploration industry. Within the Intrusion-related Gold System (IRGS) model, the depth of emplacement exhibits a strong control on not only the target type but the associated pathfinder elements as well. Furthermore, factors such as the level of erosion further complicate exploration for IRGS. Integrated geochemical and geophysical techniques will be required to test the eastward and southward limits of the TPS.

References

Mortensen, J.K., Hart, C.J.R., Murphy, D.C. and Heffernan, S. 2000. Temporal evolution of Early and mid-Cretaceous magmatism in the Tintina Gold Belt. *In:* The Tintina Gold Belt: Concepts, Exploration and Discoveries, British Columbia and Yukon Chamber of Mines, Special Volume 2, p. 49-58.

Appendix 1

Analytical Precision

The precision of lithogeochemical data obtained during the course of this study was monitored by replicate analyses of Mineral Deposit Research Unit in-house standards P-1 (granodiorite from the Coast Plutonic Complex) and BAS-1 (basalt from near Cheakamus, British Columbia). Analytical data obtained from these samples was compared to a mean of 5 previous repeat analyses and are presented in Table A.1. Duplicate analyses of these samples are precise and are within two standard deviations of the standard values.

Table A.1. Mean values and duplicate analyses of standards P-1 and BAS-1.

	P-1 (n=5)* mean	std deviation	P-1-A	P-1-B	BAS-1 (n=5) mean	std deviation	BAS-1-A	BAS-1-B
Major elements (wt. %)								
SiO_2	70.96	0.10	69.90	69.83	53.56	0.36	52.41	52.45
TiO_2	0.38	0.00	0.38	0.80	1.31	0.01	1.33	1.31
Al_2O_3	14.10	0.06	14.27	14.24	15.12	0.07	15.06	15.08
Fe_2O_3	3.90	0.00	3.89	3.85	11.16	0.05	11.09	11.10
Fe_2O_3	2.34	0.08	2.25	2.25	8.86	0.12	8.73	8.76
MnO	0.08	0.00	0.08	0.08	0.14	0.00	0.15	0.14
MgO	1.11	0.01	0.91	0.93	7.35	0.05	7.10	7.11
CaO	3.49	0.02	3.35	3.38	8.28	0.05	8.28	8.30
Na_2O	3.80	0.00	3.78	3.80	3.28	0.04	3.05	3.06
K_2O	2.12	0.01	2.19	2.21	0.56	0.02	0.61	0.60
P_2O_5	0.08	0.04	0.07	0.08	0.22	0.00	0.23	0.23
TOTAL	100.56	0.22	99.28	99.20	100.96		99.15	99.26
Trace and rare earth elements (ppm)								
Ag	0.3		<1	<1	0.28	0.08	<1	<1
Ba	724	8	825	932	194	18.55	209	184
Ce	28	1.26	25	29.5	21.8	0.75	20.5	20.5
Co	6.2	0.4	5.5	6.0	42.2	0.4	39.0	41.0
Cs	1.2	0.1	1.1	1.1	0.1	0.0	<0.1	<0.1
Cu	15.5	5.5	5.0	5.0	59.0	0.8	55.0	65.0
Dy	3.3	0.2	2.3	3.1	3.3	0.2	2.6	2.7
Er	2.1	0.1	1.9	2.1	1.5	0.1	1.4	1.4
Eu	0.8	0.0	0.7	0.7	1.3	0.1	1.0	1.0
Ga	15.0	1.1	12.0	13.0	19.6	1.0	16.0	17.0
Gd	3.1	0.1	2.7	2.5	3.8	0.1	3.0	3.3
Hf	3.8	0.1	3.0	4.0	2.4	0.1	2.0	1.0
Ho	0.7	0.0	0.5	0.5	0.6	0.0	0.5	0.5
La	13.2	0.4	14.0	16.0	9.3	0.4	10.5	9.5
Lu	0.4	0.0	0.3	0.3	0.2	0.0	0.1	0.1
Nb	3.8	0.2	2.0	3.0	8.2	0.5	6.0	6.0
Nd	13.0	0.6	10.5	12.0	13.6	0.8	11.0	11.5
Ni	-	-	<5	<5	172.0	1.9	160.0	170.0
Pb	10.2	1.5	15.0	5.0	4.4	4.3	40.0	<5
Pr	3.4	0.1	2.6	2.6	3.0	0.1	2.2	2.3
Rb	50.4	3.1	40.4	43.2	7.0	0.1	5.2	5.6
Sm	2.9	0.1	1.9	2.7	3.5	0.5	2.5	2.4
Sn	2.4	0.9	1.0	1.0	1.2	0.2	1.0	1.0
Sr	256.0	4.9	194.5	207.0	502.0	7.5	401.0	426.0
Ag	0.3	0.0	0.4	0.5	0.5	0.0	0.5	0.5
Tb	0.5	0.0	0.4	0.5	0.6	0.0	0.5	0.5
Th	4.4	-	<0.5	<0.5	0.8	0.0	<0.5	<0.5
RTl	0.3	-	<0.5	<0.5	0.1	0.0	<0.5	<0.5
Tm	0.4	0.0	0.3	0.3	0.2	0.0	0.1	0.1
U	1.5	0.1	1.5	1.5	0.3	0.0	<0.5	<0.5
V	58.2	0.4	45.0	45.0	152.0	1.1	125.0	140.0
Y	22.8	0.5	18.0	19.0	18.4	1.0	14.0	14.5
Yb	2.5	0.2	1.9	2.0	1.4	0.1	1.2	1.1
Zn	44.0	0.9	30.0	40.0	91.4	1.0	85.0	90.0
Zr	126.0	10.2	126.0	123.0	94.5	2.2	93.0	90.0

P-1 and BAS-1 are MDRU standards.
* Mean values of P-1 and BAS-1 are based on the average of 5 previous repeat analyses.
A and B are duplicate analyses of the standards that were used to test for precision.